Faculdade de Engenharia da Universidade do Porto

LEGO® House (Building a LEGO® beam/structure for civil engineering applications)

David André da Silva Araújo Faria

Dissertação de Mestrado/Masters Dissertation
Mestrado Integrado em Engenharia Mecânica

Orientador: Prof. Dr. António Torres Marques
Co-orientadores: Prof. Neil Thomas MBE
Prof. Dr. Marco Parente

Setembro de 2018

You must always strive to be the best,

but you must never believe that you are.

Juan Manuel Fangio

Agradecimentos/Agnowlegments

I would like to start thanking the people who directly influenced in the writing of this dissertation, namely Professor Neil Thomas for giving me the initial guidance and Professor Marco Parente for helping me in the simulation stage of this project.

I would also like to appreciate the work Lego has done with its customers around the world, making sure that their projects are not neglected. I hope this project takes on the same treatment.

Gostaria de agradecer aos meus pais por me darem todas as possibilidades de me tornar naquilo que sempre quis! Pelo apoio e paciencia e apoio também merecem uma menção ainda mais especial. Ainda mais especial a minha mãe por ser o meu rochedo.

Aos meus amigos, em especial à Teresa, ao Gonçalo e à Carolina por me terem dado tanto alento e me terem ouvido nos últimos meses. Gostaria de agradecer também à Sara e à Rita por estarem sempre lá para mim.

Uma palavra também à Dr. Márcia que tanto me ajudou a sair de um mau lugar nos ultimos 9 meses.

À minha avó e ao meu tio, onde quer que eles estejam…

Abstract

This report is set to document the project of a LEGO® horizontal beam that is able to support normal loads on house-bearing beams.

An introduction to the State of Art of Modular Constructions is done, giving examples of existing solutions. Then an introduction to LEGO® and the attempts to make full sized houses with this material is made. Various LEGO® particular builds are cited as inspiration for the creation of this beam.

A prototype (not a physical prototype) is projected with regards to LEGO® design potentiality and limitations.

The projected prototype goes through three simulation phases: simplification – due to the simulation with the LEGO® parts being too heavy, it would require unsustainable computational capacity, which is why a simpler solution is given; contact determination – in this phase the “stud-and-tube” contact is defined and translated into cohesive contact; validation – the cohesive contact is validated using parts equivalent to those tested in phase two, in a system equivalent to phase one. As reference, beam deflection is also simulated in a geometrically similar beam made off balsa wood.

3 point bending tests are scheduled to be carried out to validate simulation results, however due to various limitations, it was impossible at the time that this report was completed.

Resumo

Ao longo deste relatório pretende-se documentar o projeto de uma viga horizontal feita em LEGO® capaz de suportar cargas verticais, com vista à aplicação como vigas de suporte na construção de habitações.

É feita uma introdução ao estado de arte da construção para habitações, passando por um exemplo de construções habitacionais modulares já existentes. É depois feita uma introdução à LEGO® e às tentativas de fazer casas em tamanho real com este material. Serão também mencionadas alguns tipos particulares de construção em LEGO® que ajudaram ao desenvolvimento do protótipo.

É projetado um protótipo (não concebido fisicamente) com atenção às potencialidades e limitações do LEGO®

A viga projetada passa por três fases de simulação: simplificação – a simulação da viga com peças LEGO® ao ser demasiado complexa, iria exigir uma capacidade de computação insustentavel, pelo que uma alternativa é apresentada; determinação do contacto – nesta fase determinam-se os valores caracteristicos do contacto “stud-and-tube” traduzidos sobre a forma de contacto coesivo; validação – é feita a validação do contacto coesivo usando peças equivalentes às usadas na segunda fase, mas no sistema da primeira fase. Para obter uma referência, é também feita a simulação da flexão de uma viga em madeira (balsa) com o mesmo perimetro de secção, mas secção sólida para comparar a defleção.

Estão programados testes de flexão de 3 pontos para comprovar os resultados da simulação, mas devido a limitações diversas foi impossível ter um protótipo físico aquando da entrega deste relatório.

List of Contents

List of Figures

List of Tables

1. Introduction

1.1. Context and Motivation

In a fast changing world where value is everything, the largest value asset an individual has is its house. This limits the individual's mobility, as when relocation is needed, the house must be sold and replaced, as this asset generally represents most of the individual's wealth, and wouldn't be able to acquire a new one. This can be overturned by renting or leasing, however this removes the entitlement to something so personal.

Modular houses can solve this problem by making use of a LEGO®-like construction, which leads to LEGO® itself.

LEGO® parts have been in the market for over 60 years (essentially) in their current form, but due to its status as a toy, it has been grossly neglected as a construction material, despite its durability, ease of construction and disassembly, lightness and sparse availability, as proven by Atelier One's attempt. (May, 2010) This is a material that needs no building tool as an aid to its construction, it's easily modified, waterproof, non-magnetic, and generally soft.

The objective of this thesis is to try and stretch the design capability of these kinds of materials, so they can be used in civil engineering applications without the need for fabrication of specific parts (something like bricklaying or concrete building).

1.2. Problem definition

To be inhabited, a structure has to meet some legal technical requirements, usually specified via legislation. During the course of this dissertation, the housing requirements will be based on Portuguese Law.

LEGO® parts are made to be easily taken a part, something structural parts can never do, as a compromise in the structure may mean its failure. This is a particular problem when it comes to free standing sections of LEGO® parts: as the loads act over unsupported sections, the direction of it activates the

disassembling mechanism and the pieces fall apart. For this reason, the thesis object will be a 100% LEGO® beam.

As a benchmark, the mechanical behaviour of wood will be used for comparison (it was what made the passive structure in Atelier One's house, as can be seen in Figure 1).

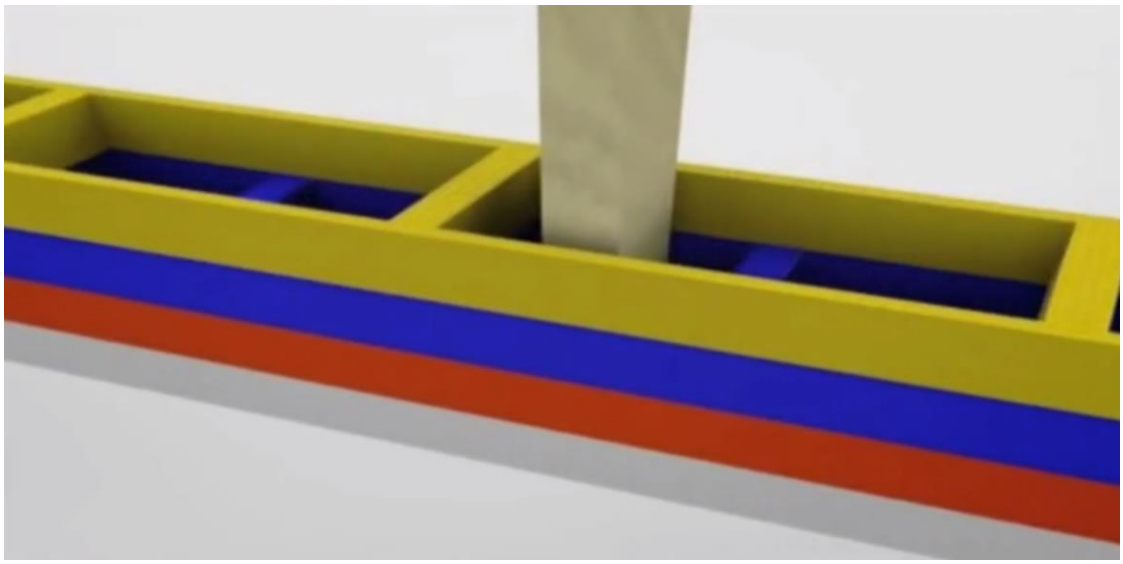

Figure 1 Wooden passive structure inside the original LEGO® House (1)

1.3. Methodology & Report Structure

This report is divided in two parts: State of Art Research and Prototype development

In the first part, a brief introduction to modular houses and one particular example is given. Then, the LEGO® company will be introduced, the way LEGO® works is described and some of the most relevant works done with the material so far is presented. As there is no academic work or relevant information regarding LEGO® as a mechanical material, many of the research done during this project has to come from alternative sources like Youtube or personal experience with LEGO®.

In the second part, a description on the expectations of the prototypes is made, based on civil engineering requirements and regulations, of how the mechanisms that hold LEGO® together work and the prototype is presented.

To verify the application of the concepts on the beam, simulations were run in three phases: simplification – where a simplified version of the beam is presented, with custom made to mimic the LEGO® beam's volume and Inertia Momentum; contact definition – the contact that connects bricks in LEGO® will be translated into cohesive contact, which were added for determined surfaces on the simulated beam (phase one); validation – a disassembly between parts geometrically similar to the one tested in phase two, but in the system of phase one was performed to validate the use of the cohesion method. As comparison for the deflection on the beam, a Wooden beam with the same cross-section and length of the LEGO® beam will be tested under the same loading conditions.

3 point bending tests on a physical prototype will verify the simulation results.

1.4. Pros&Cons

Any material or construction type comes with its pros and cons.

For LEGO® construction, that list is presented bellow in Table 1.

Advantages	Disadvanatages
+ Modability	– Cost
+ Durability	– Environmental impact
+ Availability	– Wasn't meant to be used as construction material
+ Washability	
+ Waterproofness	

Table 1 Advantages and Disadvantages of building with LEGO®

2. Chapter One: State of Art

2.1. Modular Houses

Modular houses are a cheap and efficient way to build many houses very fast. Television shows like “Extreme Makeover: Home Edition” give examples on how it is possible to build a complete house in 7 days (reuters, 2011), even though this show uses a great amount of hand labour (hundreds of people usually help on the builds), which is something very costly. The houses they build are not modular, however they follow a constant design philosophy, which sees the structure being assembled by wooden stakes and covered by prefabricated walls and roofs.

Modular construction can be very helpful in disaster stricken or generally poor areas, as their simplicity and modability allows not only for the environment sustainability (segments can be easily replaced by equal modules) and evolution, as the configuration can be changed at will.

An example of modular elements for the construction of buildings is presented in Patent #107461 from the Portuguese Patent Office, as seen in Figure 2.

This invention describes a constructive system through Modular Elements for structural walls, inner walls and ceilings, mainly destined to habitable buildings. This construction system consists in panels that are easy to assemble and disassemble and interconnected to form the floor, walls and ceiling. Each panel is constituted by a U-shaped steel tube whose external base is welded to a perforated rail (1) or a slotted one ready for clamping (11); the central part of the panel, which comprises a steel tubular structure (with rectangular cross-section) made of 3 vertical equidistant tubes (12) connected at the top and the base by 4 U-shaped (14) and 2 rectangular tubular elements placed diagonally (13), which

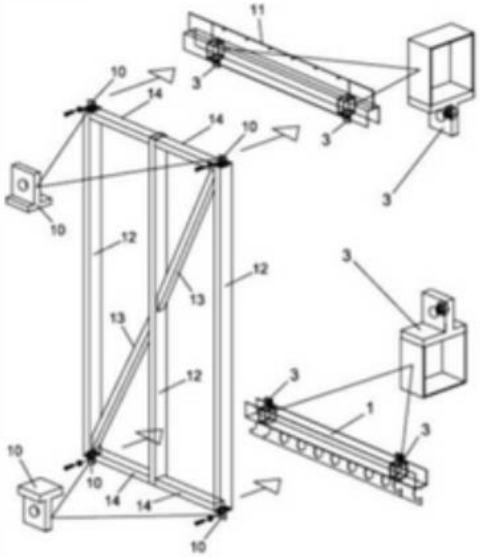

Figure 2 Patent 107461(PT) (2)

connects opposite corners of the panel. There are two male-female fixing elements (3) and (10). (Portugal Patente Nº 107461, 2017)

With these panels, architects and engineers can easily create standardized houses that have elements that have been proved to work which makes not only the build, but the project that leads to it less time consuming, meaning more projects can be put into place. This, because with this particular element, one can build all the segments of the house, be it floors, walls and roofs.

The ease of availability and standardization should allow to build houses with these panels anywhere and in a relatively simple way. The only elements that are not presented are the connecting bolts that are standardized and easily available anywhere in the world in common hardware stores. This also makes the construction much faster as the house fabrication on site, which is the most time consuming to come in the construction of the building, comes down very much, as the building blocks for this type of construction come to the construction site already assembled and as they are meant to be easily connected, a house can be erected very fast.

Figure 3 shows possible configurations for a simple T0 house, with a bathroom. The apartments are all 4 panels wide by 3 panels long, but the disposition can change. The bathrooms are always 1 panel wide by 2 panels long. These inner walls that limit the bathroom are also made from the panels seen in Figure 1, as are the floors and ceiling. The only different elements are the window and door sections that can be seen in the lateral view of Figure 2. However, these elements would be as available as the previously discussed panels and make part of the constitution.

Figure 3 Possible configurations for T0 apartments using Patent 107465(PT) (3)

2.2. LEGO®

LEGO® started as a carpentry in the 1930s when Ole Kirk Kristiansen established a shop to manufacture stepladders, ironing boards, stools and wooden toys. The company's name comes from the amalgamation of "leg godt" meaning "play well" in dannish. The word "LEGO" also means "to put together" in latin. (LEGO(r), 2018)

In 1946 the company acquires its first injection moulding machine and starts producing plastic parts. The income from this machine on its first year of production is 15 times what it costed. It's also with this machine that the current story of LEGO begins: it's thanks to it that Ole Kristiansen gets the idea to build interlocking and dissasembling bricks called "automatic building blocks" – these aren't still the current LEGO bricks we have today. (LEGO(R), 2018)

These came officially in 1958, with the stud-and-tube patent that included the patented locking mechanism that allows LEGO® to stay together better than without that system (a locking system which will be described further on). By 1964, LEGO® Elements start to get moulded in ABS, a polymer which improves the clutch power. (Denmark Patente Nº 751387, 1958)

At the same time, Godtfred Kirk Christiansen presents the company to the ten product characteristics: (LEGO(R), 2018)

1. Unlimited play potential
2. For girls and for boys
3. Fun for every age

4. Year-round play
5. Healthy, quiet play
6. Long hours of play
7. Development, imagination, creativity
8. The more LEGO®, the greater the value
9. Extra sets available
10. Quality in every detail

LEGO® Technic products get into production in 1977, meaning that LEGO® now has tension materials, allowing for bigger supported structures. (LEGO(r), 2018)

In 1985 the LEGO® Prize is founded, an international annual award of 750k DKK (100 565.63€), now increased to 1M DKK (134 087.50€) for exceptional efforts on behalf of children. In 1986, as the Group is granted the title “Purveyor to Her Majesty the Queen” by Queen Margrethe of Denmark, Godtfred Kirk Christiansen steps down from the leadership of the LEGO® Group to be replaced by his son Kjeld Kirk Kristiansen. (LEGO(r), 2018)

After some years of lower than usual sales, the company launched various products from various lines (namely the Ferrari® and Star Wars® brands that were brought to work together with LEGO®) to further popularize the brand. This all culminated in the 2014 LEGO® MOVIE, which was a commercial success and further cemented the brands image and goals: everything is possible if you believe it is. (LEGO(R), 2018)

2.2.1. How does LEGO® work

LEGO® elements can be divided into two categories: bricks and (technic) beams.

Bricks (Picture 1a) are assembled from the bottom to the top and are held together by the stud-and-tube principle (which will be discussed later), which allows them to grip to each other, but can be easily removable. This is also known as the LEGO® play system.

Beams are customarily structurally used, threaded elements. The threads hold pins (Picture 1b) which have a shape such that they snap into the position inside the threads, but can be easily pulled off, as the bricks. Beams can be

connected to each other via these pins or can be connected to a brick structure via special bricks that have pins integrated to them (Figure 4c), with the same snapping abilities of regular pins.

Figure 4a) LEGO Brick, b) LEGO® Technic pin, c)LEGO® Brick with half pin ends

2.2.2. Acrylonitrile Butadiene Styrene (ABS)

Acrylonitrile Butadiene Styrene (more commonly known as ABS) is the plastic that most LEGO® parts are produced from and the only material employed in this project.

ABS was introduced in LEGO® parts in 1963. It is the polymer used in most of the modern LEGO® parts. The material comes in bar form and is then melted into a resin and injected in the mould. The butadiene component (a derivative of natural rubber) is largely responsible for the strength and impact resistance of this polymer. The modern formula for ABS was developed as part of the war effort in the mid-1940s. Bayer AG, a German chemical company, had long been the exclusive supplier to the LEGO® group. It spun off most of its plastics business in 2004 into the newly-formed Lanxess AG. Virtually all plastic used by LEGO is a proprietary version of Lanxess' Novodur ABS, Makrolon polycarbonate (for transparent elements) and Macrolex dyes for coloring.

LEGO® parts are injection moulded. Silos of material are available with pipes that feed plastic granules to the molding machines. Each silo holds up to 33 tons of granules. The molding process is almost completely automated. The molding machines heat up the granules to a temperature of about 230°C. The polymer is then fed into molds. The machine applies high pressure to make sure the bricks are shaped with perfect accuracy. They are then cooled and ejected, which takes about 10 seconds. (Industries, s.d.)

Properties of ABS	
Young Modulus	2.07-2.76 GPa
Poisson Coefficient	0.391-0.407
Yield Strength	34.5-49.6 MPa
Specific Weight	1030-1060 kg/m^3
Price	2.50-2.66 €/kg

Table 2 Some properties of ABS (CES EduPack ®)

2.2.3. LEGO® based constructions

2.2.3.1. Sculptures

Nowadays, LEGO® constructions can be considered works of art. Some of these represent replicas made out of LEGO® of people, vehicles, objects or even monuments. Some of these sculptures are incredibly massive and from some point of view, one can wonder “how did they do that?”. Most of these pieces are made by artists who are mostly commissioned to build these artefacts.

Figure 6 represents a sculpture that impresses by expressing the soul of a LEGO® creator. The exposing of one’s inside only to reveal it made of bricks is not only startling, and could only be achieved due to the incredible craft, as at first glance it looks like a real human has ripped his skin off to reveal a “LEGO®y” interior. Only when coming closer can one truly understand the detail of this Minecraft-like construction.

Figure 5 Creation by Riccardo Zangelmi (5)

Figure 6 Creation by Nathan Sawaya (4)

Figure 5 however represents the full potential of a LEGO® structure. Mimicking Figure 6 on its Minecraft-like construction, it is a far larger piece, as there are some pictures of its creator Riccardo Zangelmi standing behind it (possibly a person could fit laid on the hands). This means this piece is very heavy. As you can see in this sculpture, the fingers are positioned in unconventional angles and despite this they are held together. This demonstrates the true virtue of the locking system in LEGO®.

There are however some private creators who can get very creative with LEGO®, building not only massive constructions, like the Big Ball Contraption ((Youtube) B. t., 2018), the “Amazing Box”, an automated box, ((Youtube) J. B., The Ultimate LEGO Machine Returns!, 2016) or mainly the “LEGO® safe” ((Youtube) J. B., Working LEGO Combination Safe, 2015), the latter being inspiration for some of the design features as will later be seen.

The Big Ball Contraption and the “Amazing Box” (Figure 7) in particular employ various elements from different ranges of the products, from beams to bricks and even Mindstorms parts. In the pieces of JK Bricks, one trend is clear: he uses brick masonry outlying a technic-based structure. This is mainly due to the fact that most of his creations have movement, where Technic elements come into play.

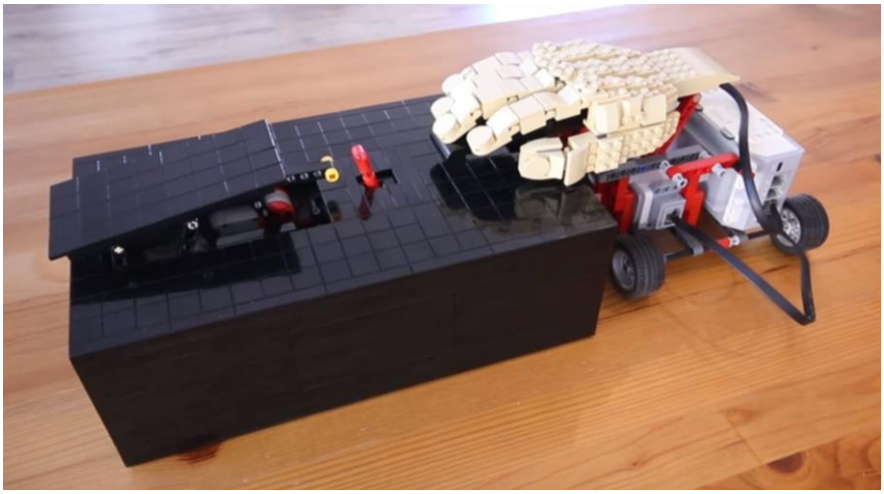

Figure 7 The "Amazing Box" and it's match-made-in-hell hand foe by JK Bricks (6)

2.2.3.2. Atelier One's LEGO® House

In 2010, in the BBC television show James May's Toy Stories, the presenter James May takes on the challenge of building a two-storey House using only LEGO® bricks. For this, and with the consulting help of Atelier One, a house is built out of LEGO® masonry, having a bypass wooden structure as the actual structural part of the building. This was not the early objective, and by the end of the show, a possible sustainable LEGO®-only structural element is built and succesfully tested. However, to this day, a fully operational LEGO® only house (apart from regulatory outboard systems like sewage and electricity) is yet to be built.

Figure 9 LEGO® House (7)

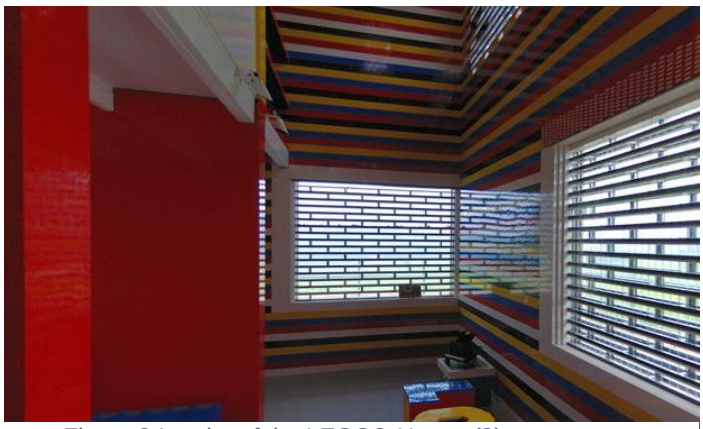

Figure 8 Interior of the LEGO® House (8)

This house, consisting of about 3.5 million LEGO® bricks, had a living room and a kitchen in the lower floor and a bedroom and bathroom in the top floor, the floors being connected by a corner staircase. All the furniture and appliances where made out of LEGO®, including water taps and sewage, cutlery, and some house hold "items" like slippers, or a cat. It was built on a vineyard in the English countryside. When asked for evaluation on the house, two real estate agents rated the house at 5 000 £ and 10 000 £ respectively. However, an Art Gallery curator rated it at 500 000 £, which closer represents the true value of the house. It was projected by Barnaby Gunning with help from Atelier One.

The main reason why the initial build wasn't considered a complete success is in the fact that the structure of the house wasn't made out of LEGO®, and LEGO® was only supported on top of this construction. This happened due to delay in development, as many solutions were tried to obtain a capable design. The main issue with LEGO® bottom to top construction is the fact that the pieces can easily delaminate and tear apart, meaning evident failure (Figure 10). During contacts with Atelier One, they expressed special concerns towards this action and should be the main concern to overcome in this project.

Figure 10 Failure of early prototypes (1)

As the main issue during this construction were the horizontal beams, this will be the sole focus of this dissertation, however, possible solutions for connectors will be provided.

3. Chapter Two: Building a LEGO® beam

3.1. Concept

3.1.1. Building Principles

3.1.1.1. "Stud-and-Tube"

LEGO® parts fit due to a feature called "Interference fit". This feature consists in locking materials together using the material's internal tensions to aggregate separate pieces. This works by superimposing the matching surfaces, in a sense that, if the parts were perfectly rigid, the matching wouldn't be possible.

Figure 11 Typical LEGO construction (3 story LEGO®-scaled lair; original construction)

However, in early LEGO® parts this connection was very weak, given that parts with more than 1 stud of width would have only the outer studs loaded, only on their exterior. This was rectified by the introduction of the interior tube (hence the LEGO® patent "stud-and-tube") which allowed for a higher surface tension between blocks which in itself turns into higher gripping force.

3.1.1.2. Snapped Beams

Technic elements (generally pins and beams) are usually used to build mechanical models that are most times equipped with gears and dynamic mechanisms to represent, to a certain extent, existing machines.

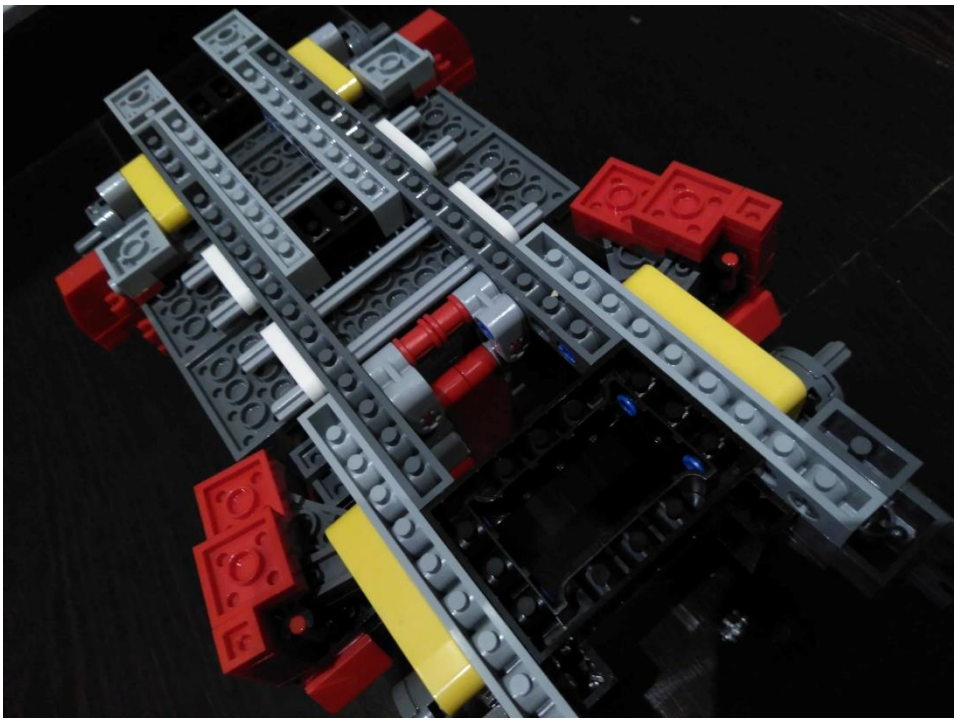

Figure 12 LEGO Ferrari F40 undertray

When combined with brick, the beams can increase the rigidity of a structure. This increase in rigidity comes in a similar way to what happens in reinforced concrete, as the technic beams support the beam under traction (as the steel rods would on concrete) and the bricks support the build under compression (like concrete itself). This type of construction allowed engineers to build higher, culminating in the skyscrapers seen in many cities throughout the world, mainly in Asia and North America.

As it can be seen in Figure 12, Technic bricks (large dark and light grey parts) are held together to provide the structure for the undertray of the car. They are connected via 2 or 3-wide pins and hold not only the body, but the engine (that represents the hole in the back) and the suspension (rigid wheel hubs in this case).

The upper element seen in Figure 13 – red L shape – includes the mounting point of the rear body (which can move up to reveal the engine bay), which represents about a quarter of the body of the car! This piece also reduces the torsion rotation along the central axis, by acting in the opposite direction to it. In essence, this type of construction, which resembles automotive monocoque construction, is based on a reverse T.

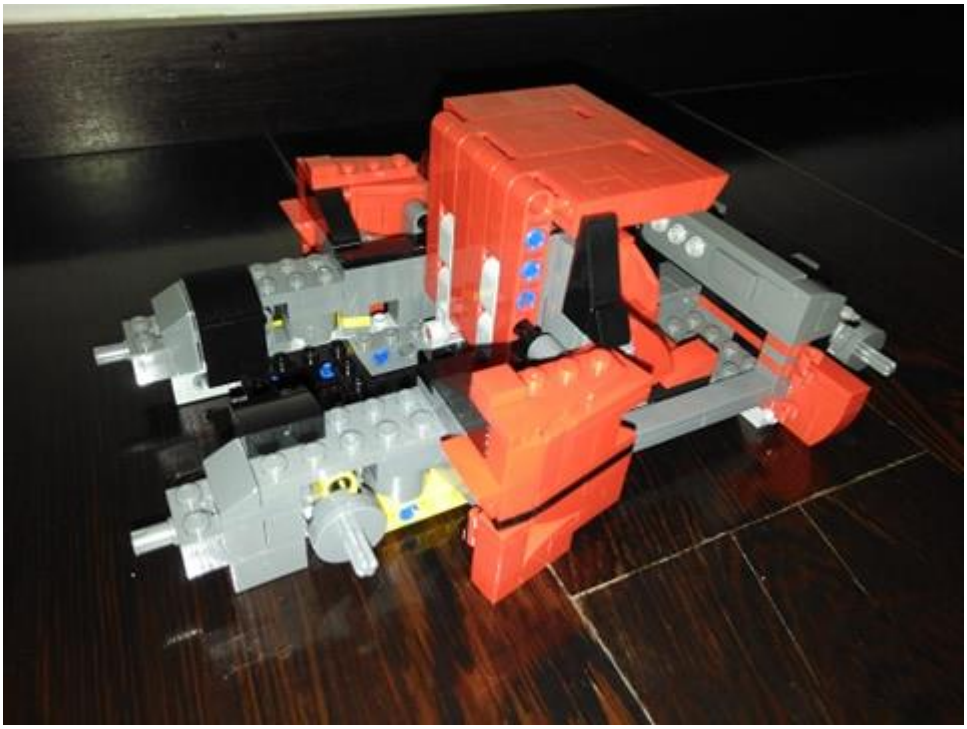

Figure 13 LEGO Ferrari F40 bare chassis

3.1.1.3. The “sleeve”

This ring-like structure is built to withstand the deflection of the beam. It does so by changing the direction of action of its rupture: unlike the central beam, it isn’t built from bottom to top, but rather in the axial direction, meaning that its natural direction of brakeage isn’t the direction on which the loads are applied.

Although not exactly alike, the inspiration for this sleeve came from the LEGO® vault (Figure 14) project by JK Brickworks, as it is a LEGO® model that could potentially be undisassembleadble, without fixing any parts. This happens due to, when in position, the safe will lock itself into a position where no piece is disassembleable. This means that a structure can now withstand loads without breaking under LEGO® construction rules, only failing when the material itself fails.

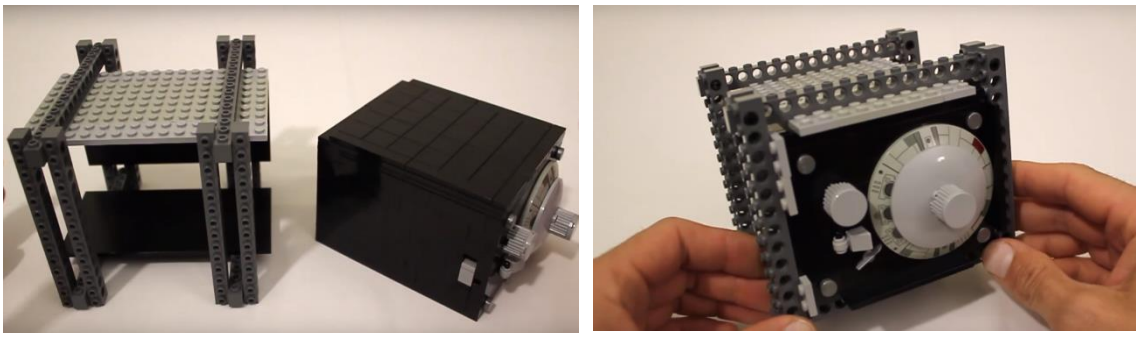

Figure 14 a) sleeve and LEGO® vault separate b) complete LEGO® vault(9)

This construction wouldn’t serve its purpose on its own, however in a stationary locked position, and allied with the technic beams working on the direction opposite to the brick separation for this situation, it does.

The inner sleeve is only meant to avoid the dislodgement of the beams in the direction opposite to the walls.

3.1.2. Design Phylosophy

Spaceframe vs Monocoque

When building a structure, there are generally two options: spaceframe (interconnected beams that are overlaid with masonry) or monocoque (where the structure and masonry are one single component).

Figure 15 Example of a monocoque structure (F1 chassis) (10)

From a mechanical point of view, monocoque has far superior characteristics when compared to spaceframe, giving it its ability to absorb loads more uniformly throughout the structure. However, due to its far more complex construction and design potential, only early prototypes were sketched. It should be noted that the ideal LEGO® House should go through this path, and should be the path to be explored in the future, but the time frame to embark on set project would surpass the duration of this project.

Figure 16 Example of Spaceframe construction (temporary accomodation) (11)

Spaceframe is still a suitable solution, given that most houses are actually built applying this principle, as it is far simpler to develop and erupt compared to monocoque, it's fairly more modable and due to that it's an easy way to expand. This should not be confused with a truss system as every connection in this structure type is clamped.

3.1.3. Building Requirements

Columns

While trying to understand how to deal with the simulation part of problem in hands, and after some talks and suggestion from Professor Cesar Sa to try and go through a discrete elements method methodology, suggested an article from Professor Paulo Lourenço from U. Minho (Paulo B. Lourenço). Despite not being the focus or orientation of this project, it clearly shows two important things: the modes of failure and possible correction solutions on columns and that it was extremely uncommon to have straight rock beams.

The modes of failure of brick laid columns can be seen in Figure 17, and as it is possible to see, the central part of the column collapses first due to shear stress. This same problem affects LEGO® constructions, and can lead to a delamination of the whole structure. A through stone is a physical rigid element that breaks diminishes the influence of the shear stress (Figure 17b) and can also be used in LEGO® construction

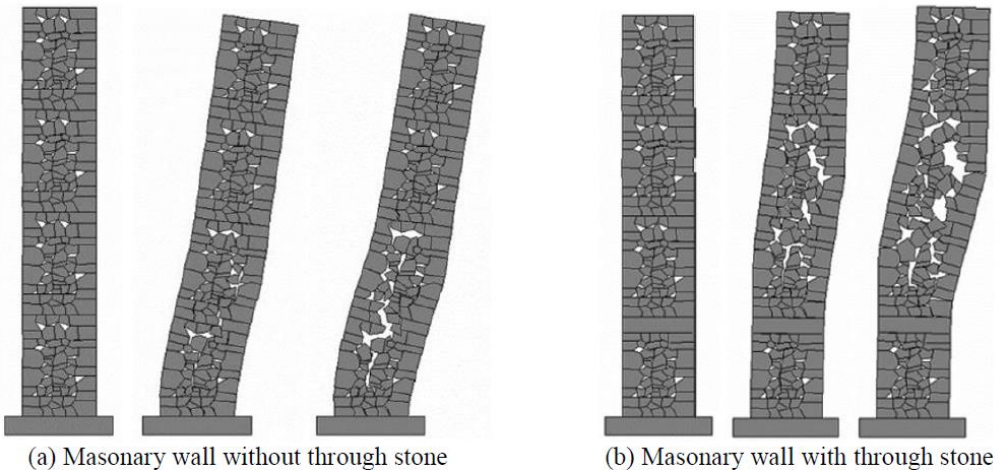

Figure 17 Progression of collapse mechanism under pushover analysis of three leave rubble masonry all a) without through stone and b) with through stone (12)

Figure 18 leads to the second conclusion that discrete elements are very difficult to build horizontally in order to support loads. For that reason, arches are usually seen in older stone constructions, as this allowed the elements to support loads on bricks that didn't even need to be cemented together. This arches distribute their load through their neutral axis (different from the centre of gravity) towards the footings (connections to the walls; ends).

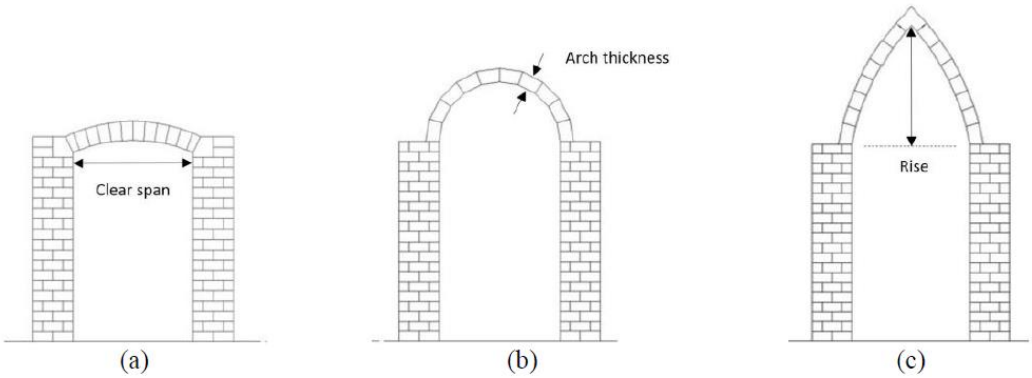

Figure 18 a) Pier and shallow arch, b) pier and deep arch, c) pier and point (gothic) arch (12)

These 3 configurations of arches show clearly how discrete element based constructions should be built, or at least were built until the introduction of LEGO®.

Floor

When building a house, the supporting force exerted for many actions based on overloads on a floor is given as: (Ministério da Admnisitração Interna, 2005)

$$S_d = 1.5 \cdot S_{Gk} + 1.5 \cdot (S_{Qk} + 0.6 \cdot S_{Wk}) \text{ (3.1.3.1)}$$

Where:

- S_d is the load applied to the beam in kN/m^2
- S_{Gk} is the effect of the weight of the floor in kN/m^2. Knowing that each beam weights about 10 kg ≈ 0.1kN, and has an area of surface of 0.184m^2, its density is 0.543 kN/m. Introducing the number of beams as *n*, and knowing that each beam has a considered area of 0.1278 m^2 for 1 m length, we get that S_{Gk}=0.0694·*n* kN/m^2. *n* Є [1,7], **N**
- S_{Qk} is the effect of the overload on the floor. The value for this action is of 4 kN/m^2, as overload requirements for offices were considered (Ministério da Admnisitração Interna, 2005)
- S_{Wk} is the effect of the wind on the floor, and will not be considered
- The values of 1.5 represent the safety coefficient for the proper weight influence and for the permanent actions

Given the above, the overload over the beams is defined as:

$$S_d = 0.1041 \cdot n + 6\ kN/m^2 \text{ (3.1.3.2)}$$

And the load applied to each beam per meter of beam is:

$$S_{di} = {}^{S_d}/_{n}\ kN/m^1 \text{ (3.1.3.3)}$$

With these principles in mind and attending to the building capabilities of LEGO®, the following solution for a LEGO® beam was developed.

[1] As the distribution of beams is constant throughout the floor, this load is only dependant of the beam's length

3.1.4. Prototypes

3.1.4.1. Elements

Horizontal Beams

A render of the final projected beam is presented in Figure 19. This horizontal beam is made of 6 components: the bottom and top plates, the two walls and the inner and outer sleeves.

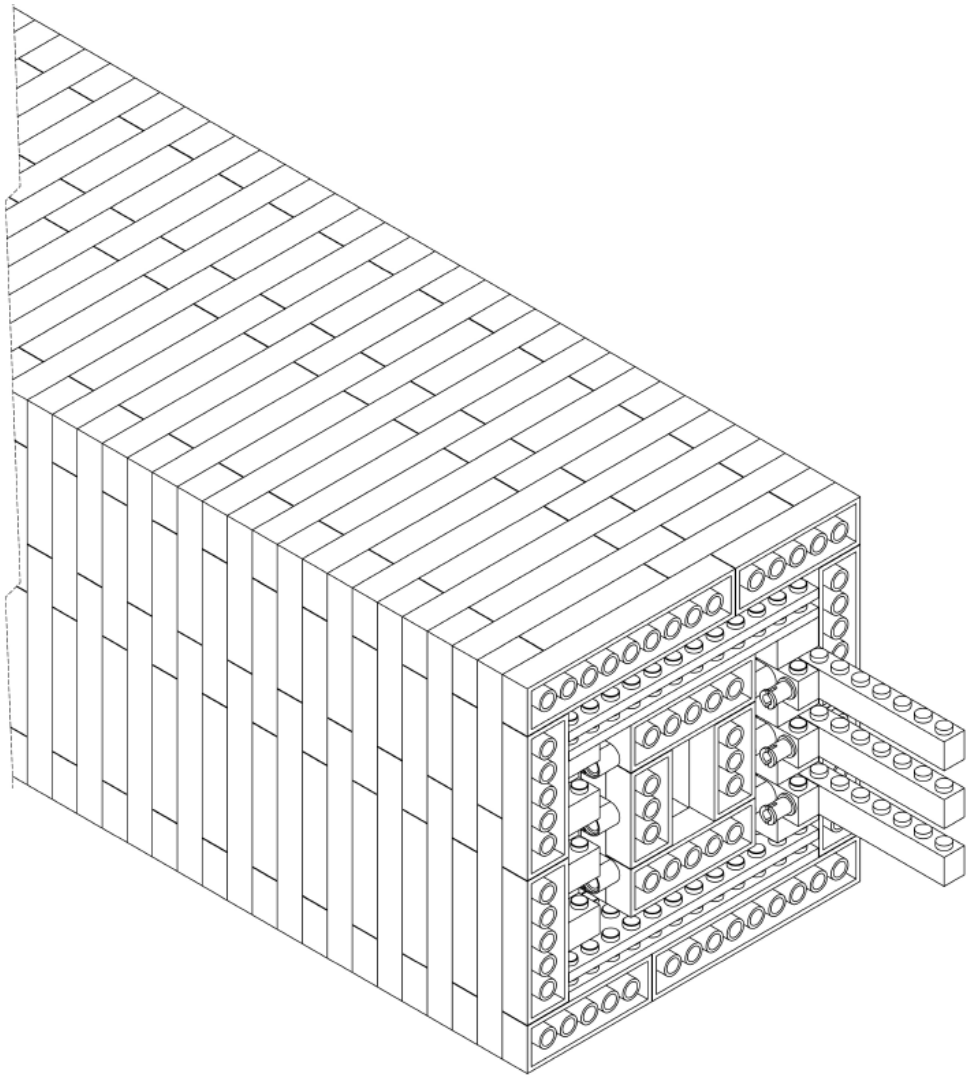

Figure 19 Rendering of part of the prototype beam (SOLIDWORKS®)

As this beam is supposed to work together with Atelier One's house, this beam has to fit inside the existing brick construction, which has an opening that is 16 stud wide in the shortest direction, being this the limit to the outer perimeter. With this in mind, the following paragraphs will define each of the sections of the beam as well as the reason for their conception.

The beam is to be built in the following order: Bottom Plate, the two Walls, Inner Sleeve, Top Plate and Outer Sleeve.

For generalization, all similar parts are the same (all the same color) for the identification of the constituents, however for easier analysis during testing, identical bricks may have different colors depending on their position in the beam.

Additionally, all technical drawings of the beam are available in the attachments section.

The Bottom Plate section is a 12.8 mm thick plate that connects the walls on bottom connection and acts as base for the beam. It's built from a 4-high 6x12 brick mesh. These meshes rely only on Interference fit for interlayer-connectivity. It also has an 8 stud wide flat tiles (16x8 tile, succeeded by two 2x4 tiles) section as to accommodate the inner sleeve, so it can slide in easily.

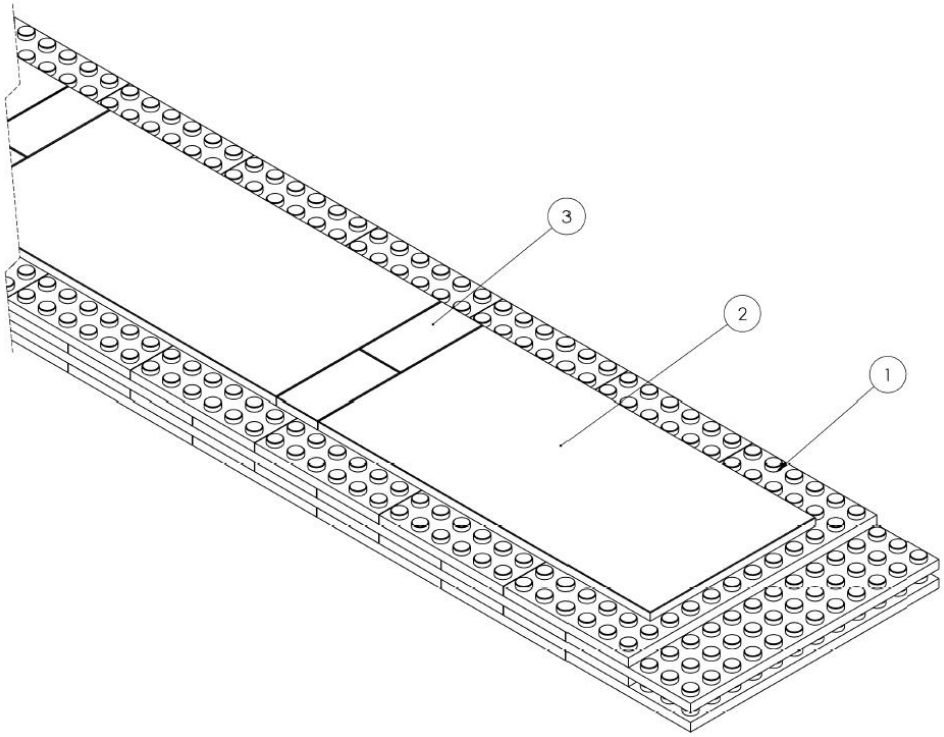

Figure 20 Rendering of part of the Bottom Plate section of the beam (SOLIDWORKS®)

	Part Name	Part Number	Quantity
1	Plate 6x12	4256149	120
2	Flat Tile 16x8	4217070 (discontinued)	10
3	Flat Tile 2x4	4560182	18

Table 3 Parts name, LEGO® identification number and quantity in the Bottom Plate section

The Top Plate section is a 16 mm thick plate similar to the bottom plate, but joins the walls on the top end. It also has 4-high 6x12 bricks, but is finished by a layer of flat tiles (one 16x8 tile outlaid in every edge except for one of the shortest by a 2 stud offset, which means ten 4x2 flat tiles and two 2x2 flat tiles for every repetition).

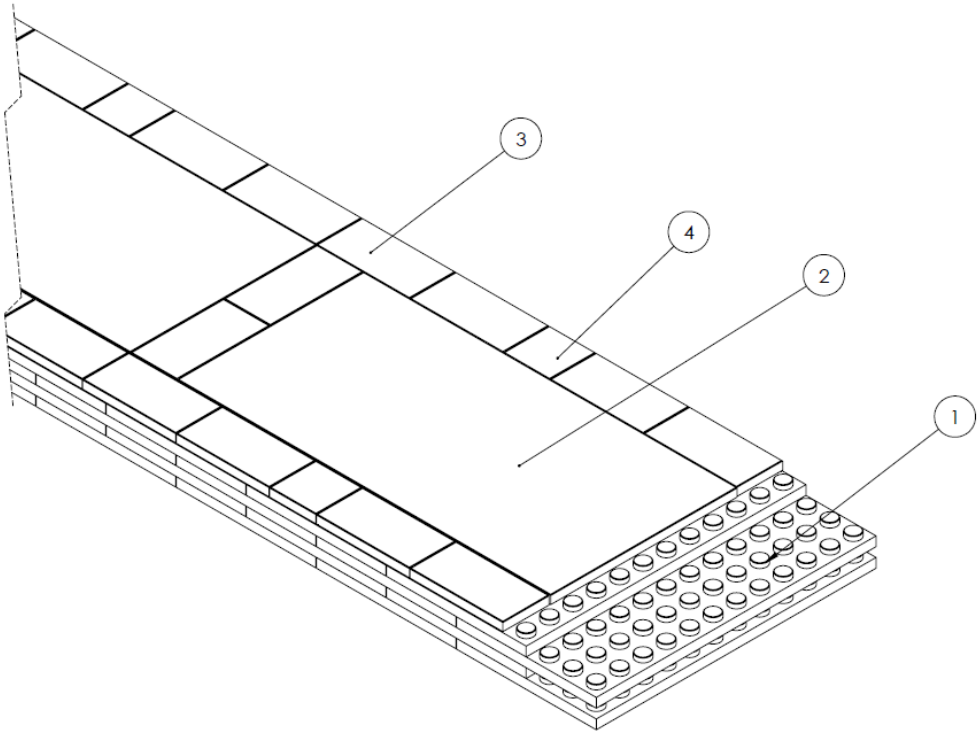

Figure 21 Rendering of part of the Top Plate section of the beam (SOLIDWORKS®)

	Part Name	Part Number	Quantity
1	Plate 6x12	4256149	120
2	Flat Tile 16x8	4217070 (discontinued)	10
3	Flat Tile 2x4	4560182	98
4	Flat Tile 2x2	306801	20

Table 4 Parts name, LEGO® identification number and quantity in the Top Plate section

The Walls are composed of simple stacked bricks interleaved with technic supported bricks. This construction allows for tension to be created over the axis of the beam during loading. This stress is supposed to stop the outer sleeve from delaminating, as the material stress between the technic beam is superior to the separation tension between levels of the sleeves (in essence, $K_{nn} << K_{tt}, K_{ss}$, as will be later demonstrated).

The wall is built by 4 rows of 2x10 bricks sandwiching 3 rows of 1x3 and 1x10 bricks, 1x2 brick with pins and the 5 stud long technic beams as seen in Figure 22.

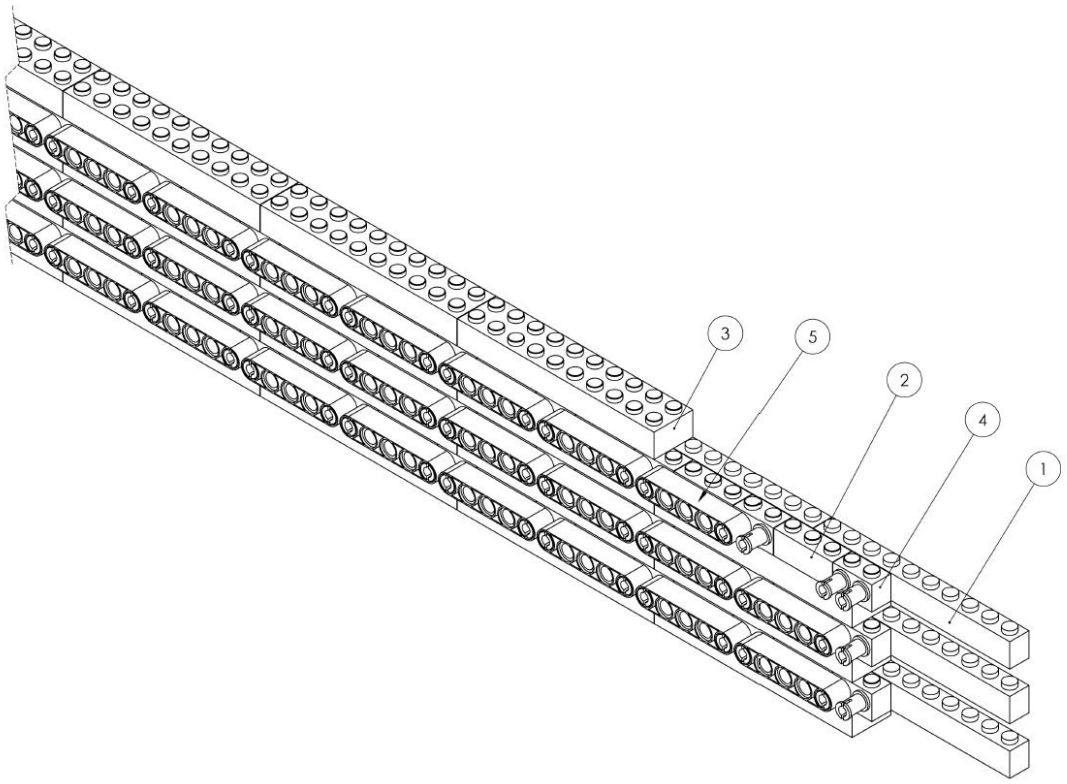

Figure 22 Rendering of part of one of the Wall sections of the beam (SOLIDWORKS®)

	Part Name	Part Number	Quantity
1	Brick 1x10	611126	54
2	Brick 1x3	362226	108
3	Brick 2x10	4617855	72
4	Brick 1x2 with 2 Pins	4210697	108
5	Technic Beam 5	4142135	108

Table 5 Parts name, LEGO® identification number and quantity in one of the Wall sections

The Inner Sleeve section acts as a brake for the technic parts not to separate from the pinned bricks under tension. It also acts as a central support for the beam, supporting the Top Plate.

It's built in a repeated mesh that has two levels that are 6 stud wide by 8 stud long: the first level is built by two 2x2 bricks and two 2x8 and top level is fixed to the lower with two 2x6 bricks and two 2x4 bricks, as seen in Figure 23.

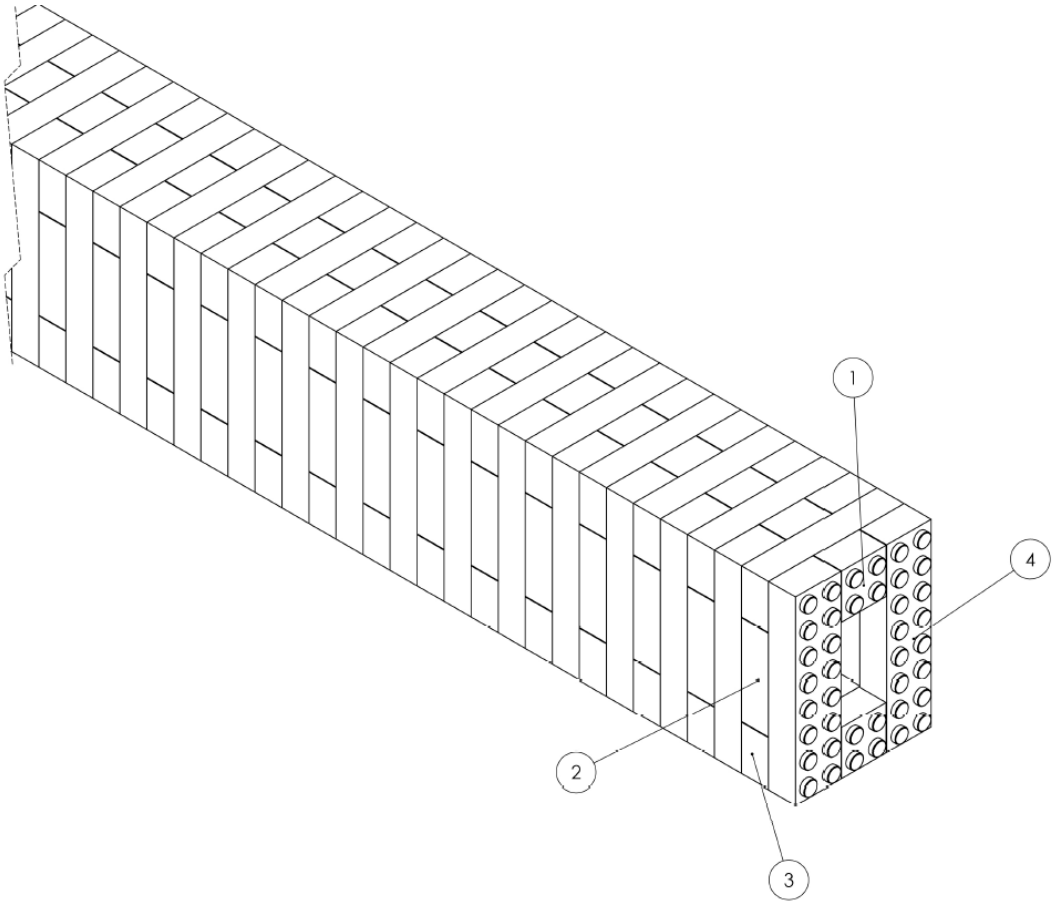

Figure 23 Rendering of part of the Inner Sleeve section of the beam (SOLIDWORKS®)

	Part Name	Part Number	Quantity
1	Brick 2x2	300301	150
2	Brick 2x4	300126	150
3	Brick 2x6	4181142	150
4	Brick 2x8	6037390	150

Table 6 Parts name, LEGO® identification number and quantity in the Inner Sleeve section

The Outer Sleeve section stops the plates from delaminating. As the load is acting on the studs, the rupture is through fracture and not cohesion, giving it increased rigidity and resistance to normal strength.

This section is built by outlaying six 2x6 bricks with two 2x10 bricks to create a 16x16 stud section, that is 2 studs wide. For every layer up, the construction should be rotated by 90º through the cross section central axis. This process can be verified in Figure 24.

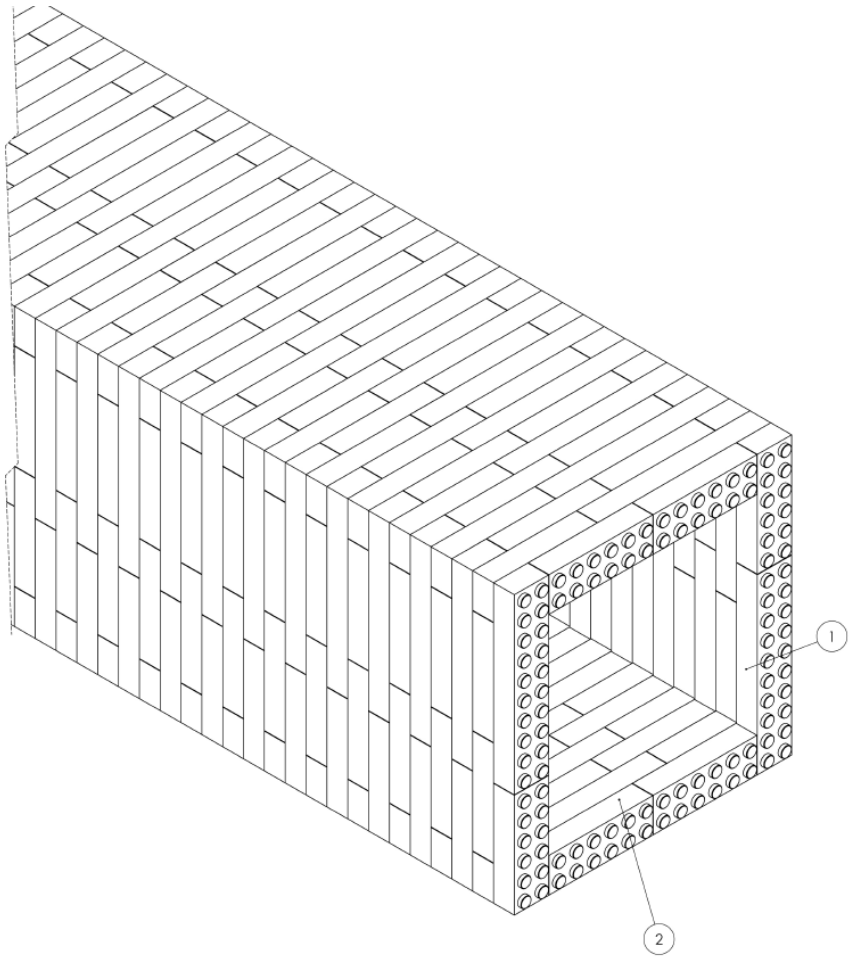

Figure 24 Rendering of part of the Outer Sleeve section of the beam (SOLIDWORKS®)

	Part Name	Part Number	Quantity
1	Brick 2x10	4617855	300
2	Brick 2x6	4181142	900

Table 7 Parts name, LEGO® identification number and quantity in the Outer Sleeve section

Connectors

Given that the main focus of this study is on the beam, not much thought was put into the connectivity of the beam with the rest of the house.

Figure 25 shows a possible way to go when it comes to the clamping of the beam 1) to a fixed point or 2) to other beams.

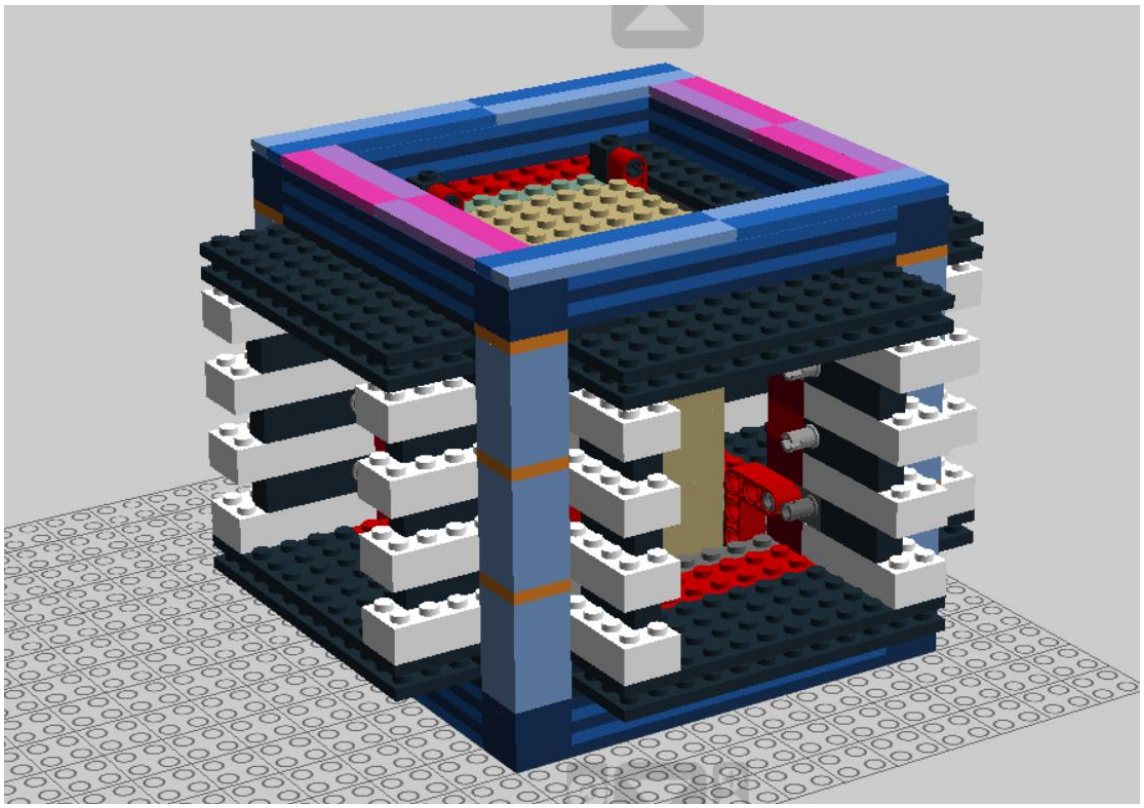

Figure 25 Rendering of a possible connector between beams (LEGO® Digital Designer)

3.2. Simulation

3.2.1. Method

The simulation was carried out using the Finite Element Method (FEM) through ABAQUS.

Interference fit is a very complicated feature to simulate in its most raw form, as it demands the readjustment of various details to guarantee there is no material overlap. In this case, given the amount of studs that have to be connected (there are 33968[2] stud connections in this beam alone!), an alternative simulation solution must be found, as this is a far too heavy solution to solve.

For this matter, the study was divided in two parts:

- In the first part, the pressure resultant from the Interference fit was determined as well as the shear force per stud, which represents respectively the normal (Knn) and tangential (Kss and Ktt) rigidity coefficient on the cohesive contact for the second part. The stresses represent the separation max stress (n direction) and the yield stress (t and s directions) respectively. This all means, that the stud-and-tube method could translated as a cohesive contact as seen in Figure 26.

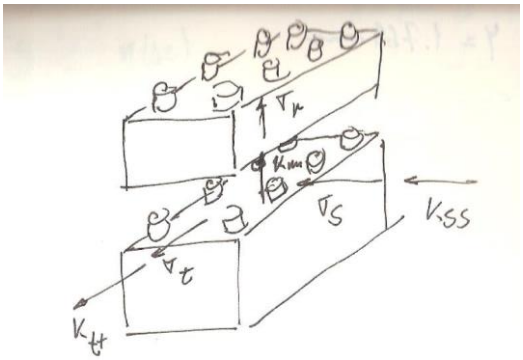

Figure 26 LEGO® connections definition

- This method was then validated using a mock up part representing the eighter piece (a hollow parallelepiped) and the separation force was determined, to ascertain if it corresponds to the brick separation force;

[2] All the existing studs are connected, apart from the tops on both sleeves, hence a simple calculation

- In the second part, and with the values from the first part, a model can be made where equivalent pieces will form an assembly and the contact between connecting faces will be modeled as a cohesive contact with normal stress equal to the Interference fit and tangential stress equal to the stud yield stress. This method is the one most suitable, as, if it could accurately represent the beam's behaviour, it's a simpler and lighter solution from a simulation point of view.

3.2.2. Finite Elements Method

3.2.2.1. Introduction

Several problems with Engineering significance can be described in terms of partially derived equations. With the exception of a few particular cases, it's not possible to obtain exact analytical solutions for these problems. The Finite Elements Method (FEM) is the most widely used numerical method to get approximated solutions for these problems. This method consists in the division of a continuous mean into sub-domains (known as elements) that retain the original mean's properties. The behaviour of these elements can be defined by differential equations that are solved through mathematical models, using computational analysis. (Roriz, 2015)

FEM had its origin in the mid-20th century, more precisely between 1943 and 1965, with the works of Courant (Courant, 1943), Argyris (Argyris, 1965) and Clough (Clough, 1960), with contributions from Zienkiewicz (O. C. Zienkiewicz, 1964). However, its application was only possible with computers, allowing algebraic equations of large dimension to be easily solved.

Due to its applicability and efficiency, FEM can be used in several exact science and biology areas as a means to, for example, analyse loads, stresses or displacements. (Roriz, 2015)

A finite element is a sub-domain of a continuous mean, with finite size. The points where the elements are connected are called nodes, or nodal points, and the process of node selection and creation of the finite elements is called discretization. (Roriz, 2015)

This method converts a problem with an infinite number of degrees of freedom (DOF) into one with a finite number of DOF, to allow for a solution (it's impossible to determine the solution for an infinite number of DOF). It also allows for an approximate solution within each element, based on a function of displacement, a function of the stress or a mixture of both, called shape functions. (Roriz, 2015)

The structural problem involves a stress field, σ, displacement, u, and loads per unit of volume, f. The displacement, u, is specified to take prescribed displacement values, ū, in the S_u part of the boundary surface S, while prescribed loads, t_e, are applied in the S_σ part. (Crisfield, 1986)

Given this problem, the following conditions must be met:

1) Compatibility:
    - u is continuous and differentiable;
    - In the boundary condition u=ū in S_u;
    - Deformation Law – displacement, e=Lu, where L is a linear operator and all the non-linear terms and dismissed.
2) Equilibrium:

$$S\boldsymbol{\sigma} + \mathbf{f} = \mathbf{L}^T\boldsymbol{\sigma} + \mathbf{f} = 0 \quad (3.2.2.1)$$

$$\mathbf{t}_i = \mathbf{t}_e \text{ in } S_\sigma \quad (3.2.2.2)$$

where t_i are internal loads and $S = \mathbf{L}^T$ is a linear operator.

3) Stress-displacement Law:

$$\boldsymbol{\sigma} = \mathbf{De} \quad (3.2.2.3)$$

where D is a symmetric matrix with fixed terms which are function of the Young's Modulus, E, and the Poisson Coefficient, ν.

A structural analysis using FEM includes the following steps:

1) Discretization of the structure – the continuous mean (geometry) is subdivided into finite elements.
2) The elements are then connected by a discrete number of nodal points in their boundaries.
3) Definition of the material properties of the elements.
4) Selection of a set of functions to define the displacement field within each finite element, in terms of its nodal displacement.
5) The displacement functions define the field of deformation within each element in terms of nodal displacement. The sum of this deformation with the initial deformation and the material's constitutive properties define the stress field through the elements.
6) Grouping the mass, damping and stiffness matrixes, which are derived from an energy method, based on shape functions. These matrixes relate the nodal displacement, velocity and acceleration in the loads applied to the nodes.
7) Determine a load system concentrated on the nodes, balancing the boundary stresses with the distributed loads.
8) Load application – forces or moments externally applied, that are concentrated or distributed.
9) Definition of the boundary conditions.
10) Solve linear algebraic equations system.
11) Determine stresses, reactions, nodal modes or other required information.

3.2.2.2. Finite Elements

Linear two node Element

Considering a beam element, placed over the global axis X (Figure 27). To determine the stiffness matrix, the first step is to relate the global coordinates X and the natural coordinates, ξ, where $-1 \leq \xi \leq 1$.

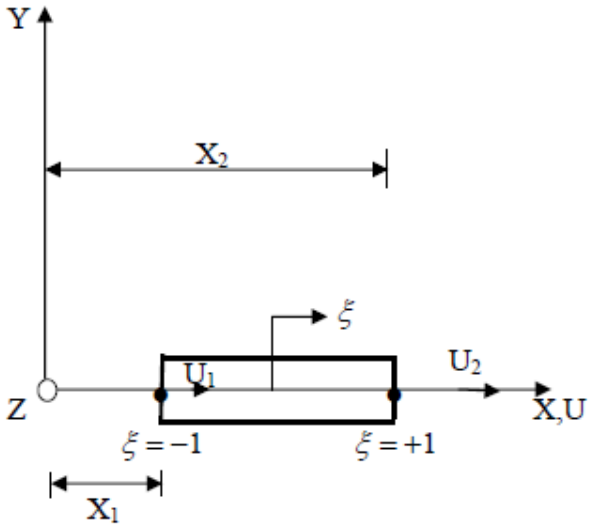

Figure 27 Beam element in the global and natural coordinate systems (13)

This relation is given by:

$$X = \frac{1}{2}(1-\xi)X_1 + \frac{1}{2}(1-\xi)X_2 \quad (3.2.2.4)$$

Or:

$$X = \sum_{i=1}^{2} N_i X_i \quad (3.2.2.5)$$

Where:

$$N_1 = \frac{1}{2}(1-\xi); N_2 = \frac{1}{2}(1-\xi) \quad (3.2.2.6)$$

Represent the shape functions that translate in a unique way the relation between coordinates X and ξ in the beam.

The global displacement in the beam is expressed in a similar way to the global coordinates:

$$\mathbf{d} = \sum_{i=1}^{2} N_i d_i \quad (3.2.2.7)$$

The interpolation of the coordinates and the elements displacement, using the same shape functions, defined in the natural coordinate system, constitutes the base for the formulation of the parametric finite elements.

The determination of the deformation is given by:

$$\varepsilon = \frac{d\mathbf{d}}{dX} = \frac{d\mathbf{d}}{d\xi}\frac{d\xi}{dX} \text{ (3.2.2.8)}$$

Where:

$$\frac{d\mathbf{d}}{d\xi} = \frac{d_2 - d_1}{2} \text{ (3.2.2.9)}$$

And

$$\frac{d\mathrm{X}}{d\xi} = \frac{X_2 - X_1}{2} = \frac{L}{2} \text{ (3.2.2.10)}$$

Where L is the length of the beam.

Henceforth, combining these equations, it is possible to obtain the deformation:

$$\boldsymbol{\varepsilon} = \frac{d_2 - d_1}{2}\frac{2}{L} = \frac{d_2 - d_1}{L} \text{ (3.2.2.11)}$$

The relation between deformation and displacement is given by:

$$\boldsymbol{\varepsilon} = \mathbf{B}\mathbf{d} \text{ (3.2.2.12)}$$

Where:

$$\mathbf{B} = \frac{1}{L}\begin{bmatrix}-1 & 1\end{bmatrix} \text{ (3.2.2.13)}$$

The stiffness matrix is given by:

$$\boldsymbol{K} = \frac{EA}{L^2}\int_{-1}^{1}\begin{bmatrix}-1\\1\end{bmatrix}\begin{bmatrix}-1 & 1\end{bmatrix} J d\xi \text{ (3.2.2.14)}$$

Where J is the jacobian, that relates the length of the element in the global coordinate system into the corresponding length in the natural system.

$$\frac{dX}{d\xi} = J = \frac{L}{2} \text{ (3.2.2.15)}$$

The stiffness matrix is then given by:

$$\boldsymbol{K} = \frac{EA}{2L}\int_{-1}^{1}\begin{bmatrix}1 & -1\\-1 & 1\end{bmatrix} dr = \frac{EA}{L}\begin{bmatrix}1 & -1\\-1 & 1\end{bmatrix} \text{ (3.2.2.16)}$$

Isoparametric eight node Element

The solution for finite elements, based on displacement, conders the principle of virtual displacement, which assumes that in a body that is in equilibrium, for whichever virtual (small) displacement, nulled for the corresponding actual displacement, imposed to the balanced body, the internal virtual work is equal to the total external virtual work.

The integral expression of equilibrium of loads in elasticity problems can be obtained through the principal of virtual work:

$$\int_{\Omega} \{\delta\boldsymbol{\varepsilon}\}^T \{\mathbf{t}\}\, d\Omega - \int_{\Omega} \{\delta\mathbf{u}\}^T \{\mathbf{b}\}\, d\Omega - \int_{S_t} \{\delta\mathbf{u}\}^T \{\mathbf{t}_s\}\, dS_t = 0 \quad (3.2.2.17)$$

Where t represents the stress vector, b is the mass forces vecto, t_s is the boundary forces vector, δu is the virtual displacement vector, δε is the virtual deformation vector, Ω is the domain and S_t part of the boundary where loads are applied.

The virtual deformation associated to the previous equation is represented by:

$$\delta\boldsymbol{\varepsilon}\left\{\frac{\partial(\delta u)}{\partial x}, \frac{\partial(\delta v)}{\partial y}, \frac{\partial(\delta w)}{\partial z}, \frac{\partial(\delta u)}{\partial y} + \frac{\partial(\delta v)}{\partial x}, \frac{\partial(\delta u)}{\partial z} + \frac{\partial(\delta w)}{\partial x}, \frac{\partial(\delta v)}{\partial z} + \frac{\partial(\delta w)}{\partial y}\right\}^T$$

(3.2.2.18)

The displacement, deformation and corresponding virtual terms are:

$$\delta\mathbf{u} = \sum_{i=1}^{n} N_i \delta d_i \quad (3.2.2.19)$$

$$\delta\boldsymbol{\varepsilon} = \sum_{i=1}^{n} B_i \delta d_i \quad (3.2.2.20)$$

Which represents carachteristcs of node I, being d_i the component of the nodal displacement vector, δd_i the virtual nodal displacement vector, N_i is the component of the shape functions matrix, B_i is the component of the global displacement/deformation matrix and n is the total number of nodes of the element.

Replacing the two latest equations on the Virtual Work equation:

$$\sum_{i=1}^{n} \{\delta d_i\}^T \left\{ \int_{\Omega} [B_i]^T \boldsymbol{t} d\Omega - \int_{\Omega} [N_i]^T \boldsymbol{b} d\Omega - \int_{S_t} [N_i]^T \boldsymbol{t}_S dS_t \right\} = 0 \quad (3.2.2.21)$$

Considering the equation as valid for any virtual displacement, the following equation for each node is obtained:

$$\int_{\Omega} \boldsymbol{B}^T \boldsymbol{t} d\Omega - \int_{\Omega} \boldsymbol{N}^T \boldsymbol{b} d\Omega - \int_{S_t} \boldsymbol{N}^T \boldsymbol{t}_S dS_t = 0 \quad (3.2.2.22)$$

The nodal displacement can be expressed through shape functions according to the following expression:

$$\boldsymbol{d}^e = \sum_{i=1}^{n} N_i^e d_i^e \quad (3.2.2.23)$$

Coordinates x, y and z of any point, of an element of nodes, is expressed under the isoparametric form, generically defined, for a three-dimensional situation is given by:

$$\begin{bmatrix} x^e \\ y^e \\ z^e \end{bmatrix} = \sum_{i=1}^{r} \begin{bmatrix} N_i^e & 0 & 0 \\ 0 & N_i^e & 0 \\ 0 & 0 & N_i^e \end{bmatrix} \quad (3.2.2.24)$$

The jacobian matrix of the transformation of natural into Cartesian coordinates is defined as follows:

$$\mathbf{J}^e = \begin{bmatrix} \frac{\partial x}{\partial \xi} & \frac{\partial y}{\partial \xi} & \frac{\partial z}{\partial \xi} \\ \frac{\partial x}{\partial \eta} & \frac{\partial y}{\partial \eta} & \frac{\partial z}{\partial \eta} \\ \frac{\partial x}{\partial \zeta} & \frac{\partial y}{\partial \zeta} & \frac{\partial z}{\partial \zeta} \end{bmatrix} = \begin{bmatrix} \sum_{i=1}^{r} \frac{\partial N_i^e}{\partial \xi} x_i^e & \sum_{i=1}^{r} \frac{\partial N_i^e}{\partial \xi} y_i^e & \sum_{i=1}^{r} \frac{\partial N_i^e}{\partial \xi} z_i^e \\ \sum_{i=1}^{r} \frac{\partial N_i^e}{\partial \eta} x_i^e & \sum_{i=1}^{r} \frac{\partial N_i^e}{\partial \eta} y_i^e & \sum_{i=1}^{r} \frac{\partial N_i^e}{\partial \eta} z_i^e \\ \sum_{i=1}^{r} \frac{\partial N_i^e}{\partial \zeta} x_i^e & \sum_{i=1}^{r} \frac{\partial N_i^e}{\partial \zeta} y_i^e & \sum_{i=1}^{r} \frac{\partial N_i^e}{\partial \zeta} z_i^e \end{bmatrix} \quad (3.2.2.25)$$

The Jacobian's inverse, J, is given by:

$$\left[\mathbf{J}^e\right]^{-1} \begin{bmatrix} \frac{\partial \xi}{\partial x} & \frac{\partial \eta}{\partial x} & \frac{\partial \zeta}{\partial x} \\ \frac{\partial \xi}{\partial y} & \frac{\partial \eta}{\partial y} & \frac{\partial \zeta}{\partial y} \\ \frac{\partial \xi}{\partial z} & \frac{\partial \eta}{\partial z} & \frac{\partial \zeta}{\partial z} \end{bmatrix} = \frac{1}{\det \mathbf{J}^e} \begin{bmatrix} \frac{\partial z}{\partial \eta} & \frac{\partial z}{\partial \xi} & \frac{\partial z}{\partial \zeta} \\ \frac{\partial y}{\partial \eta} & \frac{\partial y}{\partial \xi} & \frac{\partial y}{\partial \zeta} \\ \frac{\partial x}{\partial \eta} & \frac{\partial x}{\partial \xi} & \frac{\partial x}{\partial \zeta} \end{bmatrix} \quad (3.2.2.26)$$

The deformation field is related to the displacement field as follows:

$$\boldsymbol{\varepsilon}^e = \sum_{i=1}^{n} B_i^e d_i^e \quad (3.2.2.27)$$

B_i is the deformation matrix, and is given by:

$$\left[B_i\right]^e = \begin{bmatrix} \left(\frac{\partial N_i}{\partial x}\right)^e & 0 & 0 \\ 0 & \left(\frac{\partial N_i}{\partial y}\right)^e & 0 \\ 0 & 0 & \left(\frac{\partial N_i}{\partial z}\right)^e \\ \left(\frac{\partial N_i}{\partial y}\right)^e & \left(\frac{\partial N_i}{\partial x}\right)^e & 0 \\ \left(\frac{\partial N_i}{\partial z}\right)^e & 0 & \left(\frac{\partial N_i}{\partial x}\right)^e \\ 0 & \left(\frac{\partial N_i}{\partial z}\right)^e & \left(\frac{\partial N_i}{\partial y}\right)^e \end{bmatrix} \quad (3.2.2.28)$$

In the case of three-dimensional elements, the integral is given as:

$$d\Omega^e = \det \mathbf{J}^e d\xi d\eta d\zeta \quad (3.2.2.29)$$

The stress-deformation linear relation for every element is:

$$\boldsymbol{\sigma}^e = \boldsymbol{D}^e \boldsymbol{\varepsilon}^e = \left[\boldsymbol{D}^e\right]\left(\sum_{j=1}^{n} B_j{}^e d_j{}^e\right) \quad (3.2.2.30)$$

Picking again the following expression:

$$\int_{\Omega} \boldsymbol{B}^T \boldsymbol{t} d\Omega - \int_{\Omega} \boldsymbol{N}^T \boldsymbol{b} d\Omega - \int_{S_t} \boldsymbol{N}^T \boldsymbol{t}_S dS_t = 0 \quad (3.2.2.31)$$

The first term of this equation results in the combination of each element through the following expression:

$$\sum_{j=1}^{r} K_{ij}{}^e d_j{}^e = \int_{\Omega^e} \left[B_i{}^e\right]^T \left[\boldsymbol{D}^e\right]\left(\sum_{j=1}^{r} B_j{}^e d_j{}^e\right) d\Omega^e \quad (3.2.2.32)$$

Where K_{ij} is a sub-matrix of the elemental stiffness matrix K.

The contribution to each element of the second term of the same expression is given by:

$$\boldsymbol{f}_{bi}{}^e = \int_{\Omega^e} \left[N_i{}^e\right]^T \left\{\boldsymbol{b}^e\right\} d\Omega^e \quad (3.2.2.33)$$

For the third term of the same equation, the elemental contribution of the force vector is given by:

$$\boldsymbol{f}_{t_i}{}^{e} = \int_{S_t} \left[N_i{}^{e} \right]^T \left\{ \boldsymbol{t}_S{}^{e} \right\} dS_t \quad (3.2.2.34)$$

The stiffness matrix K_{ij} is determined numerically and is obtained through integration in natural coordinates.

$$K_{ij}{}^{e} = \int_{-1}^{1}\int_{-1}^{1}\int_{-1}^{1} \left[B_i^{e} \right]^T \left[\boldsymbol{D}^{e} \right] \left[\left[B_j^{e} \right] \right] det\, \boldsymbol{J}^{e} d\xi d\eta d\zeta = \int_{-1}^{1}\int_{-1}^{1}\int_{-1}^{1} T_{ij}{}^{e} d\xi d\eta d\zeta \quad (3.2.2.35)$$

The numeric integration follows Gauss Rule, being programmed for 2x2x2 or 3x3x3 (in 3D structures) Gauss integration points.

Naming K_{ij} the integrating function of the previous equation, the matrix develops numerically:

$$K_{ij}{}^{e} = \sum_{p=1}^{n}\sum_{q=1}^{n}\sum_{r=1}^{n} T\left(\bar{\xi}_P, \bar{\eta}_q, \bar{\zeta}_r \right)_{p,q,r} W_p W_q W_r \quad (3.2.2.36)$$

Where W_p, W_q and W_r represent respectively the rule's weight factors and the coordinates of the respective specific point.

An essential step on any finite element based calculation is the determination of the finite elements matrixes, among others, the stiffness matrix, the mass matrix or the equivalent nodal loads vector equivalent to the exterior loads.

The basic idea of the isoparametric finite elements is that the relation between the displacement in the interior of the element and the nodal displacement can be directly established through the interpolating functions (shape functions).

In a isoparametric representation, shape functions are used to interpolate the geometry and displacement. The isoparametric formulation allows the use of irregular or curved elements. The definition of the element is made from the coordinates in its actual geometry, to approximate the calculation of all the integrals to the normalized geometry of the element.

The main characteristics of the shape functions used on finite elements are their continuity interior to the element and the value those functions can assume in determined points on its domain, as the following equations impose:

$$\sum_{i=1}^{n} N_i(\xi,\eta) = 1 \quad (3.2.2.37)$$

$$N_i(\xi,\eta) = \begin{cases} 1 \Rightarrow i = j \\ 0 \Rightarrow i \neq j \end{cases} \quad (3.2.2.38)$$

Where ξ and η represent the natural coordinates of the finite element.

The shape functions thus defined are guaranteed to be continuous in the displacement field in the element's interior, making sure of a C_0 type continuity between the neighbouring elements.

Shape functions have the following properties:

- They are unitary in the node they represent and nulled in the remainder nodes.
- They are part of a unity, which means $\sum N_i = 1$

For constant deformation elements, a possible way to generate shape functions is to define an unknown function from a polynomial expression, having as much terms as the element has nodes. Write that polynomial expression with α_i coefficients for each node of the element, inverse the obtained system and determine the polynomial coefficients.

In most finite elements it is impractical to calculate de stiffness matrix K and force vector f without resorting to numerical integration. The most commonly used method on finite elements is the Gauss integration, which can be considered in one-dimensional or two-dimensional domains.

In the case of one-dimensional domains, consider a function $f(x), x \in [-1,1]$

In the Gauss integration rule, the integral:

$$I = \int_{-1}^{1} f(x)\,dx \quad (3.2.2.39)$$

Is expressed as a sum extended to p Gauss points (in the interior of the finite element) where de function value f is multiplied in those points P, by weights as:

$$I = \int_{-1}^{1} f(x)\,dx = \sum_{i=1}^{p} f(x_i) W_i \quad (3.2.2.40)$$

Where W_i are the corresponding weights on point i.

Table 8 presents the coordinates and weights for the Gauss integration technic. Note that this integration technic, of n degree, gives an exact solution for a 2n-1 polynomial.

n	$\pm x_i$	W_i
1	0.0	2.0
2	0.5773502692	1.0
3	0.774596697 0.0	0.55555555556 0.88888888889
4	0.86113663116 0.3399810436	0.3478548451 0.6521451549

Table 8 Coordinates and weights for the Gauss integration technic (up to 4 points)

As in the numeric integration in one dimension, the objective of the two dimensions numerical integration is the solution of the stiffness matrix, nodal equivalent forces vector and mass matrix integration, through the Gauss method.

The integral to a function in natural coordinates can be replaced by two sums containing the products of the Gauss weights and function in the respective Gauss points, by:

$$\int_{-1}^{1}\int_{-1}^{1} F(\xi,\eta)\,d\xi d\eta = \sum_{i=1}^{p}\sum_{j=1}^{q} w_i w_j F(\xi_i \eta_j) \quad (3.2.2.41)$$

Where p and q are the number of points in the ξ and η respectively and w_i and w_j their weights.

In particular for the stiffness matrix it is possible to determine the integral as follows:

$$\boldsymbol{K}^e = \int_{\Omega} h\boldsymbol{B}^T\boldsymbol{C}\boldsymbol{B}d\Omega^e = \int_{-1}^{1}\int_{-1}^{1} h\boldsymbol{B}^T\boldsymbol{C}\boldsymbol{B}det\mathbf{J}d\xi d\eta \quad (3.2.2.42)$$

Where h represents the thickness of the element.

Tetrahedral four node Element

On three dimension problems, the simpler continuous elements is a tetrahedral, a four node element.

The characteristics of a tetrahedral element can be defined as displacement functions, deformation, stiffness, stress and load matrixes.

In the finite element analysis, the body is approximated to a set of discrete finite elements connected at the boundaries of each element by nodal points. The displacement measured in the local x, y, z coordinate system at each point is assumed to be a function of the displacement in n points of the element.

Given a tetrahedral i, j, m, p in a space defined by x, y, z coordinates (Figure 28), the displacement state in a point is defined by the three displacement components u, v, w in the x, y, z coordinate directions.

Henceforth:

$$u = \begin{Bmatrix} u \\ v \\ w \end{Bmatrix} \quad (3.2.2.43)$$

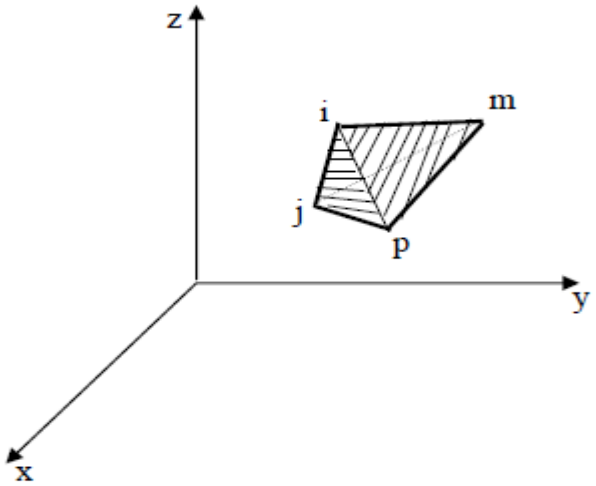

Figure 28 Tetrahedral's volume (13)

The linear variation is defined by four nodal values, being written only u (for simplification purposes) in the following way:

$$\boldsymbol{u} = \alpha_1 + \alpha_2 X + \alpha_3 Y + \alpha_4 Z \quad (3.2.2.44)$$

This equation can be presented in the form of four equations:

$$\begin{aligned} u_i &= \alpha_1 + \alpha_2 X_i + \alpha_3 Y_i + \alpha_4 Z_i \\ u_j &= \alpha_1 + \alpha_2 X_j + \alpha_3 Y_j + \alpha_4 Z_j \\ u_m &= \alpha_1 + \alpha_2 X_m + \alpha_3 Y_m + \alpha_4 Z_m \\ u_p &= \alpha_1 + \alpha_2 X_P + \alpha_3 Y_P + \alpha_4 Z_p \end{aligned} \quad (3.2.2.45)$$

Where α_1, α_2, α_3 and α_4 must be calculated.

It's possible to write the solution, using the determinant form, which means:

$$\boldsymbol{u} = \frac{1}{6V}\begin{bmatrix} (a_i + b_i X + c_i Y + d_i Z)u_i + (a_j + b_j X + c_j Y + d_j Z) + \\ (a_m + b_m X + c_m Y + d_m Z)u_m + (a_p + b_p X + c_p Y + d_p Z)u_p \end{bmatrix} \quad (3.2.2.46)$$

With

$$6V = det\begin{vmatrix} 1 & X_i & X_i & X_i \\ 1 & X_j & X_j & X_j \\ 1 & X_m & X_m & X_m \\ 1 & X_p & X_p & X_p \end{vmatrix} \quad (3.2.2.47)$$

Where V represents the volume of the tetrahedral. Expanding the other relevant determinants in their co-factors, gives:

$$\begin{aligned} a_i &= det\begin{vmatrix} X_j & Y_j & Z_j \\ X_m & Y_m & Z_m \\ X_p & Y_p & Z_p \end{vmatrix} \quad b_i = -det\begin{vmatrix} 1 & Y_j & Z_j \\ 1 & Y_m & Z_m \\ 1 & Y_p & Z_p \end{vmatrix} \\ c_i &= -det\begin{vmatrix} X_j & 1 & Z_j \\ X_m & 1 & Z_m \\ X_p & 1 & Z_p \end{vmatrix} \quad d_i = -det\begin{vmatrix} X_j & Y_j & 1 \\ X_m & Y_m & 1 \\ X_p & Y_p & 1 \end{vmatrix} \end{aligned} \quad (3.2.2.48)$$

The element's displacement is defined by 12 displacement components in the nodes as:

$$\boldsymbol{d}^e = \begin{Bmatrix} \boldsymbol{a}_i \\ \boldsymbol{a}_j \\ \boldsymbol{a}_m \\ \boldsymbol{a}_p \end{Bmatrix} \quad (3.2.2.49)$$

With

$$\boldsymbol{a}_i = \begin{Bmatrix} u_i \\ v_i \\ w_i \end{Bmatrix} \quad \boldsymbol{a}_j = \begin{Bmatrix} u_j \\ v_j \\ w_j \end{Bmatrix} \quad \boldsymbol{a}_m = \begin{Bmatrix} u_m \\ v_m \\ w_m \end{Bmatrix} \quad \boldsymbol{a}_p = \begin{Bmatrix} u_p \\ v_p \\ w_p \end{Bmatrix} \quad (3.2.2.50)$$

The displacement in any point can be given by:

$$\boldsymbol{u} = \left[\boldsymbol{I}N_i, \boldsymbol{I}N_j, \boldsymbol{I}N_m, \boldsymbol{I}N_p \right] \boldsymbol{a}^e \quad (3.2.2.51)$$

Where the shape functions are defined as follows:

$$\begin{aligned} N_i &= \frac{a_i + b_i X + c_i Y + d_i Z}{6V} \\ N_j &= \frac{a_j + b_j X + c_j Y + d_j Z}{6V} \\ N_m &= \frac{a_m + b_m X + c_m Y + d_m Z}{6V} \\ N_p &= \frac{a_p + b_p X + c_p Y + d_p Z}{6V} \end{aligned} \quad (3.2.2.52)$$

Where I represents the 3x3 identity matrix.

The deformation is obtained by deriving the displacement. This way, in a three-dimensional analysis there are six relevant deformation components, defined as:

$$\boldsymbol{\varepsilon} = \begin{Bmatrix} \varepsilon_x \\ \varepsilon_y \\ \varepsilon_z \\ \gamma_{xy} \\ \gamma_{yz} \\ \gamma_{zx} \end{Bmatrix} = \begin{Bmatrix} \dfrac{\partial u}{\partial X} \\ \dfrac{\partial v}{\partial Y} \\ \dfrac{\partial w}{\partial Z} \\ \dfrac{\partial u}{\partial Y} + \dfrac{\partial v}{\partial X} \\ \dfrac{\partial v}{\partial Z} + \dfrac{\partial w}{\partial Y} \\ \dfrac{\partial w}{\partial X} + \dfrac{\partial u}{\partial Z} \end{Bmatrix} \quad (3.2.2.53)$$

Given the following equations again:

$$\boldsymbol{u} = \frac{1}{6V} \begin{bmatrix} \left(a_i + b_i X + c_i Y + d_i Z\right) u_i + \left(a_j + b_j X + c_j Y + d_j Z\right) + \\ \left(a_m + b_m X + c_m Y + d_m Z\right) u_m + \left(a_p + b_p X + c_p Y + d_p Z\right) u_p \end{bmatrix} \quad (3.2.2.46)$$

And

$$\boldsymbol{u} = \left[\boldsymbol{I}N_i, \boldsymbol{I}N_j, \boldsymbol{I}N_m, \boldsymbol{I}N_p \right] \boldsymbol{a}^e \quad (3.2.2.51)$$

It is verified that:

$$\boldsymbol{\varepsilon} = \boldsymbol{B} a^e \left[\boldsymbol{B}_i, \boldsymbol{B}_j, \boldsymbol{B}_m, \boldsymbol{B}_P \right] \boldsymbol{a}^e \quad (3.2.2.54)$$

Where:

$$\boldsymbol{B}_i = \begin{bmatrix} \frac{\partial N_i}{\partial X} & 0 & 0 \\ 0 & \frac{\partial N_i}{\partial Y} & 0 \\ 0 & 0 & \frac{\partial N_i}{\partial Z} \\ \frac{\partial N_i}{\partial Y} & \frac{\partial N_i}{\partial X} & 0 \\ 0 & \frac{\partial N_i}{\partial Z} & \frac{\partial N_i}{\partial Y} \\ \frac{\partial N_i}{\partial Z} & 0 & \frac{\partial N_i}{\partial X} \end{bmatrix} = \frac{1}{6V} \begin{bmatrix} b_i & 0 & 0 \\ 0 & c_i & 0 \\ 0 & 0 & d_i \\ c_i & b_i & 0 \\ 0 & d_i & c_i \\ d_i & 0 & b_i \end{bmatrix} \quad (3.2.2.55)$$

Sub-matrixes B_j, B_m and B_p are obtained in a similar fashion.

For an isotropic material, with elasticity matrix D, the relation between the stress and the deformation is given by:

$$\boldsymbol{\sigma} = \boldsymbol{D}\boldsymbol{\varepsilon} \quad (3.2.2.56)$$

Where

$$\boldsymbol{\sigma} = \begin{Bmatrix} \boldsymbol{\sigma}_x \\ \boldsymbol{\sigma}_y \\ \boldsymbol{\sigma}_z \\ \tau_{xy} \\ \tau_{yz} \\ \tau_{zx} \end{Bmatrix} = \boldsymbol{D}\left(\boldsymbol{\varepsilon} - \boldsymbol{\varepsilon}_0\right) + \boldsymbol{\sigma}_0 \quad (3.2.2.57)$$

Where σ_x, σ_y and σ_z represent the normal stresses and τ_{xy}, τ_{yz} and τ_{zx} the shear stresses.

The elastic constants matrix D, for the three-dimensional state, is a function of E, which represents the elasticity modulus and ν which is the Poisson Coefficient.

$$\boldsymbol{D} = \frac{E}{(1+\nu)(1-2\nu)} \begin{bmatrix} 1-\nu & \nu & \nu & 0 & 0 & 0 \\ \nu & 1-\nu & \nu & 0 & 0 & 0 \\ \nu & \nu & 1-\nu & 0 & 0 & 0 \\ 0 & 0 & 0 & 0,5-\nu & 0 & 0 \\ 0 & 0 & 0 & 0 & 0,5-\nu & 0 \\ 0 & 0 & 0 & 0 & 0 & 0,5-\nu \end{bmatrix} \quad (3.2.2.58)$$

In the finite element solution, the equilibrium equations are not exactly satisfied in every considered point, existing two properties that are satisfied for any finite element mesh. The first property refers to the node equilibrium, while the second refers to element equilibrium.

Considering that in each finite element e the nodal force vectors are given by:

$$\boldsymbol{f}^{e} = \int_{V^e} \boldsymbol{B}^{e^T} \boldsymbol{\sigma}^{e} dV^{e} \quad (3.2.2.59)$$

Where $\boldsymbol{\sigma}^{e} = \boldsymbol{D}^{e}\boldsymbol{\varepsilon}^{e}$

According to the first property, in each node, the sum of the nodal forces is in equilibrium with the externally applied loads, given:

$$\sum_{e} \boldsymbol{f}^{e} = \boldsymbol{K}\boldsymbol{d} \quad (3.2.2.60)$$

According to the second property, each element is in equilibrium under its forces f^e. This property is satisfied, given that the interpolation matrix N^e satisfies the convergence requisites.

So, in the finite element analysis, the following conditions must be referred:

- The structure is conceived as a set of interconnected discrete nodes.
- The external loads applied are attributes to those nodes, using the virtual work principle to obtain nodal equivalent forces to the applied loads.
- The nodal equivalent forces to the external applied forces are balanced by the equivalent nodal forces to the internal stress to the element, which means:

$$\sum_{e} \boldsymbol{f}^{e} = \boldsymbol{R} \quad (3.2.2.61)$$

- The stress-deformation compatibility equations are exactly satisfied.

The stiffness matrix can be explicitly integrated, given that the deformation and stress components are constant within the element.

The general sub-matrix of the stiffness matrix is a 3x3 matrix defined as:

$$\boldsymbol{K}_{ij}^{\ e} = \boldsymbol{B}_{\boldsymbol{i}}^{T}\boldsymbol{D}\boldsymbol{B}_{j}V^{e} \quad (3.2.2.62)$$

Where V^e represents the volume of an elemental tetrahedral.

The nodal forces due to the initial deformation lead to $\boldsymbol{f}_i^e = -\boldsymbol{B}_i^T \boldsymbol{D}\boldsymbol{\varepsilon}_0 V^e$ (3.2.2.63).

3.2.2.3. Contact Formulation

FEM software ABAQUS (ABAQUS Analysis User's Manual, 2005) allows for the use of two methods to model interactions between bodies: using surfaces or contact elements. For this project, the contact between surfaces of two interacting bodies' model was used.

One of the objectives of the study of the contact between deformable bodies is to assess the evolution of the stresses throughout the bodies, as to determine their wear and this way optimize the development process. (Wriggers, 2002) For the contact model, it's necessary to define the surfaces that might be in contact, specifying the pairs of surfaces that contact one another, as to define the respective mechanical properties.

Kinematic Considerations

The contact model intends to describe the interference between two bodies through a period of time. (Cardoso, 1998) Given a point P on the surface of a body A, for the analysis of contact, and F, the point of a body B, that gets closer to P (Figure 29). If n, a vector normal to body A's surface, in the point F, the local curved axis system is represented from n and the directional coordinate ξ, defined from an initial point in body A's surface, F_0. The local Cartesian axis system is represented by the normal vector n and the vector tangent to body A's surface, t, on point F (Figure 29).

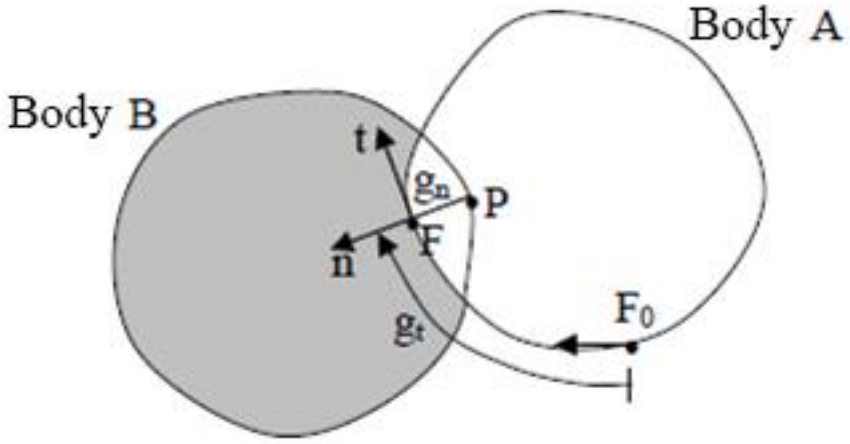

Figure 29 Kinematic Variables (14)

The kinematic in the modeling of the contact are described in a local referential associated to the geometric entities that constitute the definition of body A.

To establish an order in the vectors' orientations and to define the local referentials, it's necessary to order the geometrical entities of body A in the counter-clockwise direction, for compatibility in the numbering of the elements' nodes.

The first kinematic variables to be introduced are the normal displacement, g_n and the tangential displacement, g_t, associated to a point in body B's surface. (Cardoso, 1998)

If the current position for the node P is defined as:

$$x_P = X_P + u_P \quad (3.2.2.64)$$

Where u_p represents the displacement on the node P, then the normal displacement g_t is given by:

$$g_t = g_n n \quad (3.2.2.65)$$

$$\mathbf{g}_n = \left(x_F - x_P\right).\boldsymbol{n} \quad (3.2.2.66)$$

Where x_F defines the current postion of body A, being represented as:

$$x_F = X_F + u_F \quad (3.2.2.67)$$

Where u_F is the displacement of body A.

The tangential displacement in the curved axis system is defined as:

$$\mathbf{g}_t = \mathrm{g}_t \boldsymbol{t} \quad (3.2.2.68)$$

$$\mathrm{g}_t = \int_{F_0}^{F} d\Gamma_F = \xi\left(x_F\right) - \xi\left(x_F\right) \quad (3.2.2.69)$$

Contact Algorithm

The contact algorithm, presented in Figure 31 was conceived using the Newton-Raphson technic. (Roriz, 2015) ABAQUS uses a master-slave contact algorithm, where the nodes of a surface (slave) cannot penetrate the segments that constitute the other surface (master). The algorithm does not impose restrictions to the master surface, being this able to penetrate the slave surface, between its nodes (Figure 30). The consequence of this formulation demands for an appropriate selection of the respective surfaces, to guarantee the best contact simulation possible. One rule dictates that the slave surface must be the body with the most refined mesh, but if the mesh density is similar, the slave surface must correspond to the least rigid material.

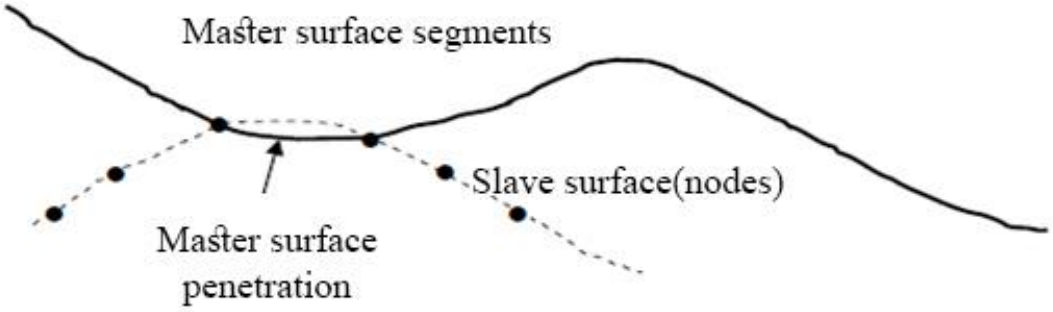

Figure 30 The master surface can penetrate the slave surface (15)

When using small-sliding formulation, ABAQUS establishes a relation between the slave nodes and the master surfaces in the beginning of the simulation, determining that the segment in the master surface establishes contact with each node in the slave surface. This relation is kept through all the analysis, without changing the surfaces they integrate.

If included in the model, non-linear geometries, the small-sliding algorithm considers any rotation and deformation of the master surface, updating the transmitted loads. If non-linear geometries are not included, the rotations and deformations are ignored, staying the loads fixed.

ABAQUS examines the state of all the contact interactions in the beginning of every increment, to verify if the slave nodes are penetrated or not. In Figure 31, p refers to the contact pressure in the slave node and h is the penetration of a single slave node in the master surface. If the node penetrates, the software determines the restriction for unpenetrated nodes. The software concludes the iteration and updates the model configuration for the calculated corrections.

Before verifying the forces or moments equilibrium, the software first checks the changes in the contact conditions in the slave nodes. Any node that is negative or nulled at the end of each iteration changes from a non-penetrated state to penetrated state. Any node whose contact pressure becomes negative changes its state from penetrated to non-penetrated. If any alteration is detected in the current iteration, the software will label it “severe discontinuity iteration” and the equilibrium verification is not concluded.

The program will modify its contact restrictions to reflect the change of contact state after the first iteration and attempts the second iteration. The software repeats this procedure until an iteration is complete without change to the contact state.

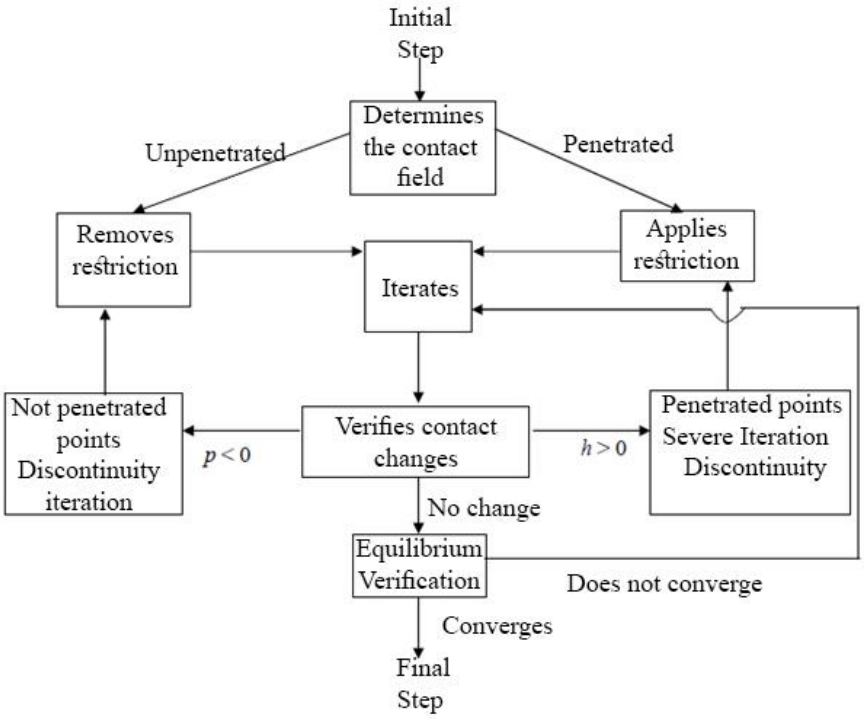

Figure 31 Contact Algorithm (13)

This iteration becomes the first equilibrium iteration and the software does a normal balance convergence verification. If the convergence fails, the software tries another iteration. Each time there is a severe discontinuity iteration, the software must set its internal balance iteration counters to zero. This iteration counter is used to determine if an increment must be abandoned due to low convergence rate. The software repeats the whole process until convergence is attained, as seen in Figure 31. (Roriz, 2015)

3.2.3. Benchmark

With the information from section 3.1.1, subsection “Floor”, it’s possible to determine the overloads and determine the term of comparison (wood; balsa in this case):

$$S_{Gk} = \rho_{balsa} \cdot A_{cross\ section} = 159.99 \cdot 0.1278^2 = 2.61 kg/m = 25.61 N/m = 0.0256\ kN/m$$

P_{balsa} is the specific weight of balsa wood in kg/m^3

$A_{cross\ section}$ is the area of the cross section of the beam, which is a 0.1278m side square

Considering *n*=4 for both cases:

$$S_d = 1.5 \cdot S_{Gk} \cdot n + 1.5 \cdot S_{Qk} = 1.5 \cdot 0.0256 \cdot 4 + 6 = 6.1536\ kN/m \quad (3.1.3.1)$$

$$S_{di} = 1.538\ kN/m$$

As the beam length, *l*, is 1440 mm, as is the LEGO® beam, the concentrated force in the centre of the beam, *F*, is:

$$F = S_{di} \cdot l = 1.538 \cdot 1.44 = 2.215\ Kn \quad (3.2.3.1)$$

Given this data, a model can be simulated in SolidWorks using the Simulation tool, as for simpler beams and standalone parts, this tool has a much more simplified interface, just introducing the geometry, mechanical properties, loads and fixtures, giving the displacement and Von Mises Stress by default.

As it is observable in Figure 32, the beam has its highest deflection at the centre, with a value of 0.3122 mm, which constitutes the benchmark value.

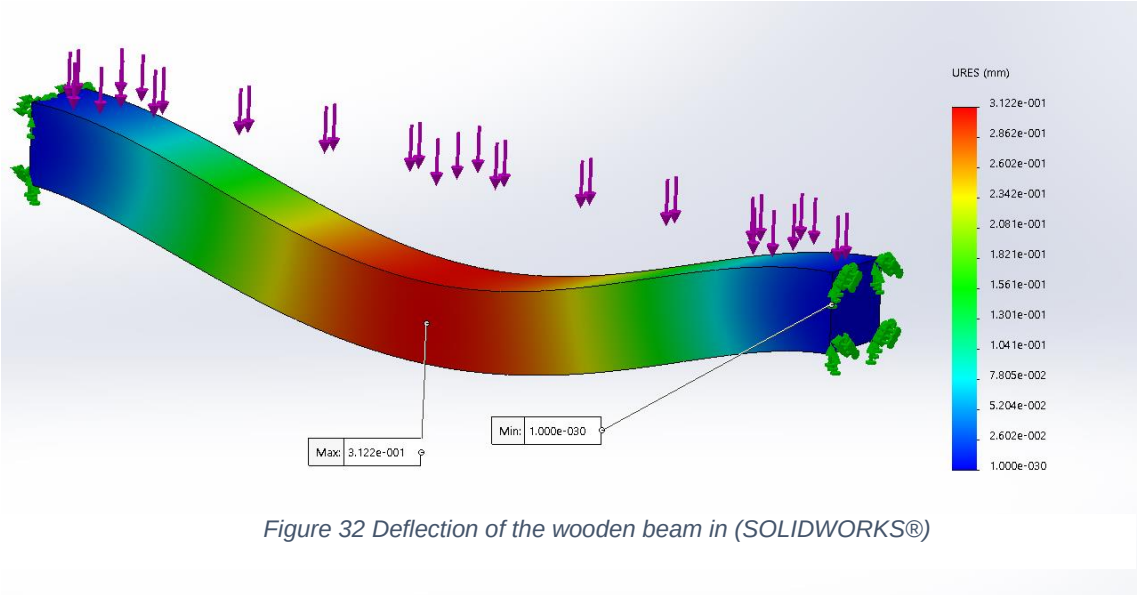

Figure 32 Deflection of the wooden beam in (SOLIDWORKS®)

Figure 33 represents the failure of the structure. If there were red spots, the beam would have failed and collapsed in those areas, but as it is blue, the beam has succeeded in the test.

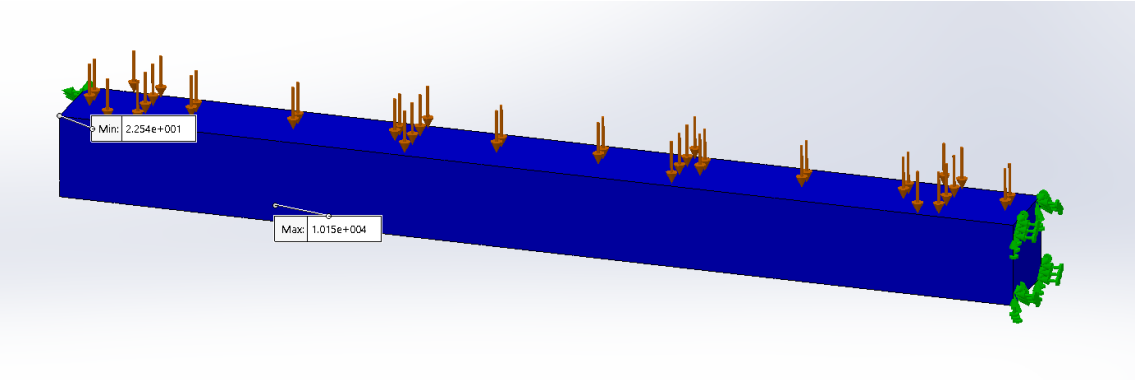

Figure 33 The von Mises Failure critireum for the wooden beam (SOLIDWORKS®)

Figure 34 shows the typical mechanical behaviour of a clamped beam. For reference, red parts are under traction and blue parts are under compression. Therefore, and looking at the figure, given a downwards applied force, the beam is seen as being under compression on the top of the central section of the beam and in the underside of the mountings and under tension in the lower part of central section and on the top of the mountings.

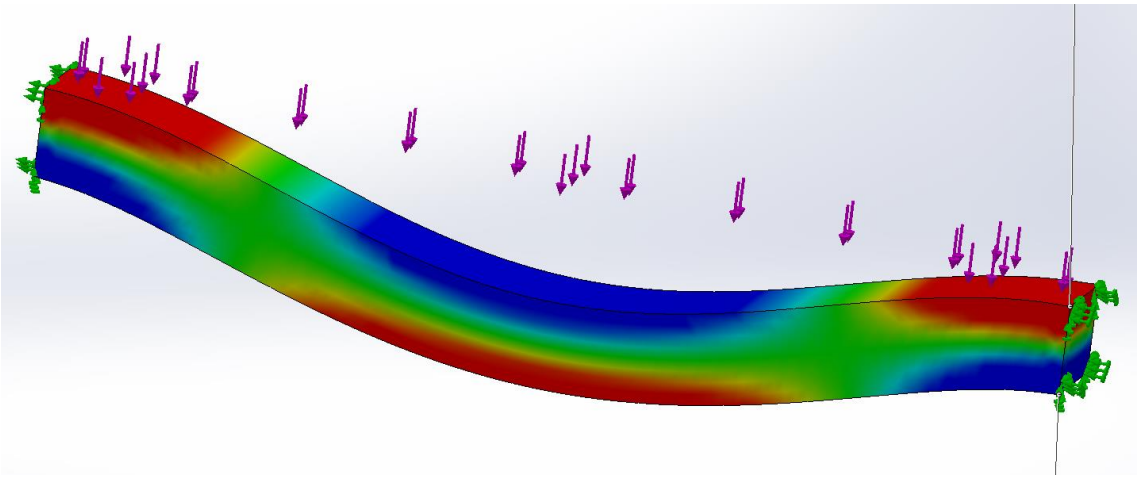

Figure 34 Distribution of normal tension on the beam (SOLIDWORKS®)

3.2.4. Simulation Preparation

3.2.4.1. Contact definition

The first step is to define the normal force exerted to the contact, with the use of Interference fit on LEGO® pieces (based on the pieces used for the beam model built in SolidWorks). The interference fit simulation was undertaken by two 2x4 bricks with all eight studs connected, as seen in Figure 36.

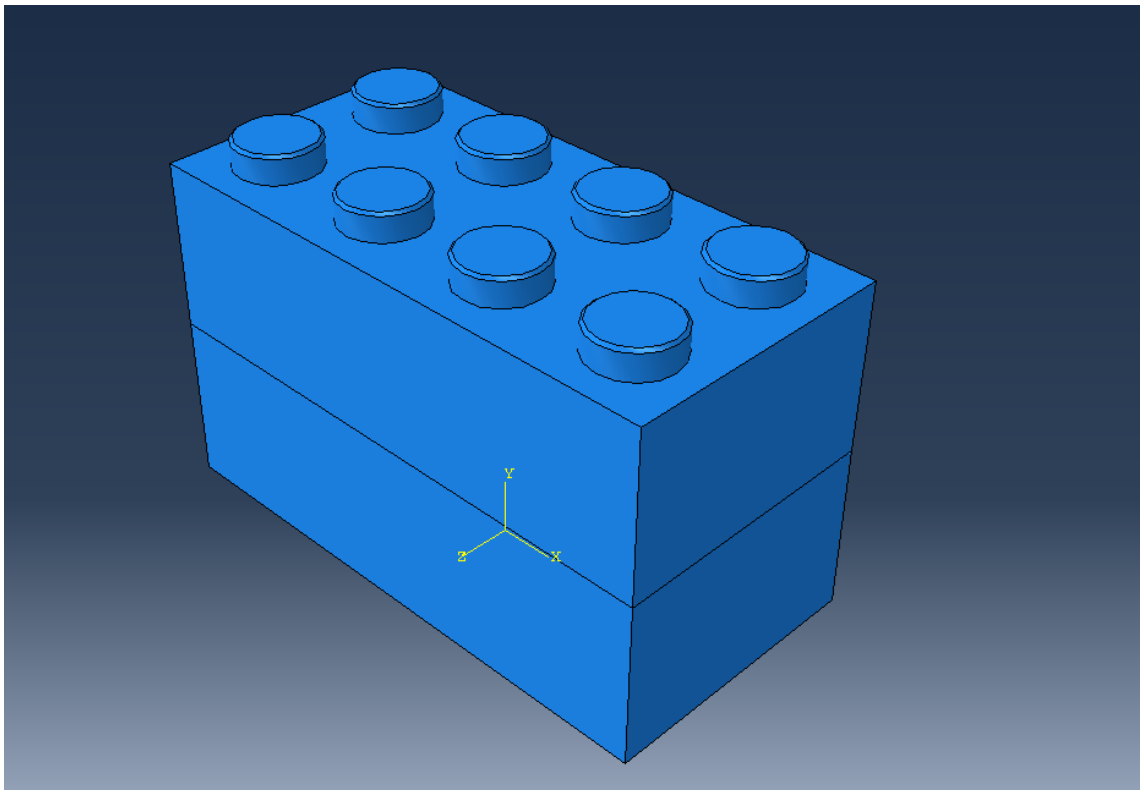

FIgure 35 Simulation assembly for the determination of the separation force per stud (ABAQUS®)

Mesh

The piece was automatically meshed in ABAQUS® using tetrahedral elements. As this is a very sensitive point of the study, this mesh had to be as refined as possible, as to guarantee that both parts have their intersecting parts effectively intersecting.

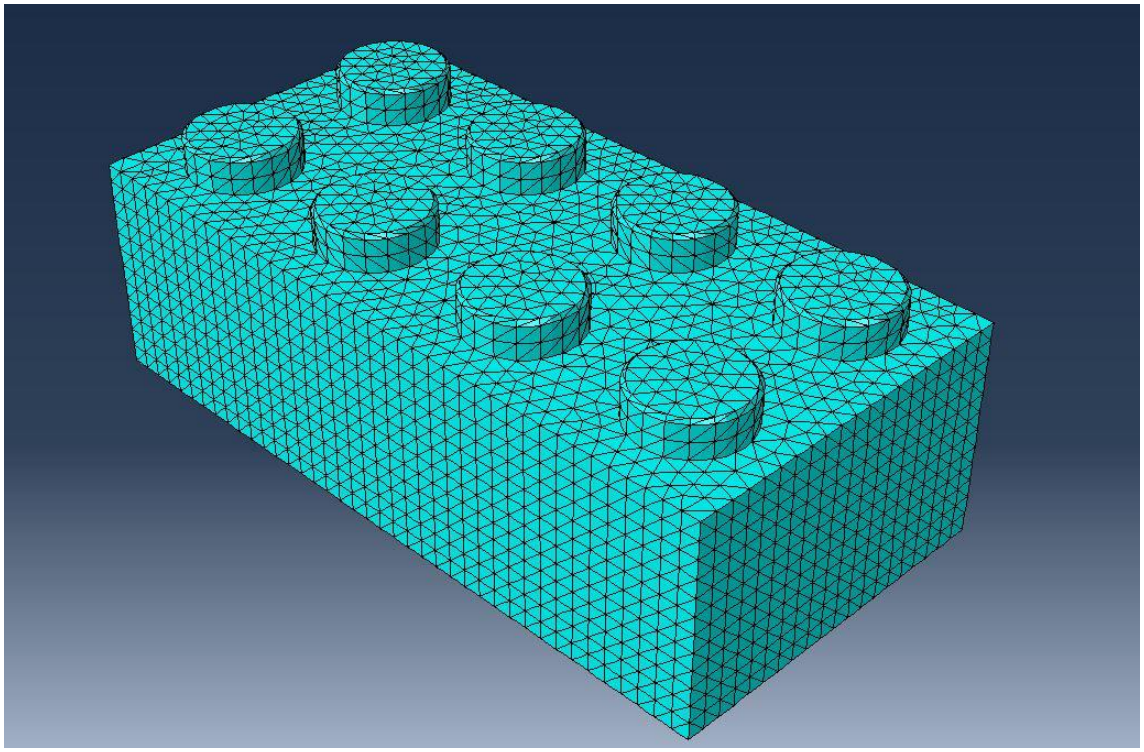

Figure 36 Meshed "Eighter" (ABAQUS®)

Step

The first step serves to eliminate the interference between the parts, while the second step defines their separation.

The initialization has to be very slow, as not to upset the interference fit.

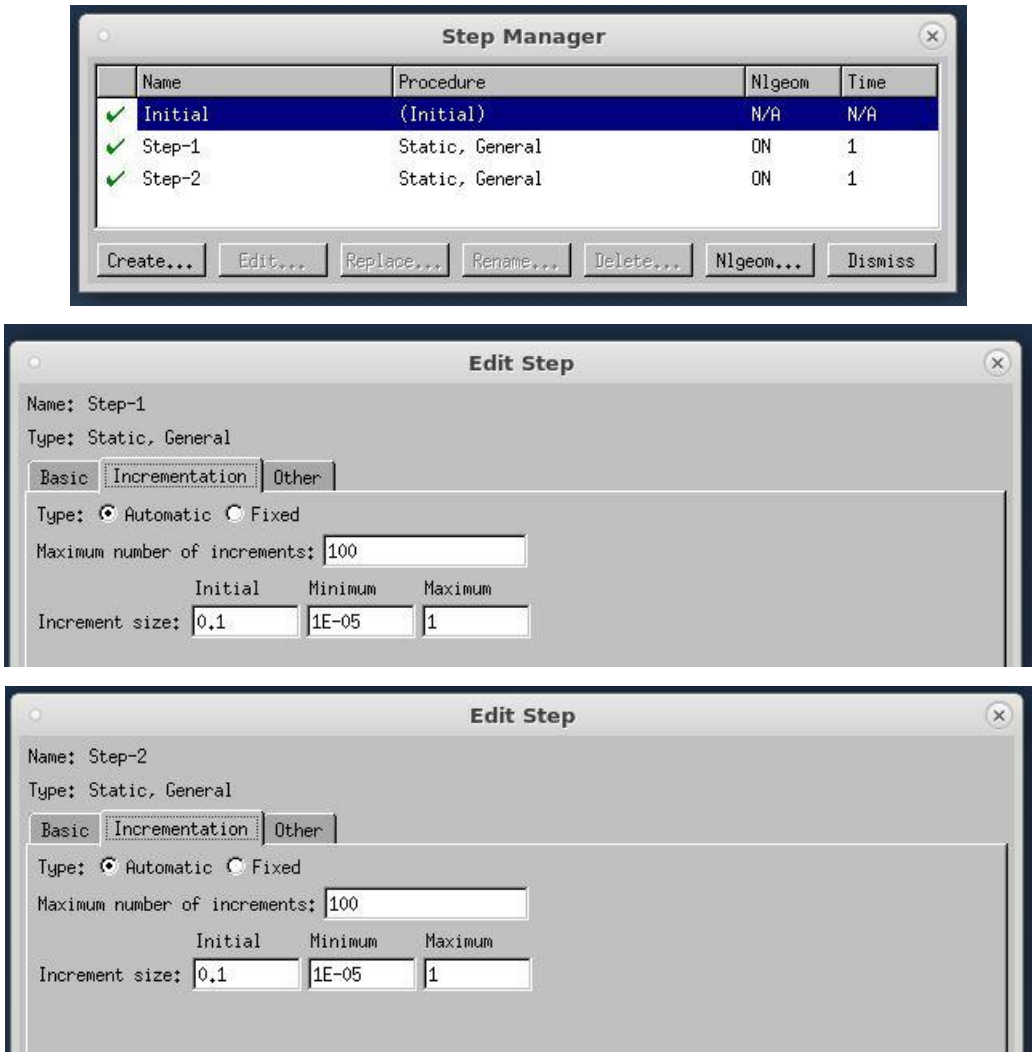

Figure 37 Steps of the Separation Simulation (ABAQUS®)

Contact

Contact between the studs and tubes/interior walls

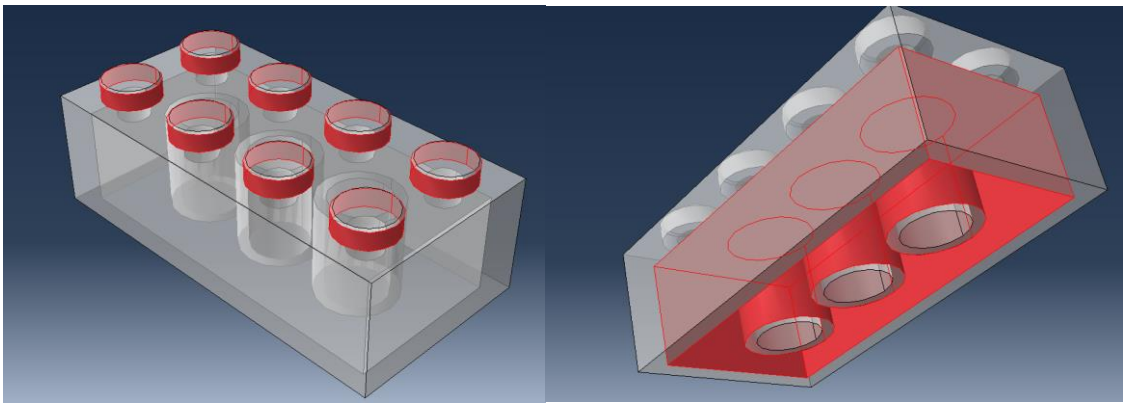

Figure 38 Highlighted contact surfaces a) studs and b) tubes and walls (ABAQUS®)

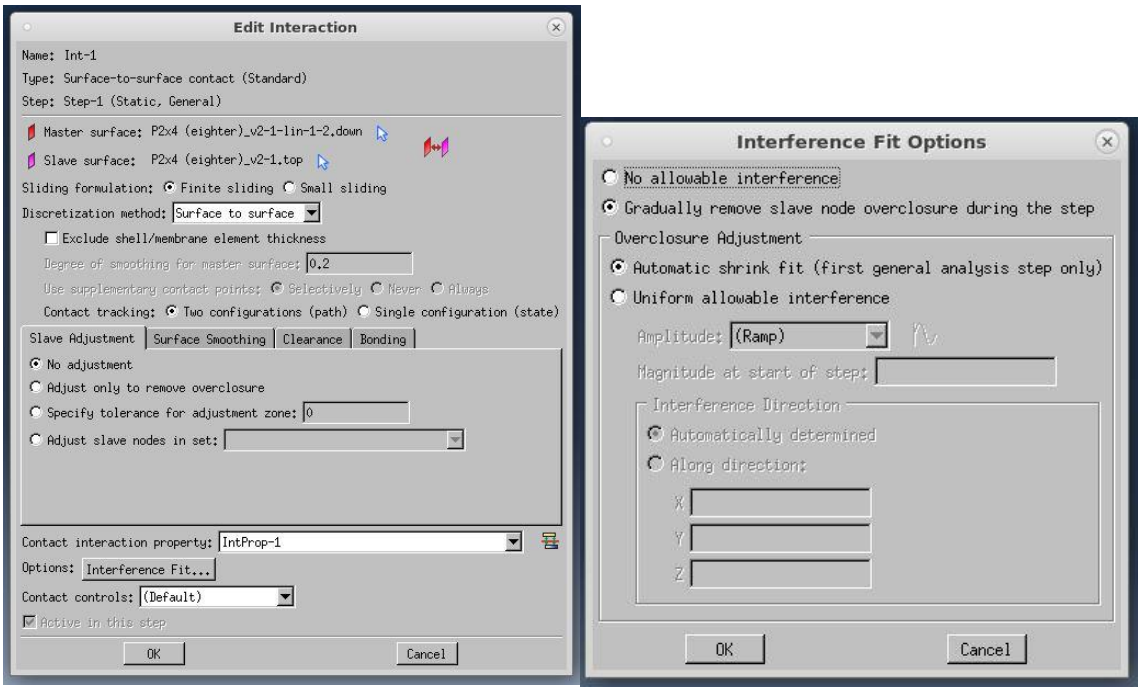

Figure 39 Definition of the interference fit (ABAQUS®)

Boundary Conditions

BC1 is defined by the region comprising the area of the base of the walls

BC2 is defined as the region comprising the area of the top of the studs

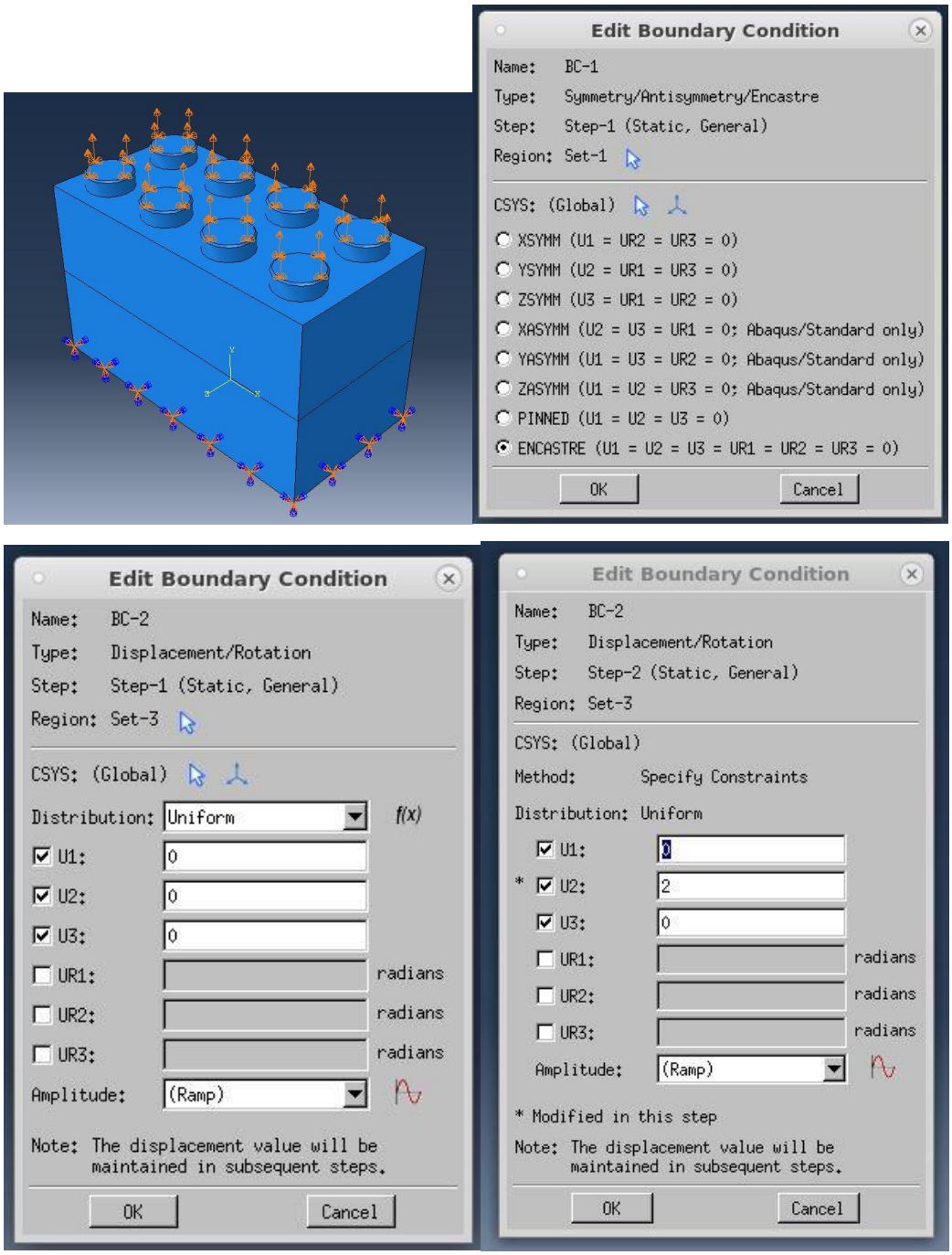

Figure 40 Boundary Conditions definition (ABAQUS®)

Results and visualization

As it is seen here, the first increment of the step has the two parts interfering where they connect (Figure 40).

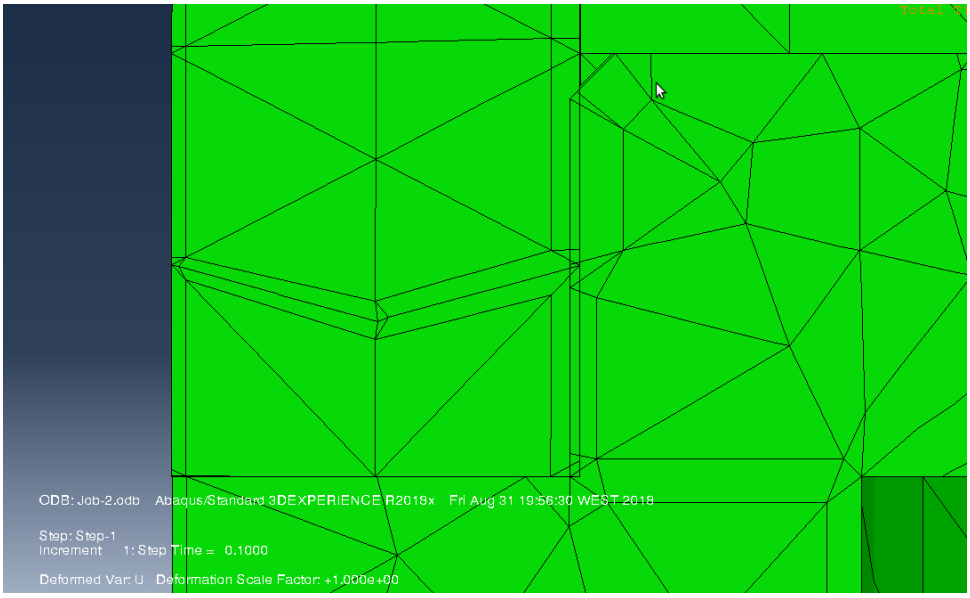

Figure 41 Connection before interference fit - step 1, increment 1(ABAQUS®)

Due to the Interference Fit Feature from ABAQUS®, it is possible to see in the last increment of this first step (Figure 41) that the parts have been adjusted to fit snugly with each other.

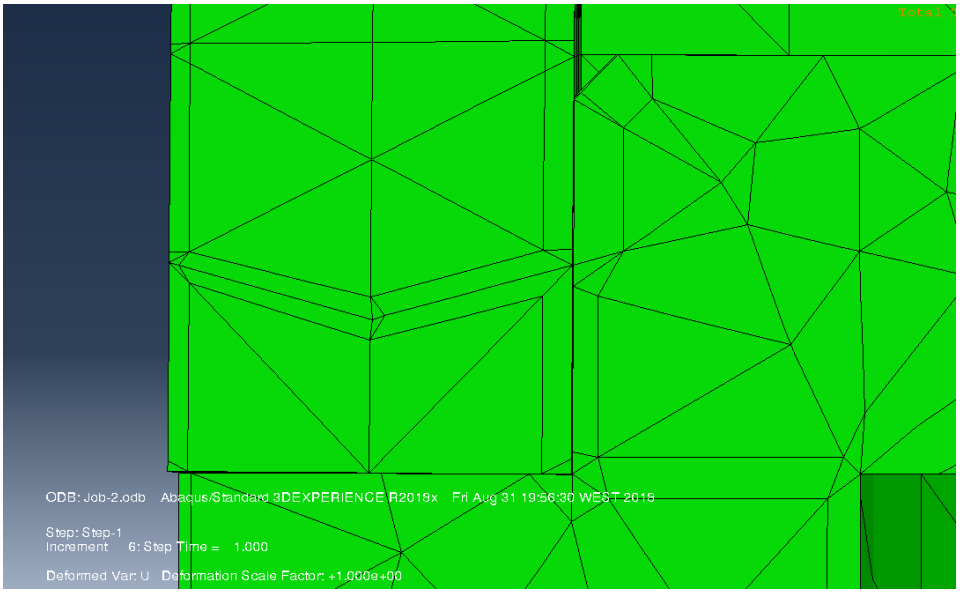

Figure 42 Connection after interference fit - step1, increment 6 (ABAQUS ®)

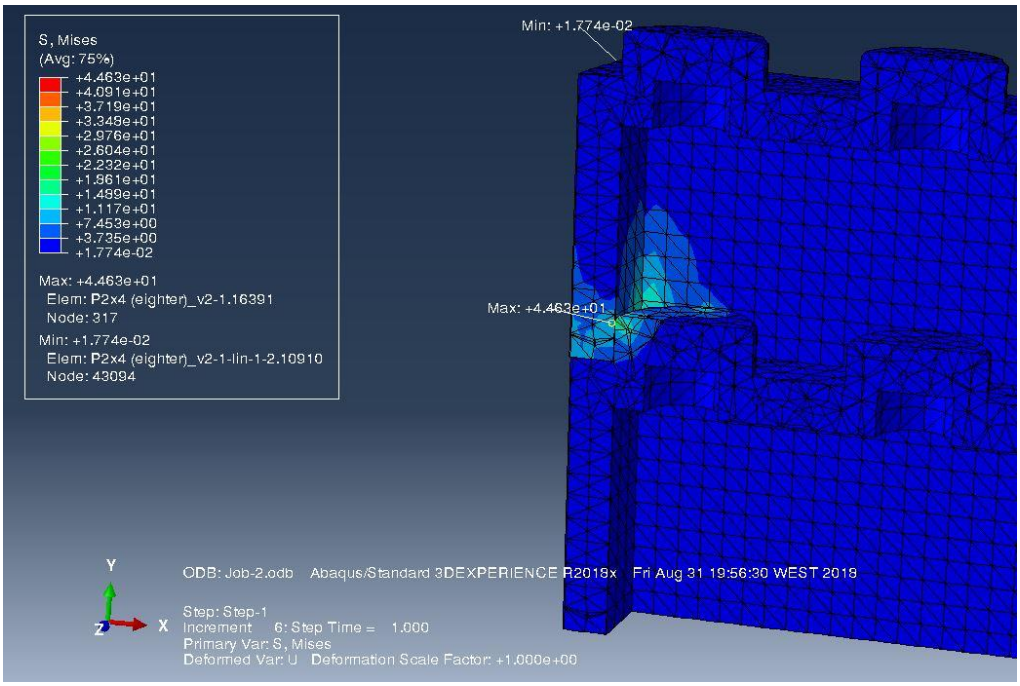

Figure 43 Highlight of Highest strained area (ABAQUS®)

Maximum Von Mises Stress: 44.63 MPa < 45 MPa (almost on elastic limit of the material)

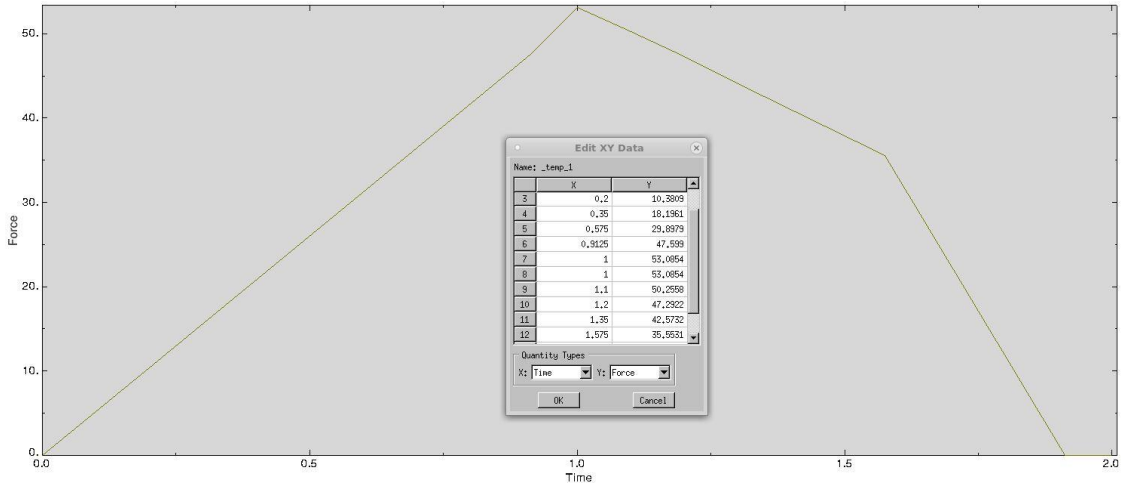

Figure 44 Separation Force in function of time graph (ABAQUS®)

Maximum separation force: 53.0854 N

As it is possible to acertain from the Figure bellow, every stud is in contact in all the predicted places. However, the tension is much greater in the studs that are further away from the centre of the beam.

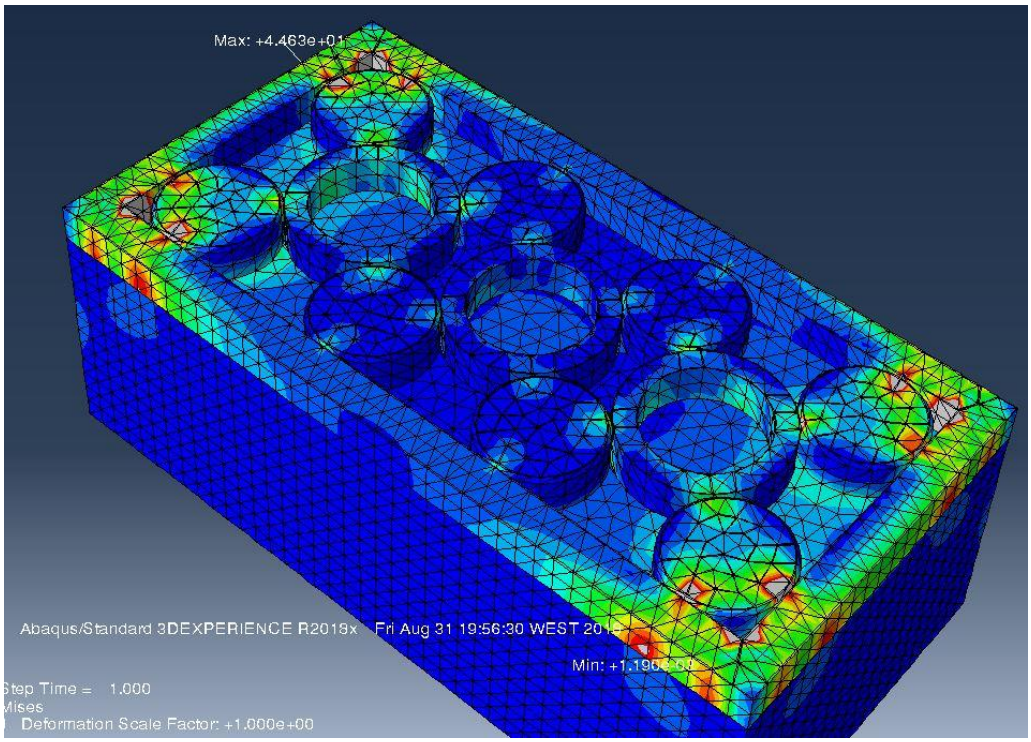

Figure 45 Contact between pieces translated into surface tension (ABAQUS®)

After determining the force needed to separate the blocks, a mean value of the force per stud can determined, Although the force per stud is not equal for every stud in a connection, this will be assumed as truth as a simplification.

The Force displacement Method is given by:

$$F = K \cdot d \therefore K = \frac{F}{d} \text{ (3.2.4.1)}$$

Giving:

$$K_{nn} = \frac{F_S}{h_s} \text{ (3.2.4.2)}$$

Where:

- K_{nn} is the elasticity coefficient normal to the plain of contact
- F_s is the mean force per stud
- h_s is the height of each stud (=1.6mm)

F_S is determined as follows:

$$F_S = \frac{F_T}{n_S} \text{ (3.2.4.3)}$$

Where:

- F_T is the total force of separation of this particular assembly (53.0854 N)
- n_S is the number of studs connected (=8)

$$K_{nn} = \frac{\frac{F_T}{n_S}}{h_s} = \frac{6.636}{1.6} = 4.148\ N/mm$$

Another element to consider, when introducing cohesive contact, is the point of its rupture, therefore a value for a “yield” strength for this definition must be set as well, which can be defined as:

$$\sigma = \frac{F_T}{A_b} = 0.106\ N/mm^2 \text{ (3.2.4.4)}$$

Where:

- A_b is the area of the base of the brick (15.8x31.8=502.44 mm^2)

After determining the separation force, the shear force can be determined analytically, as the stud can be analysed as a clamped beam with a force applied to its free end. Knowing this force, it is possible to determine the coefficients Ktt and Kss of cohesive contact.

The following model defines the maximum force applied to the stud before yielding, as well as its corresponding deflection:

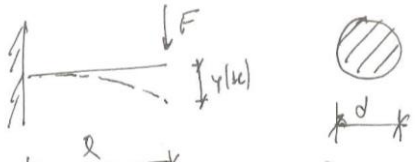

Figure 46 deflection of the stud

Considering:

T_{xy}= 45 MPa

$S=A_o=d^2\pi/4$= 18.096 mm^2

$I_z= d^4\pi/64$=26057 mm^4

b=d=4.8 mm

l=1.6 mm

E=2.5 GPa

Based on didactic material for Material Resistance Classes: (Camanho, 2015)

$$\tau_{xy} = \frac{V \cdot S}{I_Z \cdot b} \quad (3.2.4.5)$$

$$\frac{d^2y}{dx^2} = \frac{M(x)}{E \cdot I_Z} \quad (3.2.4.6)$$

Given this, a maximum value for the transverse strength can be determined:

$$V = 311.0252\ N$$

And the deflection:

$$y(1.6) = -0.01304\ mm$$

Knowing that F=Ky:

$$K_{ss} = K_{TT} = 23855.89\ N/mm$$

The principal stress in the shear direction is the same as ABS.

The values of K_{nn}, K_{ss} and K_{tt} define the value of these coefficients per stud, meaning that for each contact, the number of studs must be taken into account, meaning:

$$K_{NN\,contact} = K_{NN} \cdot number\ of\ studs\ in\ contact \quad (3.2.4.7)$$

In a similar way the actual values of K_{ss} and K_{tt} are obtained.

3.2.4.2. Contact Validation

A validation is needed when it's necessary to verify the mathematical veracity of a simulation model.

To validate the use of the cohesive contact, a simulation in similar conditions to the one previously, but in the alternative simulation system, must take place.

The contact is defined by the coefficients K_{nn}, K_{ss} and K_{tt} which are defined as an eight stud contact:

K_{nn}= 33.184 N/mm

K_{ss}=K_{tt}= 190847 N/mm

The normal stresses can be defined as in Figure 46

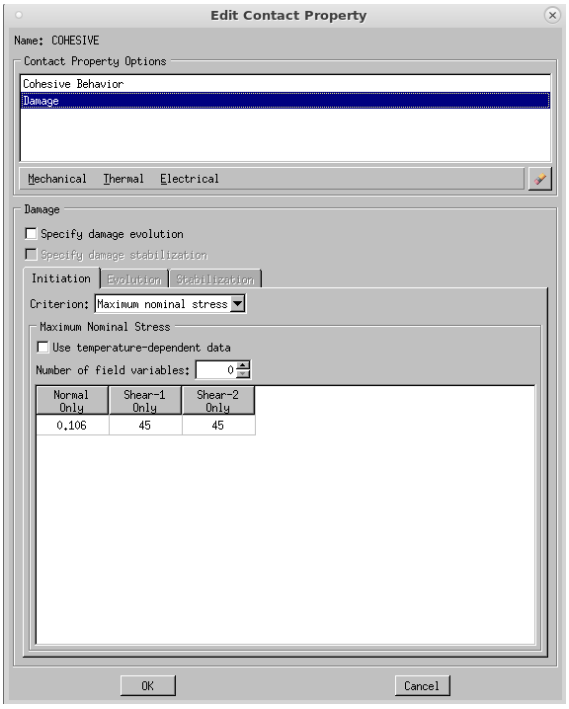

Figure 47 Stress definition on cohesive contact

The graph of Figure 46 shows the force needed to separate the two bricks, and with a maximum of almost 50 N, it is very close to the separation force verified in the LEGO® parts separation, validating this approach

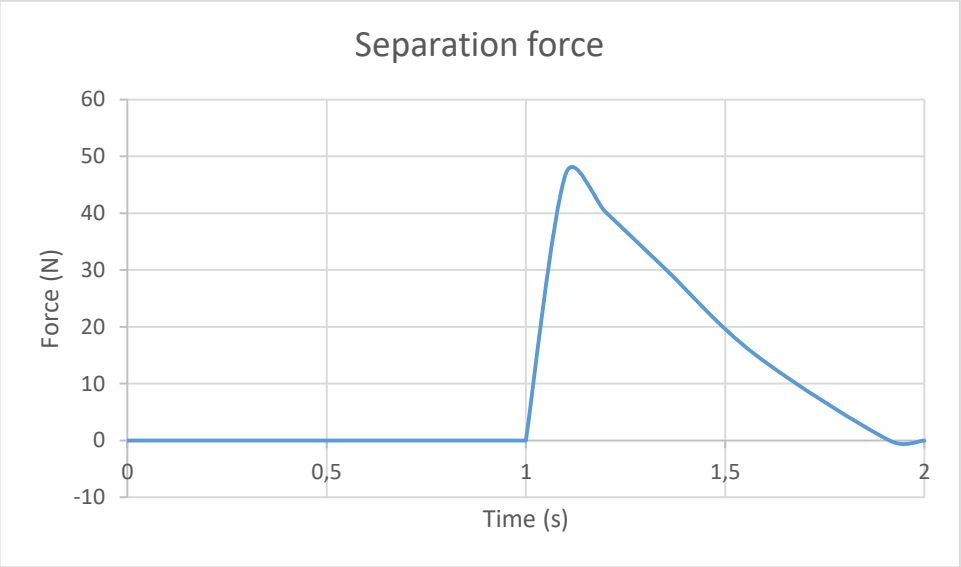

Figure 48 Separation force in the validation model (ABAQUS®)

As a means of comparison, this simulation took 13 seconds to solve, while the simulation with the actual LEGO® parts took 18 minutes and 20 seconds to conclude.

3.2.5. Simulation Model (Mock Beam)

Knowing the values of K_{nn}, K_{ss} and K_{tt}, and with the construction as seen in Figure 46, the contact parameters are defined. The beam will be clamped in both ends.

The beam is constituted of 6 different pieces: beam long sections that are meant to represent the technic-brick construction, blocks representing 2x10 bricks, two plates representing the bottom and top plates, inner and outer sleeve mock ups. The overall material volume of this beam is the same as on the other beam and their cross sections are very similar.

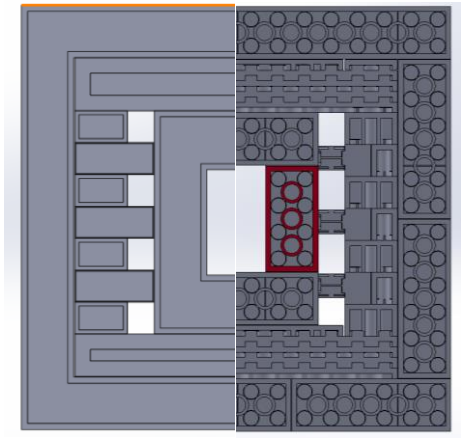

Figure 49 Cross Section comparison between a) converted beam b) original LEGO® beam (SOLIDWORDS®)

To try and maintain the volume of the structure, the parts have to guarantee the same volume as the sum of the parts they are meant to represent. For example, part 2 only represents a 2x10 Brick, so its volume has to be the same as one 2x10 Brick, but part 4 is replicating 16 Bricks, which means that each instance of part 4 has to have the same volume as the sum of those 16 Bricks. The volumes calculation is presented in the Excel document “volumes” and “swparts”. It is assumed that the pieces that constitute one part don’t separate and are thus rigidly connected.

Due to the unavailability of the 8x16 flat tile, it will not be considered in the final beam. The remaining flat tiles will not be considered in this part either, as their influence for the geometry is negligible. Also, for a matter of simplification, the material volume of parts 3.1 and 3.2 are the same (as their construction is relatively similar), yet due to construction simplifications, their cross section is slightly different. Part 5 has also suffered some changes in the light of this.

All the parts are meshed using hexahedral elements, that require a minimum amount of nodes to work, hence making the simulation lighter. To guarantee this, all parts were partitioned in rectangles before the parts were meshed.

After the description of the parts, the characterization of the contacts and border conditions is followed. There are 2 types of surface contacts in this beam: normal contact (the surfaces just touch) and the cohesive contact. The cohesive contact is simulated in ABAQUS® with the previously attained values by automatically assuming a 0.1 mm thick adhesive between the patched surfaces.

To make sure that the simulation is as efficient as possible, partitions had to be made to the parts so they could accommodate hexahedral meshes (based on isoparametric elements).

For part 1, the volume of the 1x2 Brick with Pin is considered as a 1x3 brick and the Technic Beam 5 is approximated to a 1x5 Brick.

All matching surfaces were defined as a contact. Contact 1 through 6 are of cohesive behavior and Contacts 7 through 9 are of normal behavior.

The beam will be clamped on both ends and will be subjected to a distributed load on the upper surface (which will be turned into a pressure, given the thickness of the beam, b).

Part1

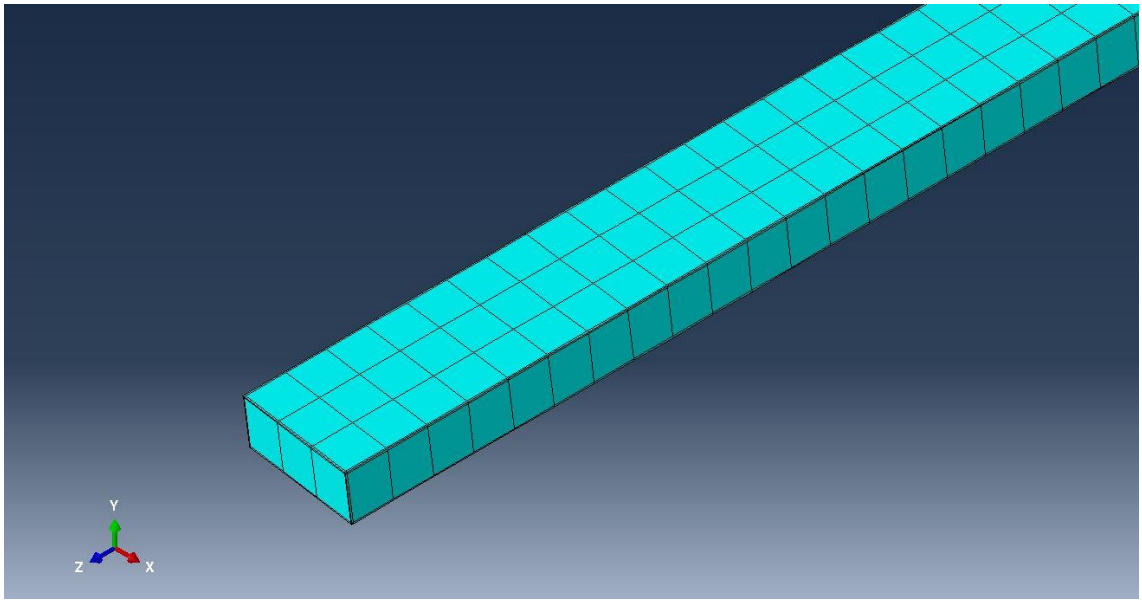

Figure 50 Meshed Part 1 (ABAQUS®)

Represents a 3 stud-wide, beam-long section made of 4 pieces: Brick 1x3, Brick 1x8, Brick 1x2 w Pin and Technic Beam 5.

Total volume (18 1x10 Brick, 36 1x3 Brick, 36 1x2 Brick with 2 Pin and 36 Technic Beam 5))

111517,8 mm^3

Dimensions 23.8x9.6x1440 mm^3

Which gives a wall thickness of 0.276 mm

Part 2

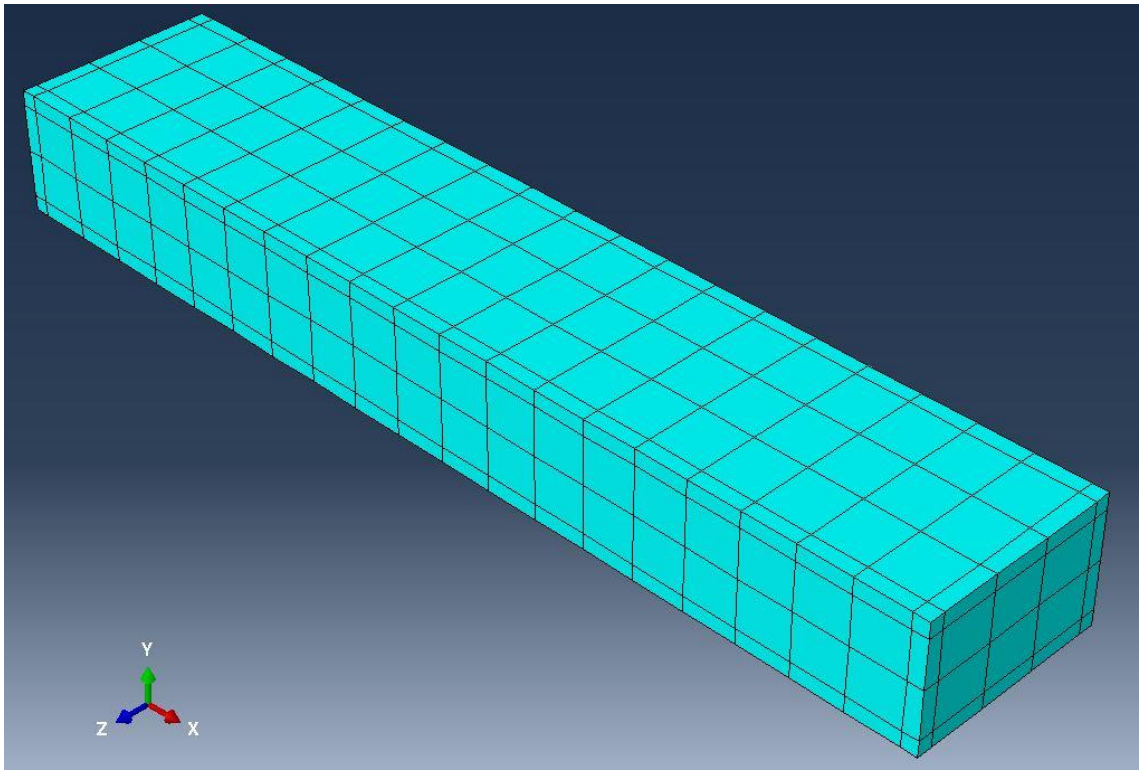

Figure 51 Meshed Part 2 (ABAQUS®)

Represents a single 2x10 brick.

Total volume (1 2x10 brick)

4600,358 mm^3

Dimensions 15.8x9.6x79.8 mm^3

Which gives a wall thickness of 1.189 mm

Part 3.1

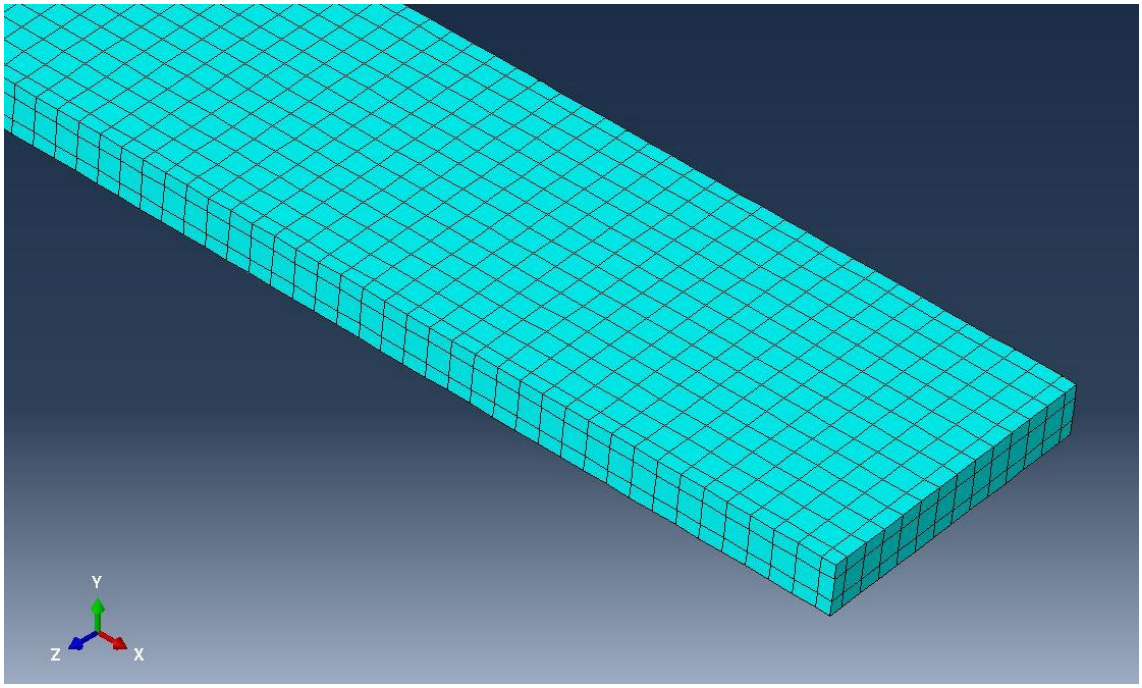

Figure 52 Meshed Part 3.1 (ABAQUS®)

Represents the upper plate section of the beam consisting of a stack of 4 pieces: plate 6x12, flat tile 8x16, flat tile 2x2, flat tile 2x4.

Total volume (120 6x12 plates)

1332422 mm^3

Dimensions 95.8x16x1440 mm^3

Which gives a wall thickness of 4.48 mm

Part 3.1

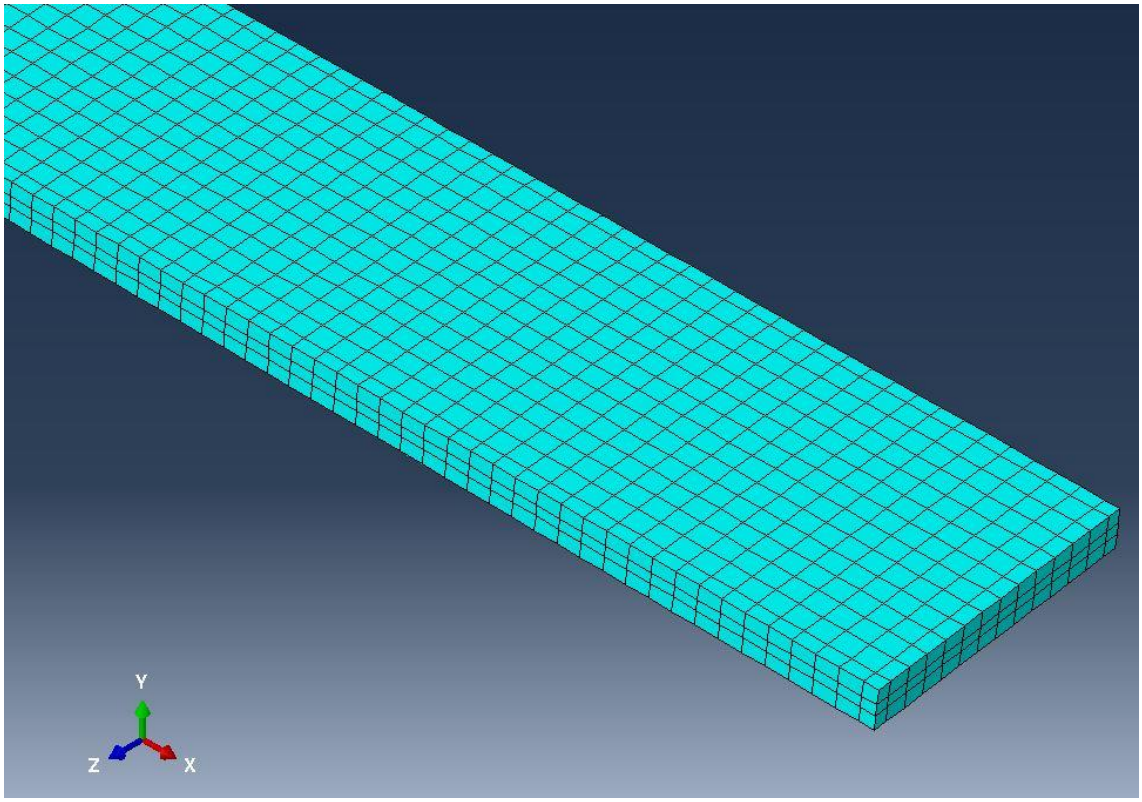

Figure 53 Meshed Part 3.2 (ABAQUS®)

Represents the lower plate section of the beam consisting of a stack of 3 pieces: plate 6x12, flat tile 8x16, flat tile 2x4.

Total volume (120 6x12 plates)

1332422 mm^3

Dimensions 95.8x12.8x1440 mm^3

Which gives a wall thickness of 4.649 mm

Part 4

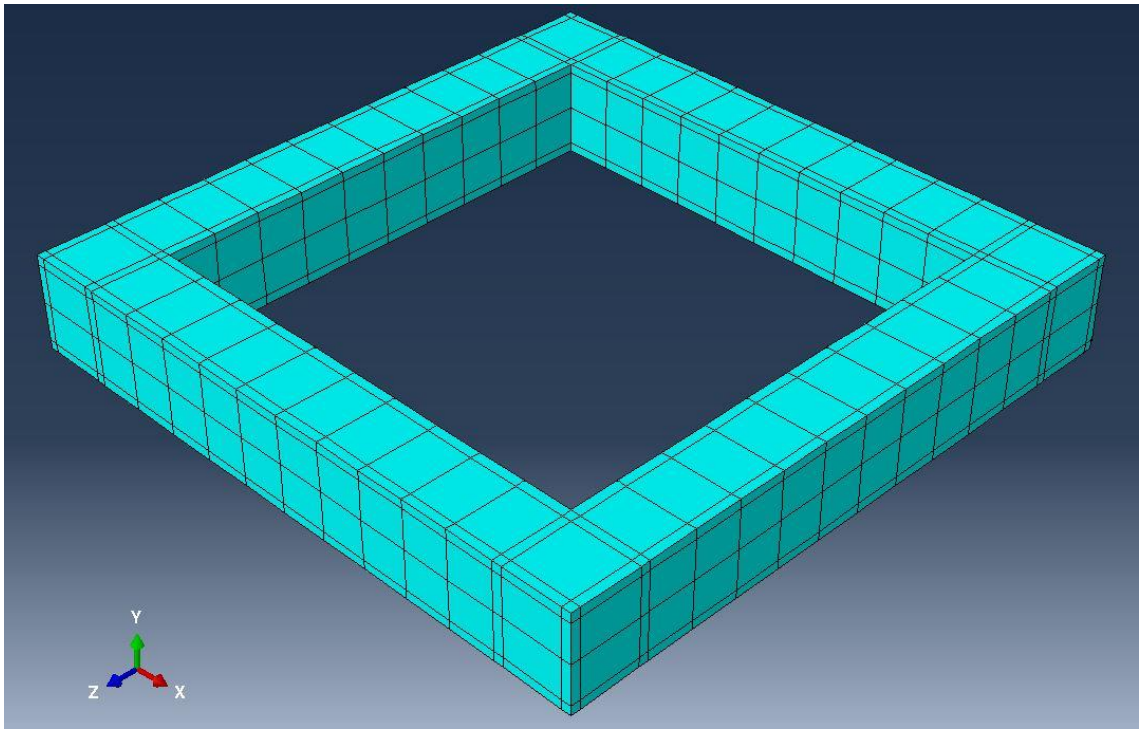

Figure 54 Meshed Part 4 (ABAQUS®)

Represents a 2 brick high stack of the outer sleeve consisting of 2 pieces: brick 2x6, brick 2x10

Total volume (4 2x10 Brick and 12 2x6 Brick)

51745,1 mm^3

Dimensions 127.8x127.8x19.2 mm^3 (inner square 96.2x96.2 mm^2)

Which gives a wall thickness of 1.844 mm

Part 5

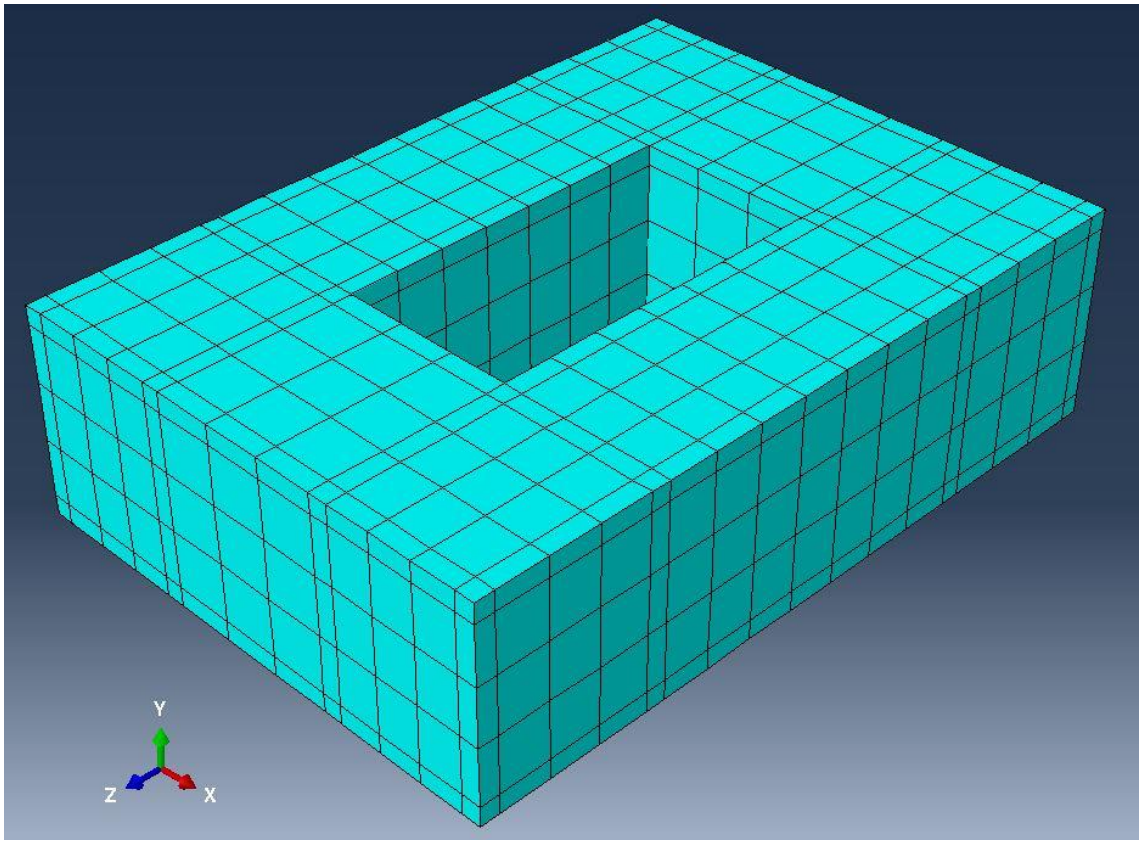

Figure 55 Meshed Part 5 (ABAQUS®)

Represents a 2 brick high stack of the inner sleeve consisting of 4 pieces: brick 2x2, brick 2x4, brick 2x6, brick 2x8

Total volume (2 2x2 Brick, 2 2x4 Brick, 2 2x6 Brick, 2 2x8 Brick)

18585,67 mm^3

Dimensions 47.8x67.2x19.2 mm^3 (inner rectangle 16.2x32.2 mm^2)

Which gives a wall thickness of 1.768 mm

Contacts (geometrical definition in attachments)

Contacts 1-6 are defined as follows:

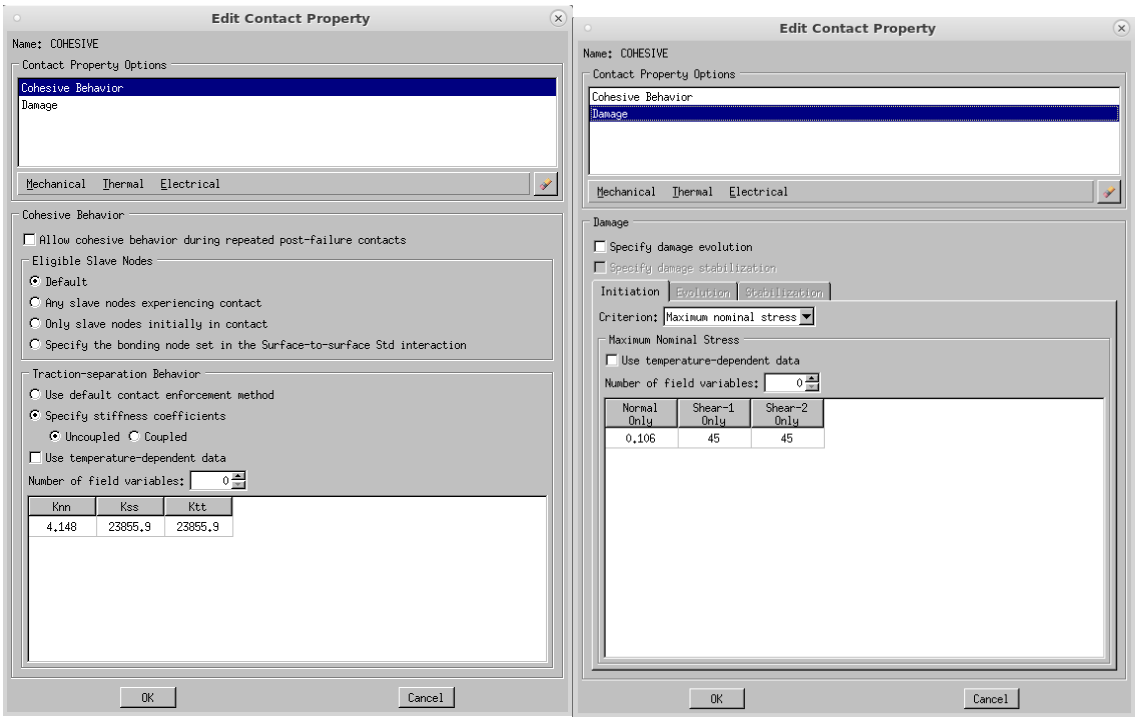

Figure 56 Property definition of cohesion (ABAQUS®)

Given that contacts 1 and 2 are differently defined from contacts 3-6, these different definitions must be found. This means only multiplying the presented values of K_{nn}, K_{ss} and K_{tt} by the number of connected studs in each contact.

Contact 1 has 112 connected sutds:

K_{nn}= 464.58 N/mm

K_{ss}=K_{tt}= 2671860 N/mm

Contact 2 has 40 connected sutds:

K_{nn}= 165.92 N/mm

K_{ss}=K_{tt}= 954236 N/mm

Contact 3-6 have 20 connected sutds:

K_{nn}= 82.96 N/mm

K_{ss}=K_{tt}= 477118 N/mm

The stresses are not dependant of the number of studs and are always defined as in the right window on Figure 55.

To overcome a limitation in ABAQUS (which doesn't allow to add cohesive and normal behavior in the same model; or at least not in a straightforward fashion). For that, the following steps must be followed: (Ismail, 2017)

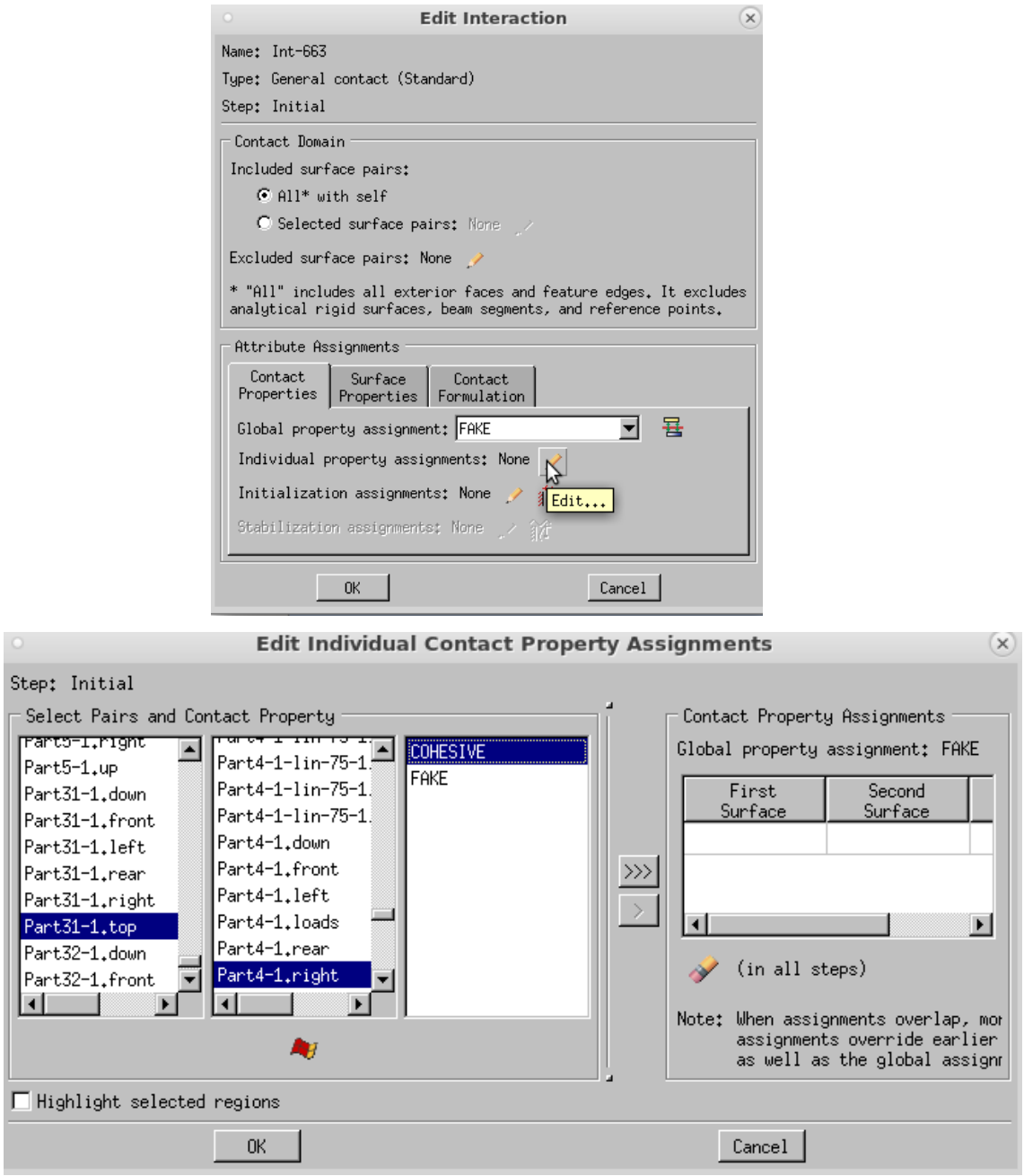

Figure 57 Overcoming Software Limitations (ABAQUS®)

Contacts 7-9 are defined as follows:

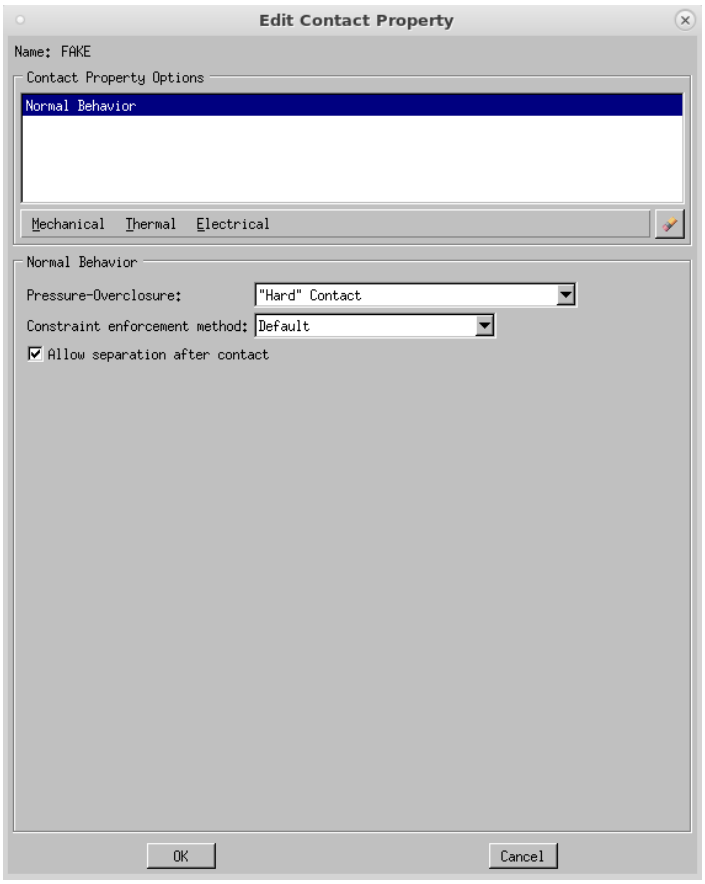

Figure 58 Definition of General Contact (ABAQUS®)

Boundary Conditions

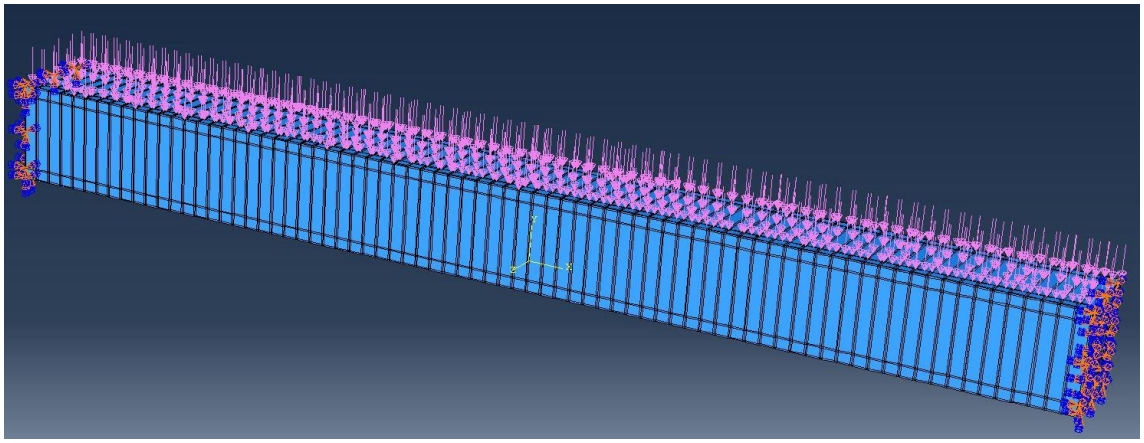

Figure 59 Loads represented over the length of the beam (ABAQUS®)

As it is seen from Figure 58, a distributed load equivalent to the 4kN/m^2, as previously defined, is applied to the upper surface of the beam

In Figure 59 it is clear by the red highlighted parts that the beam is clamped in almost every element of the boundary faces. Only the 2x10 brick mock-ups are not clamped.

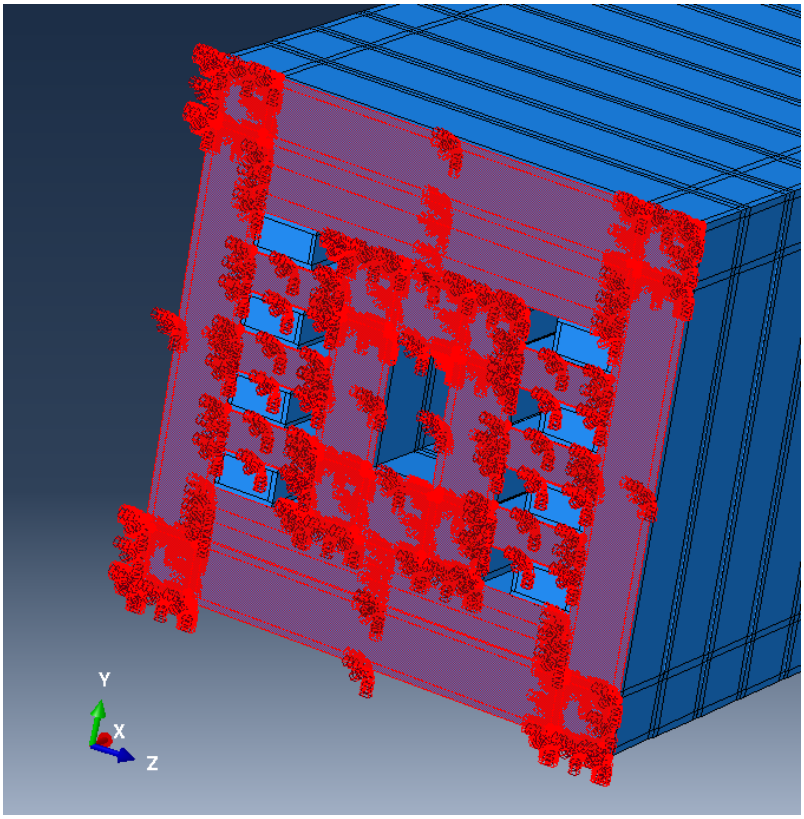

Figure 60 Highlighted Boundary Condition on one end of the beam (same on both sides) (ABAQUS®)

3.2.6. Results

As the simulation, even if simplified, is still too heavy for regular users' utilization, a solution has to be found, as to have a base value for the comparison between the beam and the benchmark simulation on wood.

As such, an analytical model was created, where a continuous beam, clamped on both ends, subjected to a distributed load and with the cross section defined as the cross section on a point of the mock beam:

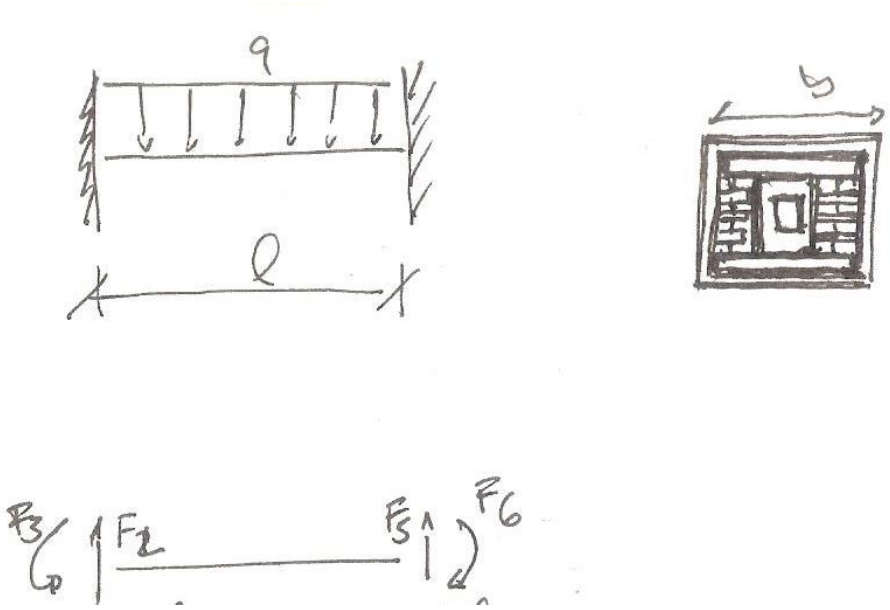

Figure 61 Analytical model of the beam deflection (very simplified)

Where:

q=1.569N/mm

l=1440 mm

b=127.8 mm

$$F2 = \frac{q \cdot l}{2} \quad F5 = \frac{q \cdot l}{2}$$

$$F3 = \frac{q \cdot l^2}{12} \quad F6 = -\frac{q \cdot l^2}{12} \text{ (3.2.6.1)}$$

$$\tau_{xy} = \frac{V \cdot S}{I_Z \cdot b} \text{ (3.2.4.5)}$$

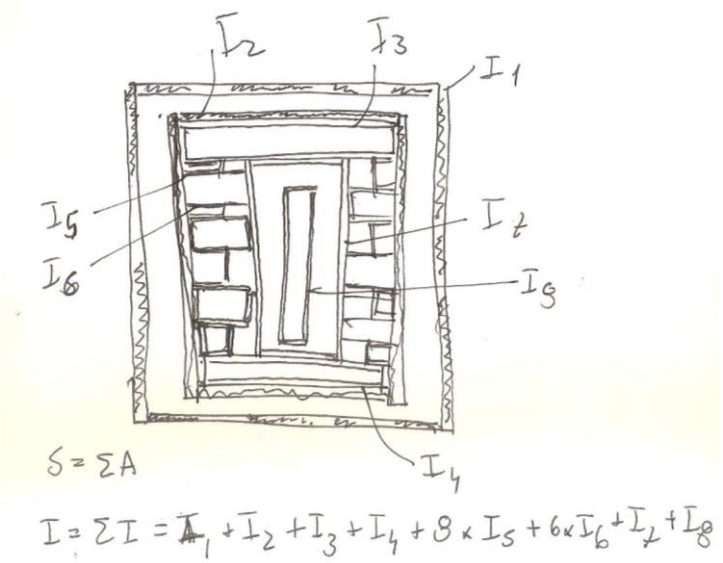

Figure 62 Cross section of the calculated beam, showing its geometry

The Values for the area of each element and their respective inertia moments can be found in the excel file “inertia_area”.

Known the values for I_Z and S:

V=ql/2= 1129.7 N

S= 4664.3mm^2

I_z=3972681 mm^4

b=127.8 mm

And the shear stress on the centre of the beam is:

$$\tau_{xy} = 0.0104\ MPa$$

To determine the displacement on the centre of the beam, equation (3.2.4.6) is used again :

$$y\ (l/2) = -1.769\ mm$$

3.2.7. Observations

The stresses on this beam are lower than when compared to the wooden beam, but the deflection is higher. This is justified by the fact that the stress is only function of the shape of the cross section ($\frac{S}{I_Z}$) and the deflection is function of the material's rigidity (E) and the moment of Inertia ($\frac{1}{E \cdot I_Z}$). Given that the wood has E.I= 67e^9 Nmm^2 and ABS has EI=9.93e^9 Nmm^2 it is predictable that the ABS beam would deform further. However, from a mechanical point of view, both beams showed positive results as in none of the beams is there evidence that they would get close to their yield stress.

3.3. Testing

3.3.1. 3 point bending test

When testing the bending capability of beams, it is usual to conduct a 3 or 4 point bending test. Given that the available test is 3 point bending, this will be the one undertaken.

This test consists of 2 supports separated by l, in which a beam will be supported and then an actuator presses on the top of the beam as seen in Figure 62.

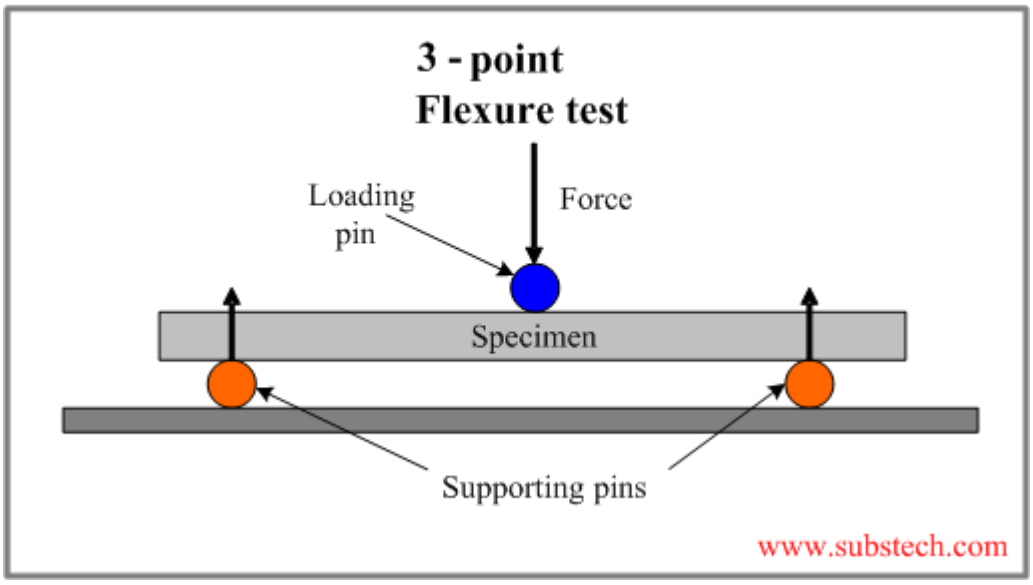

Figure 63 Representation of the 3 point bending test (16)

3.3.2. Test procedures

The beam must be clamped at the ends, so the tested length is 1440mm. The force should be applied at the centre of the beam (l=720mm).

To access the influence of each part in the project, the following constructions should be followed to evaluate the influence of the Technic Beams and the Sleeves.

- Beam alone

ITEM Num	Name	Quantity
1	PLATE 6X12	240
2	FLAT TILE 2X4	120
3	BRICK1X10	108
4	BRICK1X3	216
5	BRICK2X10	144
6	BRICK 1X2 w 2pin	216
8	FLAT TILE 2X2	20

Table 9 Beam Alone part list

- Beam + technic

ITEM Num	Name	Quantity
1	PLATE 6X12	240
2	FLAT TILE 2X4	120
3	BRICK1X10	108
4	BRICK1X3	216
5	BRICK2X10	144
6	BRICK 1X2 w 2pin	216
7	TECHNIC BEAM 5	216
8	FLAT TILE 2X2	20

Table 10 Beam + Tecnhic part list

- Beam + technic + sleeve out

ITEM Num	Name	Quantity
1	PLATE 6X12	240
2	FLAT TILE 2X4	120
3	BRICK1X10	108
4	BRICK1X3	216
5	BRICK2X10	144
6	BRICK 1X2 w 2pin	216
7	TECHNIC BEAM 5	216
8	FLAT TILE 2X2	20
10	BRICK 2X6	900

Table 11 Beam + Tecnhic + Outer Sleeve part list

- Beam + technic + sleeve in

ITEM Num	Name	Quantity
1	PLATE 6X12	240
2	FLAT TILE 2X4	120
3	BRICK1X10	108
4	BRICK1X3	216
5	BRICK2X10	294
6	BRICK 1X2 w 2pin	216
7	TECHNIC BEAM 5	216
8	FLAT TILE 2X2	20
9	BRICK 2X2	150
10	BRICK 2X6	150
11	BRICK 2X4	150
12	BRICK 2X8	150

Table 12 Beam + Tecnhic + Inner Sleeve part list

- Beam + technic + sleeve out + sleeve in (only one simulated)

ITEM Num	Name	Quantity
1	PLATE 6X12	240
2	FLAT TILE 2X4	120
3	BRICK1X10	108
4	BRICK1X3	216
5	BRICK2X10	444
6	BRICK 1X2 w 2pin	216
7	TECHNIC BEAM 5	216
8	FLAT TILE 2X2	20
9	BRICK 2X2	150
10	BRICK 2X6	1050
11	BRICK 2X4	150
12	BRICK 2X8	150

Table 13 Beam + Tecnhic + Outer Sleeve +Inner Sleeve part list

3.3.3. Test specimens

To carry out these tests, all the pieces must be ordered from LEGO®. This order can be seen divided into 4 separate orders as in Excel file “order”, to accommodate for the Pick-a-Brick section of the LEGO® shop. This method was selected as it was the fastest way for the parts to arrive, however due to incompatibility between the financing entity and LEGO® singular part orders (namely the incapability of the later to produce pro-forma invoices for the selected parts) didn’t allow for the order, despite approval from the financing entity for this spending.

Other ways might be tried, namely trying to contact the LEGO® CEO directly, contacting the person with the original idea (James May) and retry contacts with Atelier One.

Given this restraint, the tests were not carried out.

4. Conclusions

4.1. Final regards

Without any test results, it's hard to conclude if the beam would work. However, the simulated results have given promising indication.

Also, without the data from the simulation model, it's impossible to assess if this is a viable alternative simulation method when building LEGO® beams, when compared to a simulation of the true contacts between LEGO® parts.

When analysing the data on the beam, further improvements may be done, mainly positioning more LEGO® Technic beams in the lower part of the beam as this is the most traction strained region and could be further developed.

4.2. Future works

- Continue the beam development, and find a final solution for the connection between them.
- Try and follow the monocoque construction solution.
- Develop plumbing and wiring solutions.

5. References

(Youtube), B. t. (Director). (2018). *World's Longest LEGO Great Ball Contraption! Brickworld Chicago 2018* [Motion Picture].

(Youtube), J. B. (Director). (2015). *Working LEGO Combination Safe* [Motion Picture].

(Youtube), J. B. (Director). (2016). *The Ultimate LEGO Machine Returns!* [Motion Picture].

ABAQUS Analysis User's Manual. (2005).

Argyris, J. H. (1965). Matrix displacement analysis of anisotropic shells by triangular elements. *J. Roy. Aero. Soc. 69*, 801-805.

Camanho, P. P. (2015). *Diapositivos das Aulas de Mecanica dos Solidos.* Porto: FEUP.

Cardoso, R. P. (1998). *Desencolvimento de modelos para regeneração adaptativa e contacto em processo de enformação plástica.* Porto.

Christiansen, G. K. (1958). *Denmark Patent No. 751387.*

Clough, R. W. (1960). The finite element method in plane stress analysis. *Proc. 2nd A.S.C.E. COnf. in Electronic Computation.* Pittsburgh, Pa.

Courant, R. (1943). Variational methods for the solution of problems of equilibrium and vibration. *Bull. Am. Math. Soc. 49*, 1-23.

Crisfield, M. A. (1986). *Finite Elements and solution procedures for structural analysis Vol I: Linear analysis.* UK.

Industries, C. (n.d.). *which plastic material is used in lego sets?* Retrieved from Craftechind: http://www.craftechind.com/which-plastic-material-is-used-in-lego-sets/

Ismail, M. (2017). *Abaqus Cohesive Contact (Interaction Behaviour)*. Retrieved from https://www.youtube.com/watch?v=YW-5zZV0b_4&t=348s

José Luis Pereira Rebelo Fernandes, S. -P. (2017). *Portugal Patent No. 107461.*

LEGO(R). (2018). *LEGO(R) History*. Retrieved from LEGO(R) website: https://www.lego.com/en-us/aboutus/lego-group/the_lego_history

LEGO(r). (2018). *The LEGO Group History - 1930s*. Retrieved from LEGO(r) Website: https://www.lego.com/en-us/aboutus/lego-group/the_lego_history/1930

LEGO(R). (2018). *The LEGO Group History - 1940*. Retrieved from LEGO(R) Website: https://www.lego.com/en-us/aboutus/lego-group/the_lego_history/1930

LEGO(r). (2018). *The LEGO Group History - 1970*. Retrieved from LEGO Website: https://www.lego.com/en-us/aboutus/lego-group/the_lego_history/1970

LEGO(r). (2018). *The LEGO Group History - 1980*. Retrieved from LEGO(r) Website: https://www.lego.com/en-us/aboutus/lego-group/the_lego_history/1980

LEGO(R). (2018). *The LEGO Group History -1960*. Retrieved from LEGO(R) Website: https://www.lego.com/en-us/aboutus/lego-group/the_lego_history/1960

May, J. (2010). James May's Toy Stories: LEGO(r) House. England: BBC.

Ministério da Admnisitração Interna. (2005). Regulamento de Segurança e Ações para Estruturas de Edifícios e Pontes. 21. Porto Editora.

O. C. Zienkiewicz, Y. K. (1964). The finite element method for analysis of elastic isotropic and anisotropic slabs. *Proc. Inst. Civ. Eng.*, 471-488.

Paulo B. Lourenço, E. M. (n.d.). Discrete Element modeling of Masonry Structures: Verification and Validation.

reuters. (2011). "Extreme Makeover" helps build seven Joplin homes in a week. *Reuters*.

Roriz, G. T. (2015). *Parto computacional assistido.* Porto.

Wriggers, P. (2002). *Computational Contact Mechanics.* Germany: John Wiley & Sons Ltd.

Picture References

(1) https://vimeo.com/120572139 (2016)

(2) José Luis Pereira Rebelo Fernandes, S. -P. (2017). *Portugal Patent No. 107461.* (08/2018)

(3) Fernando Faria (2017) (08/2017)

(4) http://www.nathansawaya.com/ (03/2018)

(5) http://www.brickvision.it/archives/1011 (03/2018)

(6) https://youtu.be/g5y1pdPVDx8?t=62 (2016)

(7) https://static1.squarespace.com/static/54172b75e4b03dbd0c07d1ed/t/59f20d0751a58425f25b3cd7/1509035400402/Copyright+Barnaby+Gunning.jpg?format=1500w (07/2018)

(8) https://static1.squarespace.com/static/54172b75e4b03dbd0c07d1ed/t/59f20d2280bd5e69367e4cb5/1509035400404/200_12.min+%281%29.jpg?format=1500w (07/2018)

(9) https://www.youtube.com/watch?v=H8z0f7kPQEw&t=1s~ (2016)

(10) https://racecarsdirect.com/content/UserImages/84512/471498.jpg?v=0 (07/2018)

(11) https://3.imimg.com/data3/VS/OX/MY-1114444/space-frame-500x500.jpg (07/2018)

(12) Paulo B. Lourenço, E. M. (n.d.). Discrete Element modeling of Masonry Structures: Verification and Validation.

(13) Roriz, G. T. (2015). *Parto computacional assistido.* Porto.

(14) Cardoso, R. P. (1998). *Desencolvimento de modelos para regeneração adaptativa e contacto em processo de enformação plástica.* Porto.

(15) *ABAQUS Analysis User's Manual.* (2005)

(16) http://www.substech.com/dokuwiki/lib/exe/fetch.php?w=&h=&cache=cache&media=3-point_flexure.png (06/2018)

Attachments

Attachment 1 Contact 1 – between two Parts 4 (SOLIDWORKS®)

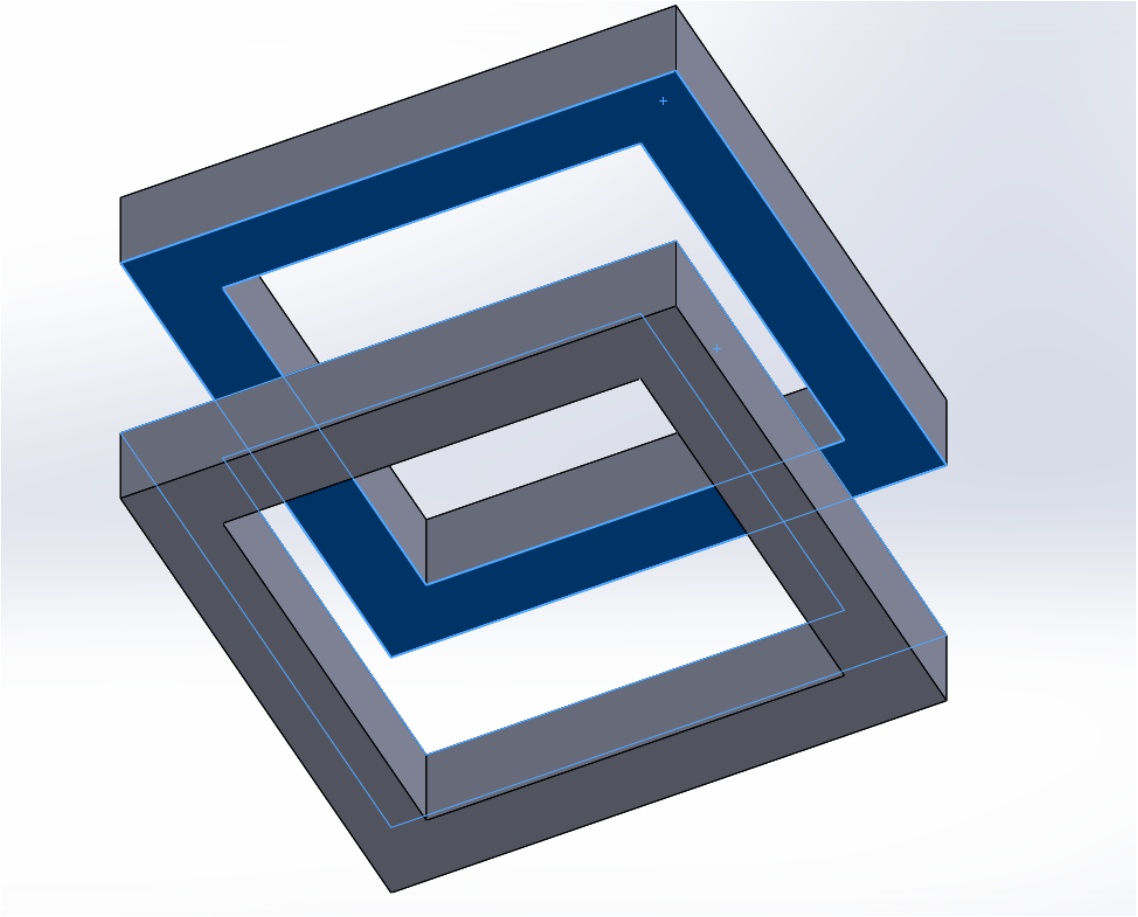

Attachment 2 Contact 2 – between two Parts 5 (SOLIDWORKS®)

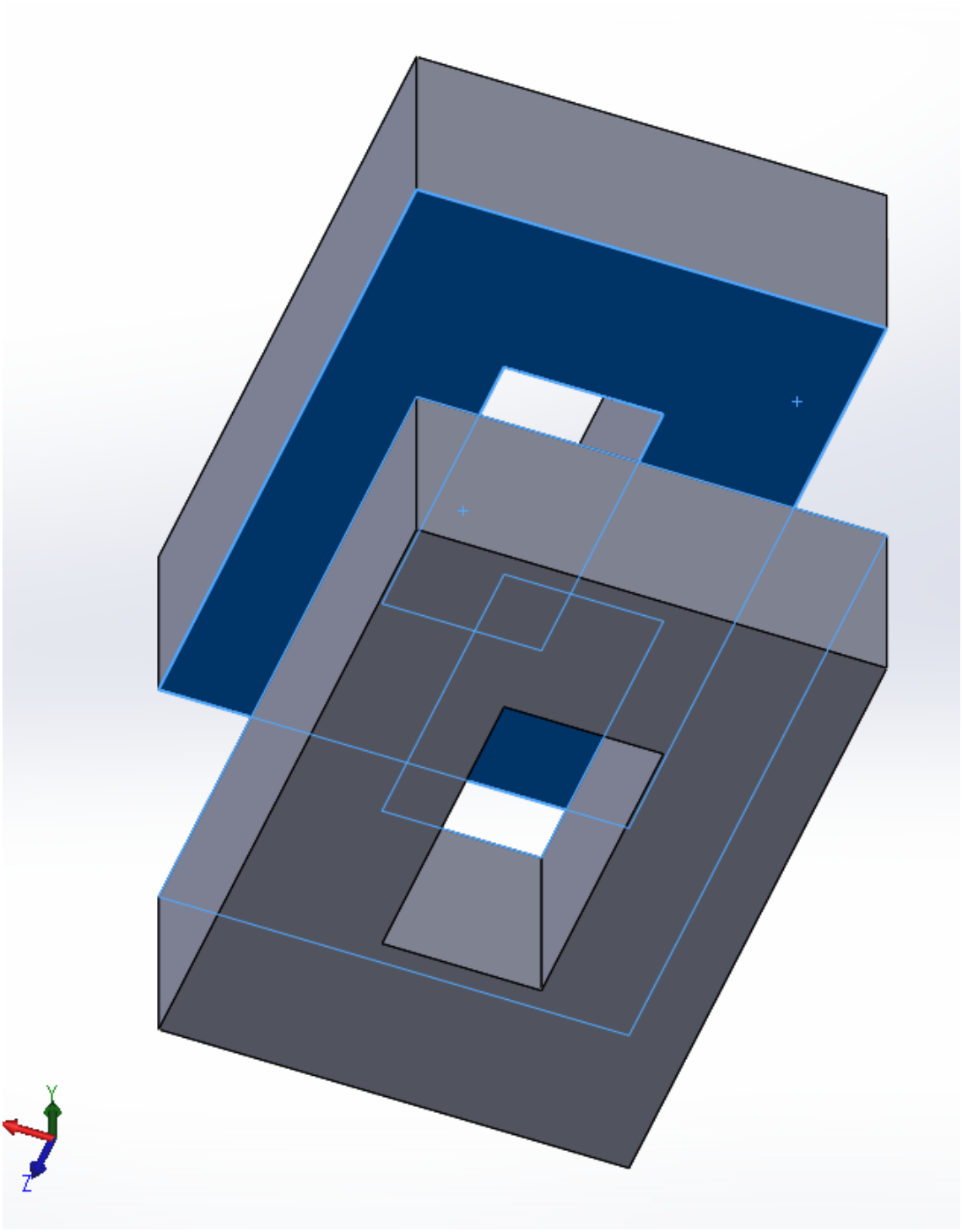

Attachment 3 Contact 3 – between Part 3.2 and Part 2 (SOLIDWORKS®)

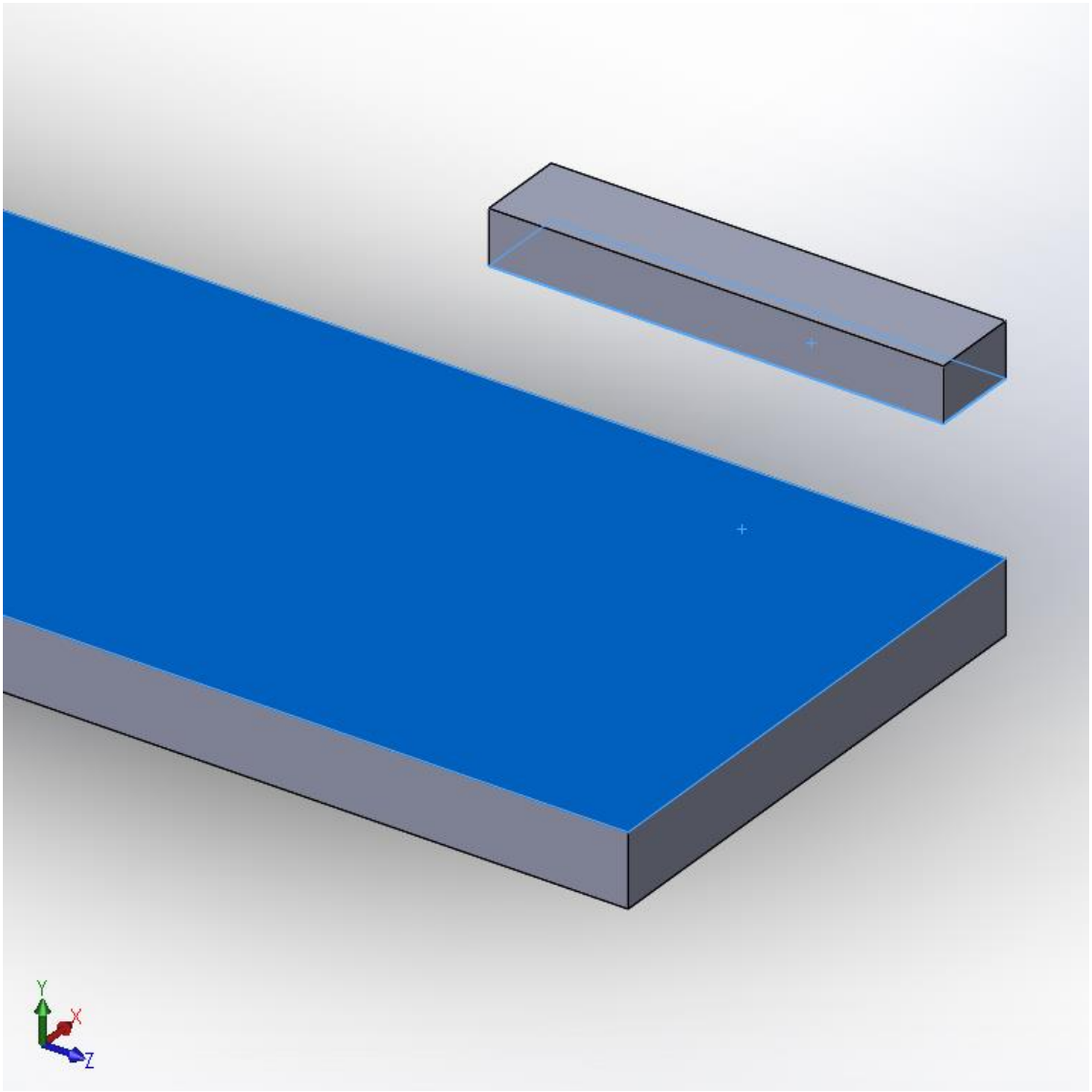

Attachment 4 Contact 4 – between Part 2 and Part 1(SOLIDWORKS®)

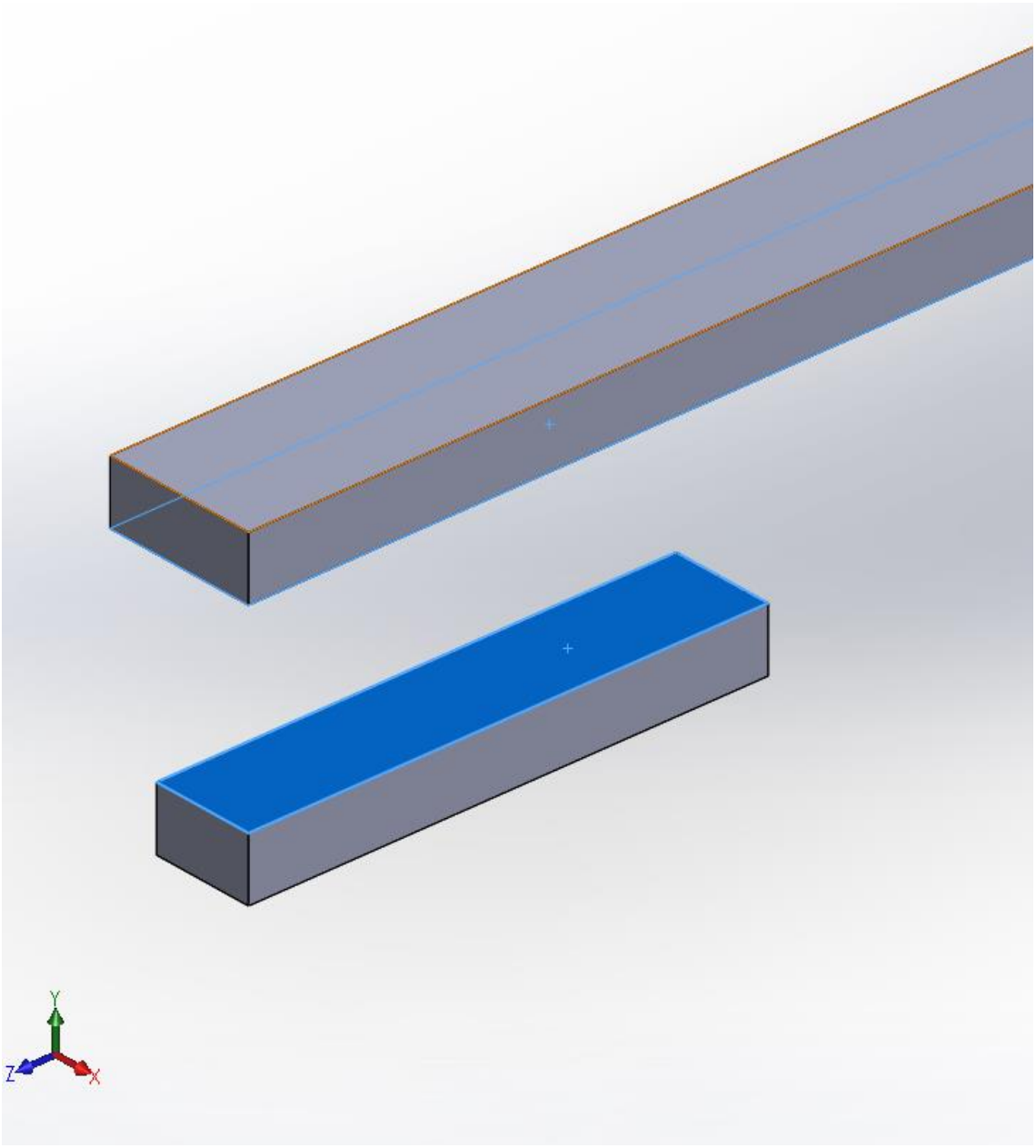

Attachment 5 Contact 5 – between Part 1 and Part 2(SOLIDWORKS®)

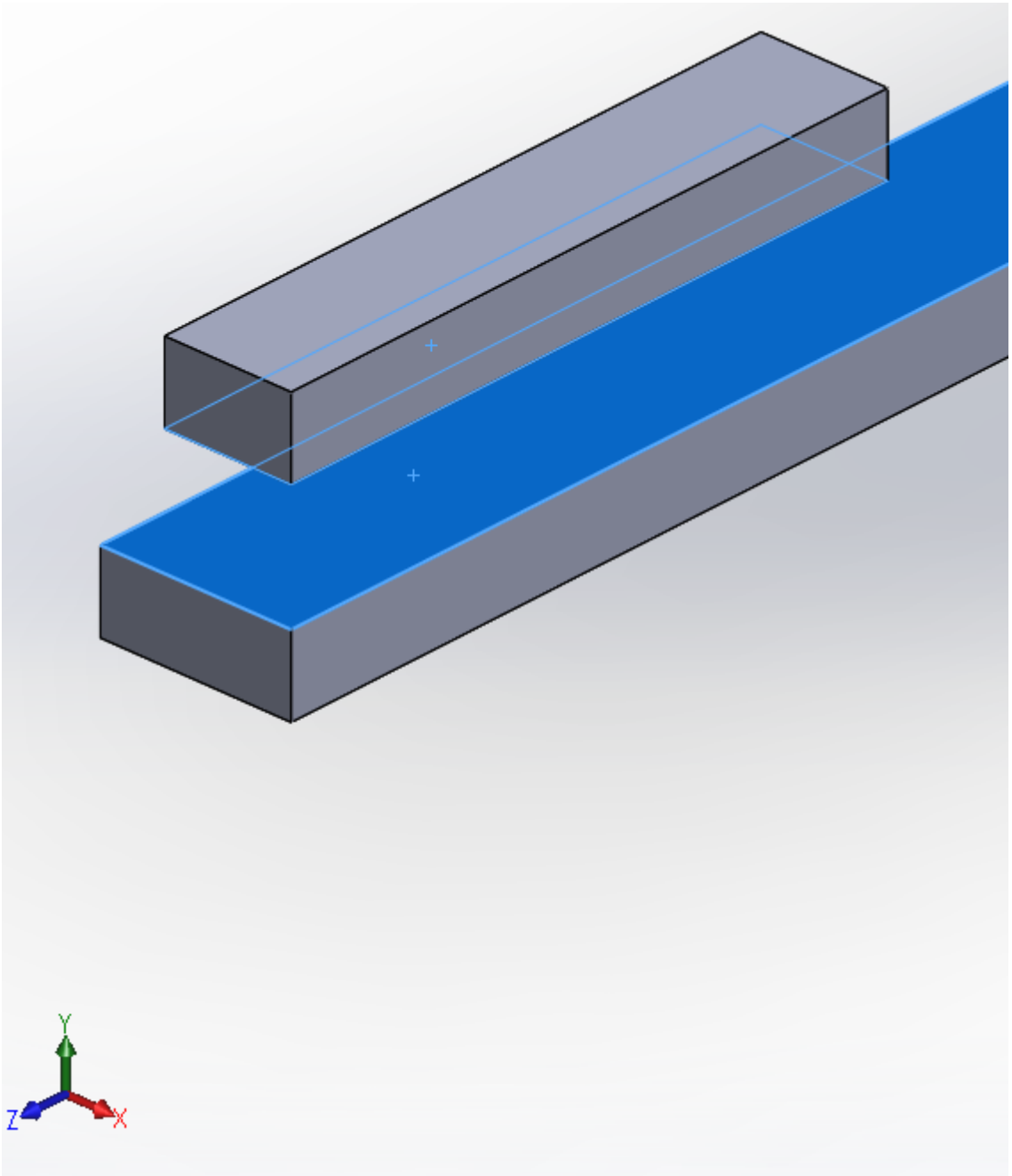

Contact 6

Attachment 6 Contact 6 – between Part 2 and Part3.1(SOLIDWORKS®)

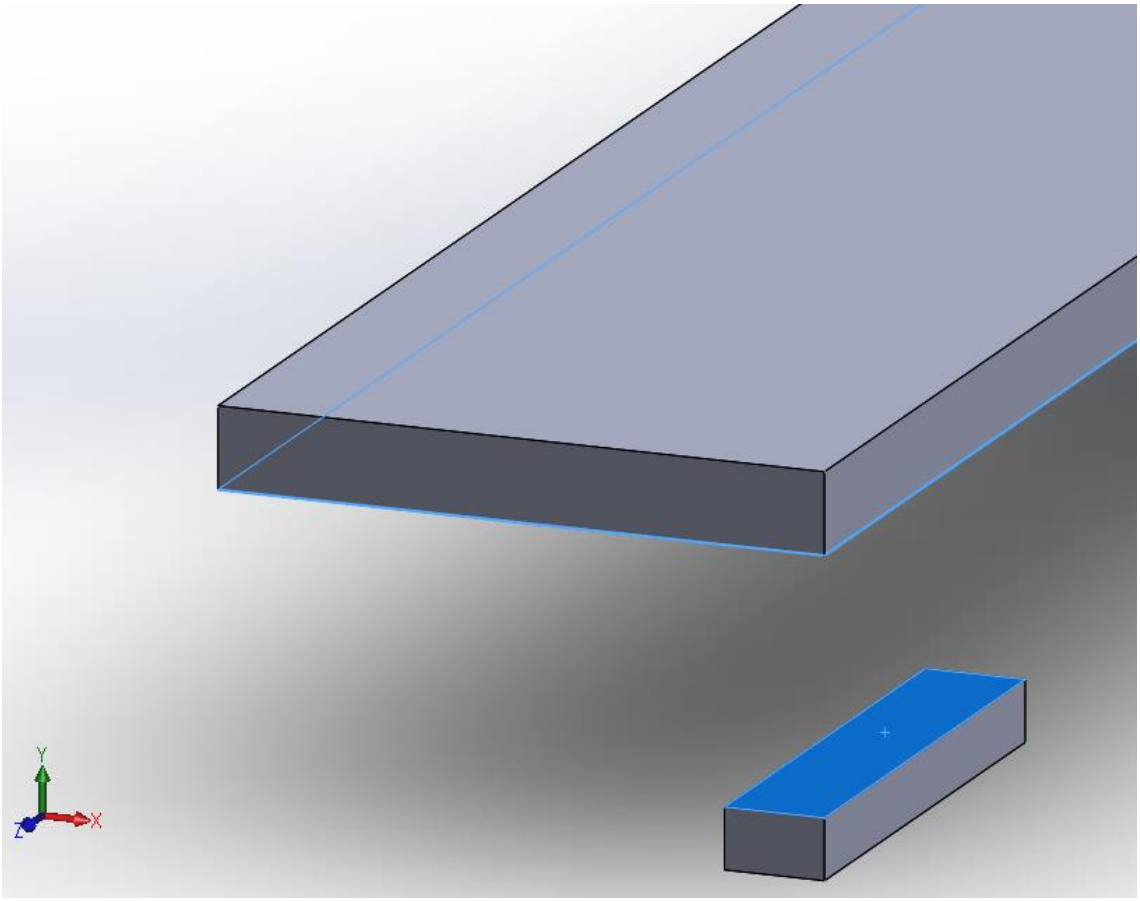

Contact 7

Attachment 7 Contact 7 – between Part 3.1 and Part 4 (SOLIDWORKS®)

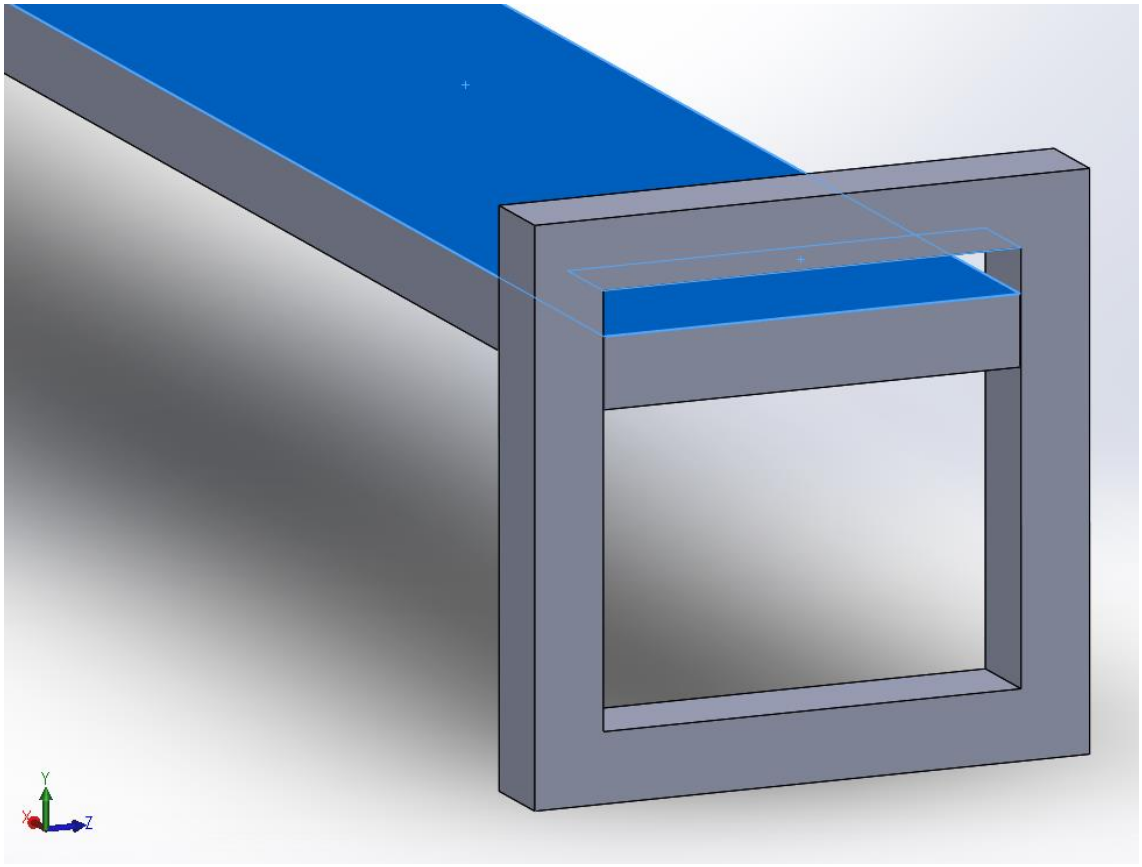

Attachment 8 Contact 8 – between Part 5 and Part 3.1 (SOLIDWORKS®)

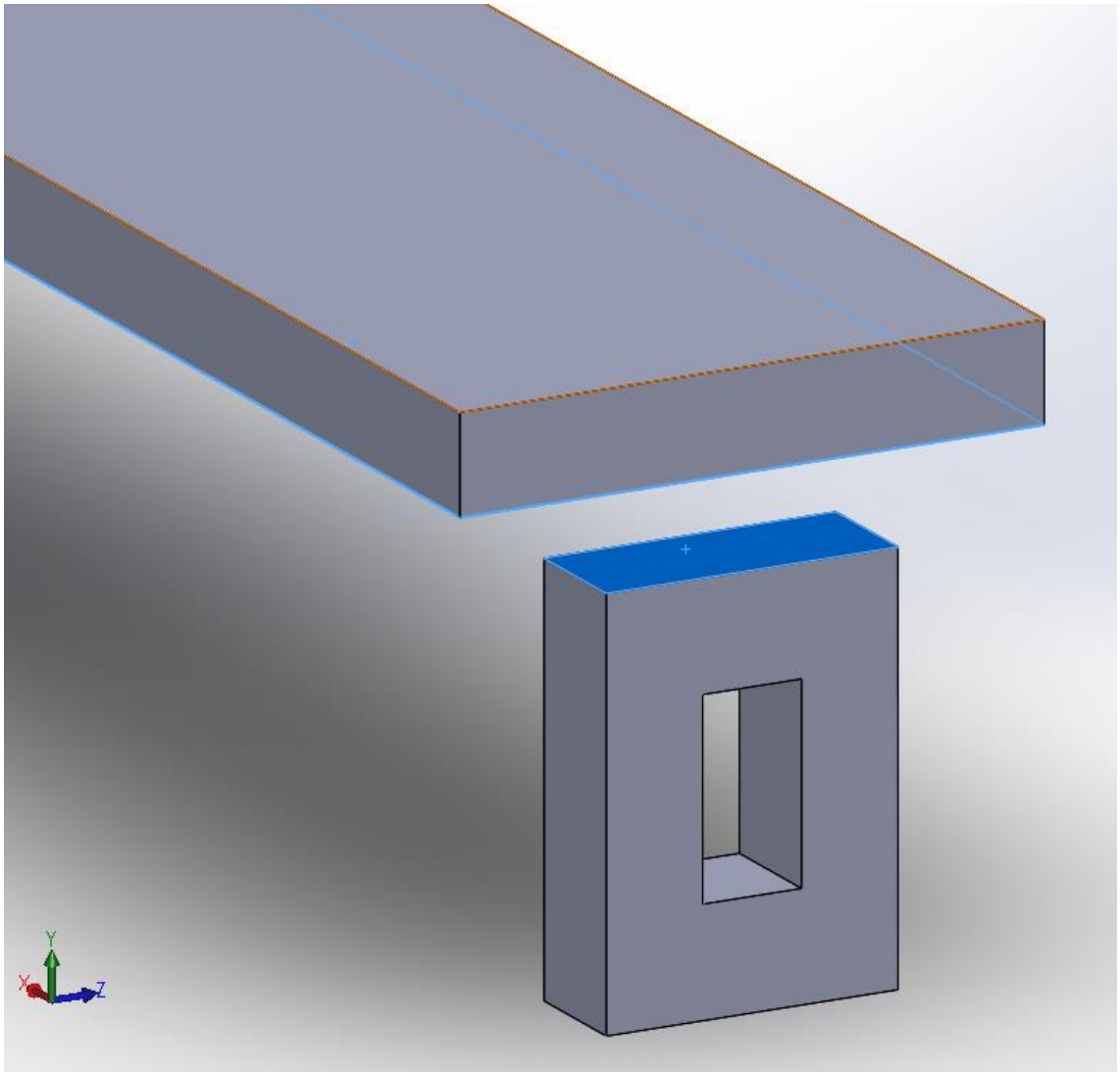

Attachment 9 Contact 9 – between Part 3.2 and Part 5(SOLIDWORKS®)